NATIONAL AERONAUTICS AND SPACE ADMINISTRATION

Technical Report 32-1363

The Mariner V Flight Path and its Determination from Tracking Data

G. Pease

R. Bourke

S. McReynolds

K. Thuleen

J. Borras

R. Mitchell

JET PROPULSION LABORATORY

CALIFORNIA INSTITUTE OF TECHNOLOGY

PASADENA, CALIFORNIA

July 1, 1969

NATIONAL AERONAUTICS AND SPACE ADMINISTRATION

Technical Report 32-1363

The Mariner V Flight Path and its Determination from Tracking Data

G. Pease
R. Bourke
S. McReynolds
K. Thuleen
J. Borras
R. Mitchell

JET PROPULSION LABORATORY
CALIFORNIA INSTITUTE OF TECHNOLOGY
PASADENA, CALIFORNIA

July 1, 1969

Prepared Under Contract No. NAS 7-100
National Aeronautics and Space Administration

Preface

The work described in this report was performed by the Mission Analysis Division of the Jet Propulsion Laboratory, under the cognizance of the *Mariner* Venus 67 Project.

This document consists of four sections, each describing a different aspect of the *Mariner V* flight path. Part I, Orbit Determination from DSIF Tracking Data, by G. Pease, discusses real-time orbit determination activities during the pre-midcourse maneuver, cruise, and encounter phases of the mission. A description of the tracking data system by H. Palmiter is included.

Part II, Nongravitational Forces, by R. Bourke, S. McReynolds, and K. Thuleen, analyzes the attitude control telemetry on *Mariner V* to determine the disturbance torques and nonconservative translational forces acting on the spacecraft during the flight. These act as a corrupting influence on the flight path determination, since only gravitational and solar radiation forces are calculated by the inflight orbit determination and trajectory programs.

Part III, Mission Trajectory, by J. Borras, describes the trajectory parameters of the flight and the near-Venus encounter geometry as it relates to occultation zones and viewing angles.

Part IV, The Midcourse Maneuver Program, by R. T. Mitchell, discusses the computational aspects of midcourse maneuver strategy. This program uses some of the results of Parts I and III in computing the parameters of a correction to the flight path.

Acknowledgments

Special acknowledgments are due to members of the Jet Propulsion Laboratory staff for their contribution to the results presented in this document. The flight path analysis was coordinated by H. J. Gordon, *Mariner V* Flight path Director. Early trajectory analysis was accomplished by D. A. Tito. Data editing and preparation of data types were performed by S. J. Reinbold and A. O. Kiesow. Computer programming support was furnished by G. A. Madrid and A. J. Donegan.

The following personnel contributed much valuable assistance in the operational phase of the mission: J. E. Ball, S. K. Wong, H. D. Palmiter, R. N. Wimberly, N. Thomas, M. Kirby, J. D. Anderson, G. W. Null, N. A. Mottinger, W. L. Sjogren, J. A. Borras, N. R. Haynes, T. H. Thornton, and D. W. Trask.

Contents

Contents (contd)

Tables

Figures

Contents (contd)

Figures (contd)

Contents (contd)

Figures (contd)

Abstract

This report contains the results of the *Mariner V* inflight oribt determination, trajectory evaluation, midcourse maneuver analysis, and the nongravitational force evaluation. During the orbit determination procedure, many physical constants of scientific interest were measured. The inflight values obtained for many of these constants, such as the mass of Venus, the astronomical unit, the earth-moon mass ratio, and the geodetic locations of the Deep Space Network tracking stations are listed.

The principal concern in flight operations was the prediction of the near-Venus trajectory quantities. This problem is discussed in its various aspects in each of the parts of this report. Nominal, predicted, and achieved aiming points are presented along with the relevant parameters pertaining to each case; these include desirable and excluded aiming zones, the effect of a midcourse maneuver, the effect of altitude control jets, and the least-squares solution for orbital parameters from radio tracking data.

The *Mariner V* Flight Path and its Determination from Tracking Data

Part I. Orbit Determination from DSIF Tracking Data

G. Pease

1. Introduction

Part I describes the real-time orbit determination activity during the *Mariner V* mission. The results are far from definitive, as they do not include the post-mission processing. The postprocessing results fall in the area of celestial mechanics investigation and are to be found in the appropriate journals, such as the *Astronomical Journal.*

For the sake of convenience, the mission has been separated into three distinct phases in this section: premidcourse, cruise, and encounter. The first of these, the premidcourse maneuver phase, is examined in Part I, Section II; it describes the orbit analysis during the 5-day interval from launch to midcourse maneuver. These results define how the entire trajectory would have appeared had there been no midcourse maneuver, such information being necessary to the planning of the maneuver. The manner in which orbit determination was used to measure the *a posteriori* maneuver execution errors in thrust magnitude and pointing direction is also described.

The cruise phase least squares orbit solutions for physical constants are given in Part I, Section III-B. These constants include the coefficient of spacecraft solar reflectivity, tracking station locations, and the lunar gravitational constant. Part I, Section III-C, discusses the cruise orbit solutions numerically integrated to Venus encounter. The target plots show the cruise orbit determination dispersion mapped to Venus.

The encounter phase physical constant solutions and aiming point estimates are described in Part I, Section IV-A. These results are based on radio tracking data collected after five days prior to closest approach to Venus and up to five days after closest approach.

II. Early Mission Performance and Results

A. Tracking Data Coverage

1. Description. During the nonpowered transfer flight period between 0629 GMT, June 14, and 2307 GMT June 19, near-continuous tracking coverage was obtained by DSS 11(Goldstone Pioneer), 41(Woomera), 42(Canberra), 51(Johannesburg), and 61(Madrid). As shown in Table 1, DSS 41 and 51 participated only briefly in the early phase of this period. The data types used in determining the orbit of the spacecraft (Ref. 1) are as follows:

(1) Hour angle and declination (HA, DEC) this data type is the pointing angle of the tracking antenna expressed in degrees; it is only used in the very early orbits.

(2) S-band phase, coherent counted doppler (CC3) this is a measure of the topocentric radial velocity of the spacecraft, and is the prime orbit data type. Units: 1 m/s $\simeq$15.3 Hz (Fig. 1).

2. Summaries. The tracking data available in the premaneuver orbits are shown in Table 1. Angle data were obtained until $07^h\,03^m\,57^s$ GMT, approximately 40 min after injection into transfer orbit. The angles from DSS 51 were biased until this time at which it was discovered the antenna had been tracking on a side lobe. Orbit *PROR XA* is corrupted by these biased angles. The DSS 42 angles in orbits *PROR YA* and *ICEV XA*, two early real-time orbits, are effectively biased, due to an incorrect station latitude used in the computations of these orbits.

3. Compressed data. In Table 1, the number of doppler points are either tagged by a *U* or *C*. The *U* indicates the data were counted over a period of 10 or 60 s. The later orbits in Table 1 are identical with a pass number listed under data type and always refer to phase-coherent two-way doppler (CC3) data. The first two digits indicate the sample time of the data, in seconds; the last three digits identify the pass number from that station. If the number of points is tagged by a *C*, this means the data has been compressed, or averaged, over 600-s intervals. This smoothing process is reflected in improved statistics for individual points.

4. Controlled roll data. The spacecraft was in a controlled roll mode until approximately 2250 GMT, June 14. Since the antenna was offset from the CG at the

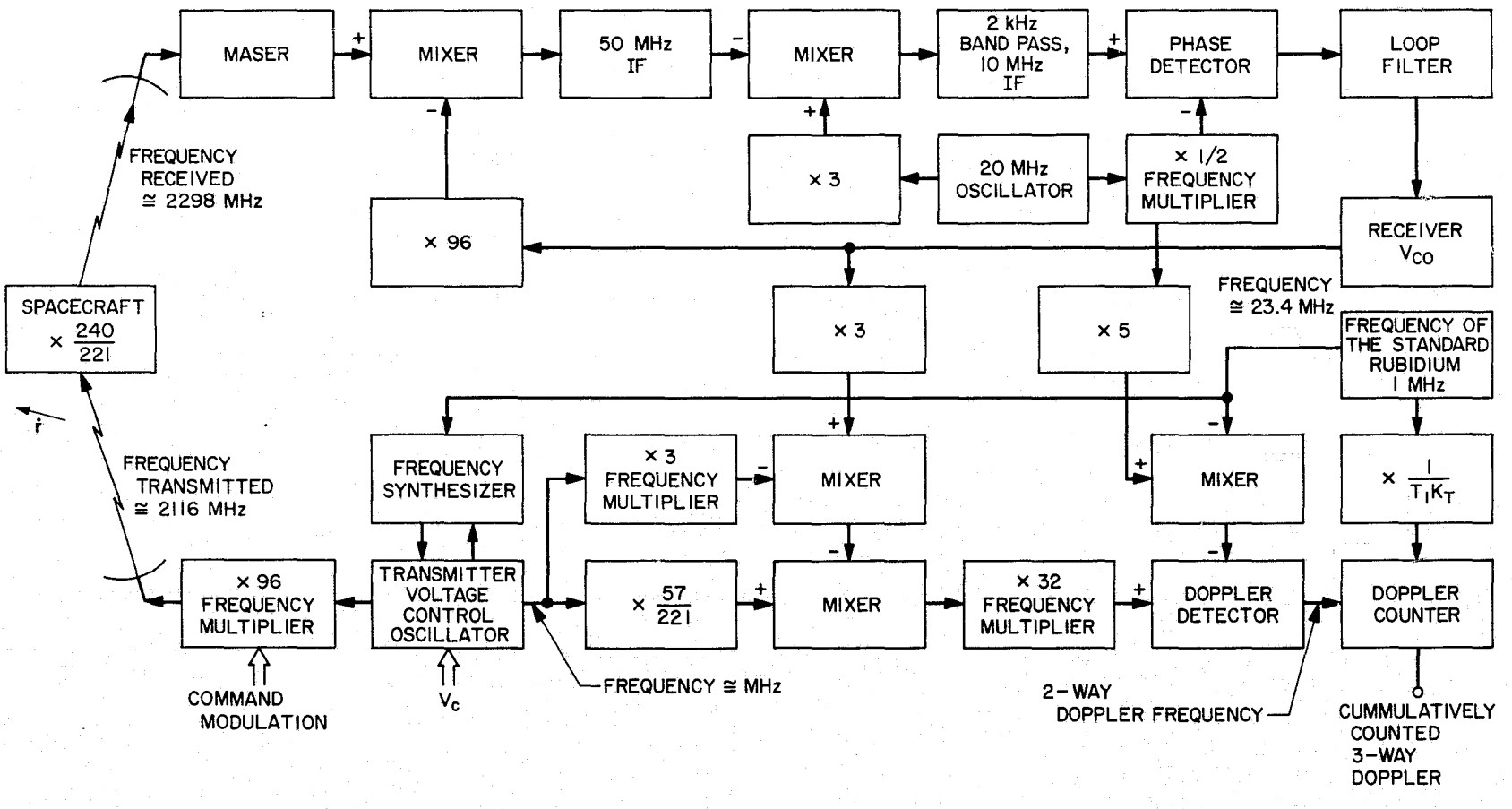

Fig. 1. S-band two-way configuration

spacecraft, a sine curve resulted in the observed −computed doppler residuals with an amplitude of about 0.02 Hz; this may be seen in the DSS 11 residual curve of Fig. 2. In referring to Table 1, it must be remembered that statistics on this portion of the doppler tracking data were corrupted by this effect.

5. Time resolver doppler. Normally, doppler cycles are counted to the nearest cycle at a fixed sample rate under control of the station clock. For this mission, however, DSS 11 utilized a special device for incrementing the sample time to the exact time of zero phase delay (±10) ns between transmitter and receiver. This has the advantage

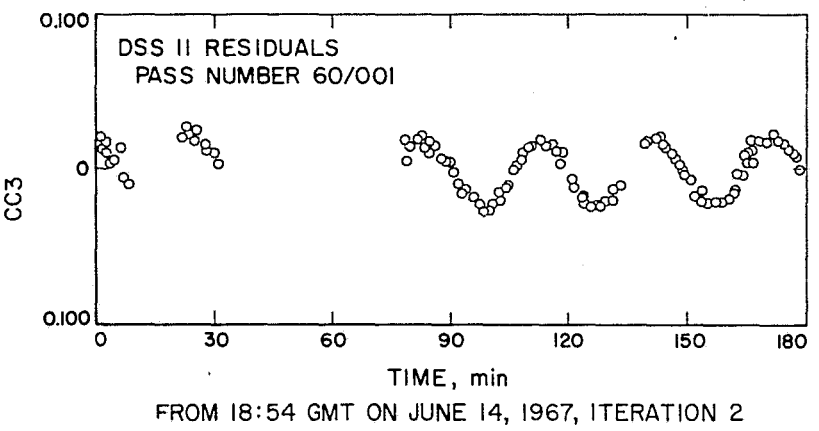

Fig. 2. DSS 11 residuals, pass 60/001

Table 1. DSIF premaneuver tracking data for *Mariner* Venus 67 orbit computations

Orbit identification[a]	DSIF station	Data type	Begin data, date / h:min:s	End data, date / h:min:s	No. of points	Standard deviation, units: deg for HA and DEC; Hz for CC3	Rms, units: deg for HA and DEC; Hz for CC3	Mean error, units: deg for HA and DEC; Hz for CC3	Remarks
PROR XA	51	HA	6/14 06:29:32	6/14 06:50:42	24	0.00887	0.00899	−0.00141	Biased DSS 51 angles
PROR XA	51	DEC	6/14 06:29:32	6/14 06:50:42	24	0.0538	0.0538	−0.00178	
ICEV XA	41	HA	6/14 06:53:42	6/14 08:20:02	87	0.0515	0.0852	0.0678	
ICEV XA	41	DEC	6/14 06:53:42	6/14 08:20:02	87	0.0328	0.161	−0.157	
ICEV XA	42	HA	6/14 06:58:42	6/14 08:19:02	42	0.247	0.644	−0.594	Incorrectly computed DSS 42 angles
ICEV XA	42	DEC	6/14 06:58:42	6/14 08:19:02	42	0.303	0.811	0.752	
ICEV XA	51	HA	6/14 07:04:02	6/14 08:18:02	97	0.00719	0.0672	0.0669	
ICEV XA	51	DEC	6/14 07:04:02	6/14 08:18:02	97	0.0405	0.203	−0.199	
ICEV XA	51	CC3	6/14 07:03:57	6/14 08:17:32	94 *U*	0.310	0.317	0.0671	
ICEV YA	42	CC3	6/14 08:36:32	6/14 08:56:32	14 *U*	No summary printed			
ICEV YA	51	HA	6/14 07:04:12	6/14 09:00:02	186	0.00659	0.00696	0.00223	
ICEV YA	51	DEC	6/14 07:04:12	6/14 09:00:02	186	0.00459	0.00464	0.0007	
ICEV YA	51	CC3	6/14 07:03:57	6/14 08:29:32	162 *U*	0.103	0.107	−0.0296	
ICEV XB	42	CC3	6/14 08:34:32	6/14 09:29:32	54 *U*	0.0125	0.0131	0.00387	
ICEV XB	51	CC3	6/14 07:03:57	6/14 10:45:32	132 *U*	0.0303	0.0308	−0.00564	
PROR YA	41	HA	6/14 07:04:12	6/14 07:27:02	27	0.0554	0.206	0.198	
PROR YA	41	DEC	6/14 07:04:12	6/14 07:27:02	27	0.156	0.331	−0.291	
PROR YA	42	HA	6/14 07:10:52	6/14 07:26:02	55	0.0242	0.453	−0.452	Incorrectly computed DSS 42 angles
PROR YA	42	DEC	6/14 07:10:52	6/14 07:26:02	55	0.109	0.612	0.602	
PROR YA	51	HA	6/14 07:04:12	6/14 07:16:51	79	0.280	0.179	0.177	
PROR YA	51	DEC	6/14 07:04:12	6/14 07:16:51	79	0.517	0.367	−0.364	
PROR YA	51	CC3	6/14 07:04:17	6/14 07:16:48	77 *U*	0.290	0.291	0.142	
MDPR YA	42	CC3	6/14 08:36:32	6/14 08:56:32	19 *U*	0.00726	0.00727	0.000514	
MDPR YA	51	CC3	6/14 07:04:17	6/14 08:29:32	152 *U*	0.0574	0.0574	−0.000437	
PREL YA	42	CC3	6/14 08:36:32	6/14 08:56:32	19 *U*	0.00680	0.0136	0.000185	
PREL YA	51	CC3	6/14 07:04:17	6/14 08:29:32	151 *U*	0.0562	0.0567	−0.00708	
PREL YB	42	CC3	6/14 08:36:32	6/14 09:29:32	48 *U*	0.0133	0.0133	0.000346	
PREL YB	51	CC3	6/14 07:03:57	6/14 13:20:32	228 *U*	0.0325	0.0325	−0.00135	
PREL YB	61	CC3	6/14 11:40:32	6/14 12:32:32	41 *U*	0.0161	0.0162	0.00164	
DACO YA	51	CC3	6/14 08:36:32	6/14 17:40:32	306 *U*	0.0297	0.0297	−0.00123	
DACO YA	61	CC3	6/14 11:40:32	6/14 17:09:32	149 *U*	0.0163	0.0163	0.000934	
GLPR YA	42	CC3	6/14 08:36:32	6/14 09:29:32	48 *U*	0.0131	0.0131	−0.000	

[a]The orbit determination designations are represented as follows: *PROR*, predict orbit; *ICEV*, initial condition evaluation orbit; *MDPR*, Madrid predicts orbit; *PREL*, preliminary evaluation orbit; *GLPR*, Goldstone predicts orbit; *DACO*, data consistency orbit; *NOMA*, nominal maneuver orbit; *LAMC*, last maneuver calculation orbit; *LAPM*, last premaneuver orbit; *POST*, post maneuver orbit.

Table 1 (contd)

Orbit identification[a]	DSIF station	Data type	Begin data, date / h:min:s	End data, date / h:min:s	No. of points	Standard deviation, units: deg for HA and DEC; Hz for CC3	Rms, units: deg for HA and DEC; Hz for CC3	Mean error, units: deg for HA and DEC; Hz for CC3	Remarks
GLPR YA	51	CC3	6/14 07:03:57	6/14 18:25:32	379 *U*	0.0459	0.0460	−0.00190	
GLPR YA	61	CC3	6/14 11:40:32	6/14 17:09:32	149 *U*	0.0164	0.0164	0.0008	
NOMA 5	11	60001	6/14 18:54:32	6/15 01:53:02	168 *U*, 19 C	0.0141	0.0141	−0.00004	All data
NOMA 5	11	60002	6/15 19:38:02	6/15 21:37:02	13 C	0.00212	0.00323	−0.00244	
NOMA 5	11	60003	6/16 19:39:02	6/17 01:21:32	51 C	0.00227	0.00287	−0.00175	
NOMA 5	11	60004	6/17 19:07:02	6/17 21:29:32	5 C, 87 *U*	0.00277	0.00277	0.00004	
NOMA 5	42	60001	6/14 08:36:32	6/14 09:29:32	48 *U*	0.0135	0.0138	−0.00248	
NOMA 5	42	60002	6/15 02:10:02	6/15 11:13:02	57 C	0.00214	0.00232	0.000917	
NOMA 5	42	60003	6/16 00:30:02	6/16 11:11:02	61 C	0.00355	0.00404	−0.00194	
NOMA 5	42	60004	6/17 01:41:02	6/17 11:12:02	26 C	0.00250	0.00383	−0.00291	
NOMA 5	51	10001	6/14 07:04:22	6/14 07:04:22	1 *U*	0.000	0.0371	0.0371	
NOMA 5	51	05001	6/14 07:13:11	6/14 07:18:11	6 *U*	0.00811	0.00827	−0.00163	
NOMA 5	51	60001	6/14 07:20:32	6/14 18:25:32	273 *U*	0.0158	0.0159	−0.00155	
NOMA 5	61	60001	6/14 11:40:32	6/14 17:09:32	149 *U*	0.0157	0.0159	−0.00259	
NOMA 5	61	60002	6/15 11:25:32	6/15 19:22:32	58 C	0.00551	0.00572	0.00153	
NOMA 5	61	60003	6/16 11:28:32	6/17 12:03:32	47 C	0.00481	0.00481	0.00007	
NOMA 5	61	60004	6/17 12:14:02	6/17 18:34:02	25 C	0.00237	0.00304	−0.00191	
NOMA 6	11	60001	6/14 22:55:02	6/15 01:53:02	19 C	0.00372	0.00376	−0.00056	Post roll
NOMA 6	11	60002	6/15 19:38:02	6/15 21:42:28	14 C	0.00175	0.00286	−0.00227	
NOMA 6	11	10002	6/15 21:43:17	6/15 21:44:02	2 *U*	0.00171	0.00173	−0.0002	
NOMA 6	11	60003	6/16 19:39:02	6/17 01:21:32	51 C	0.00248	0.00248	0.00005	
NOMA 6	11	60004	6/17 19:10:02	6/18 02:08:32	14 C, 271 *U*	0.00258	0.00259	0.000149	
NOMA 6	11	60005	6/18 18:51:32	6/18 19:04:32	14 *U*	0.00208	0.0158	0.0157	
NOMA 6	42	60002	6/15 02:10:02	6/15 11:13:02	57 C	0.00285	0.00287	−0.000291	
NOMA 6	42	60003	6/16 00:30:02	6/16 11:11:02	61 C	0.00329	0.00331	−0.000408	
NOMA 6	42	60004	6/17 01:41:02	6/17 11:12:02	26 C	0.00221	0.00274	−0.00162	
NOMA 6	42	60005	6/18 02:19:32	6/18 11:12:32	443 *U*	0.00443	0.00444	0.000312	
NOMA 6	61	60002	6/15 11:25:32	6/15 19:22:32	58 C	0.00522	0.00543	0.00148	
NOMA 6	61	60003	6/16 11:28:32	6/17 12:03:32	47 C	0.00500	0.00505	0.000758	
NOMA 6	61	60004	6/17 12:14:02	6/17 18:34:02	42 C	0.00232	0.00274	−0.00145	
NOMA 6	61	60005	6/18 11:52:32	6/18 18:36:32	193 *U*	0.00805	0.00821	0.00163	
NOMA 7	11	60001	6/14 18:54:32	6/15 01:53:02	168 *U*, 19 C	0.0141	0.0141	0.000324	All data
NOMA 7	11	60002	6/15 19:38:02	6/15 21:37:02	13 C	0.00192	0.00329	−0.00267	
NOMA 7	11	60003	6/16 19:39:02	6/17 01:21:32	51 C	0.00227	0.00252	−0.00109	
NOMA 7	11	60004	6/17 19:10:02	6/18 02:07:02	44 C	0.00209	0.00209	0.00010	
NOMA 7	11	60005	6/18 18:56:02	6/18 19:03:02	2 C	0.000732	0.0144	0.000208	
NOMA 7	42	60001	6/14 08:36:32	6/14 09:29:32	48 *U*	0.0137	0.0139	−0.00246	
NOMA 7	42	60002	6/15 02:10:02	6/15 11:13:02	57 C	0.00209	0.00233	0.00104	
NOMA 7	42	60003	6/16 00:30:02	6/16 11:11:02	61 C	0.00364	0.00402	−0.00170	
NOMA 7	42	60004	6/17 01:41:02	6/17 11:12:02	26 C	0.00246	0.00363	−0.00267	
NOMA 7	42	60005	6/18 02:24:02	6/18 11:08:02	53 C	0.00201	0.00202	0.00006	

Table 1 (contd)

Orbit identification[a]	DSIF station	Data type	Begin data, date / h:min:s	End data, date / h:min:s	No. of points	Standard deviation, units: deg for HA and DEC; Hz for CC3	Rms, units: deg for HA and DEC; Hz for CC3	Mean error, units: deg for HA and DEC; Hz for CC3	Remarks
DACO YB	11	CC3	6/14 18:54:32	6/14 21:25:32	87 U	0.0206	0.0244	0.0132	
DACO YB	42	CC3	6/14 08:36:32	6/14 09:29:32	48 U	0.0131	0.0154	−0.00795	
DACO YB	51	CC3	6/14 07:03:57	6/14 18:25:32	379 U	0.0464	0.0465	−0.00275	
DACO YB	61	CC3	6/14 11:40:32	6/14 17:09:32	149 U	0.0193	0.0194	0.00113	
NOMA 1	11	CC3	6/14 18:54:32	6/15 01:53:32	341 U	0.0197	0.0204	−0.00507	
NOMA 1	42	CC3	6/14 08:36:32	6/15 11:13:32	553 U	0.00978	0.00979	−0.000441	
NOMA 1	51	CC3	6/14 07:03:57	6/14 18:25:32	378 U	0.0468	0.0470	−0.00200	
NOMA 1	61	CC3	6/14 11:40:32	6/15 18:30:32	538 U	0.0114	0.0118	0.00286	
NOMA 2	11	60001	6/14 22:30:32	6/15 01:53:32	191 U	0.00855	0.0216	−0.0198	Estimated station locations solar pressure and AU
NOMA 2	11	60002	6/15 19:33:32	6/15 21:42:28	116 U	0.00700	0.0210	−0.0198	
NOMA 2	11	10002	6/15 21:42:58	6/15 21:44:07	7 U	0.0240	0.0273	−0.0130	
NOMA 2	11	60003	6/16 19:34:32	6/16 20:25:32	52 U	0.00804	0.0230	−0.0215	
NOMA 2	42	60002	6/15 02:05:32	6/15 11:13:32	505 U	0.00441	0.0205	−0.0200	Post roll
NOMA 2	42	60003	6/16 00:25:32	6/16 11:13:32	515 U	0.00530	0.0229	−0.0223	
NOMA 2	61	60002	6/15 11:25:32	6/15 19:23:32	428 U	0.00739	0.0210	−0.0197	
NOMA 2	61	60003	6/16 11:28:32	6/16 19:13:32	371 U	0.00839	0.0244	−0.0229	
NOMA 3	11	60001	6/14 18:54:32	6/15 01:53:02	168 U, 19 C	0.0157	0.0157	0.000473	All data
NOMA 3	11	60002	6/15 19:38:02	6/16 21:37:02	13 C	0.00232	0.00285	−0.00165	
NOMA 3	11	60003	6/16 19:39:02	6/16 22:50:32	6 C, 103 U	0.00757	0.00816	−0.00305	
NOMA 3	42	60001	6/14 08:36:32	6/14 09:29:32	48 U	0.0135	0.0138	−0.00252	
NOMA 3	42	60002	6/15 02:10:02	6/15 11:13:02	57 C	0.00217	0.00232	0.000822	
NOMA 3	42	60003	6/16 00:30:02	6/16 11:11:02	61 C	0.00359	0.00445	−0.00263	
NOMA 3	51	10001	6/14 07:04:22	6/14 07:04:22	1 U	0.000	0.0371	0.0371	
NOMA 3	51	05001	6/14 07:11:16	6/14 07:18:11	7 U	0.00742	0.00755	−0.00140	
NOMA 3	51	60001	6/14 07:20:32	6/14 18:25:32	273 U	0.0158	0.0158	−0.00164	
NOMA 3	61	60001	6/14 11:40:32	6/14 17:09:32	149 U	0.0159	0.0161	−0.00275	
NOMA 3	61	60002	6/15 11:25:32	6/15 19:22:32	58 C	0.00541	0.00551	0.00104	
NOMA 3	61	60003	6/16 11:28:32	6/16 19:13:32	46 C	0.00488	0.00495	−0.000860	
NOMA 4	11	60001	6/14 22:30:32	6/15 01:53:02	39 C	0.00876	0.00905	−0.00228	Post roll
NOMA 4	11	6002	6/15 19:38:02	6/15 21:37:02	13 C	0.00165	0.00200	−0.00113	
NOMA 4	11	6003	6/16 19:39:02	6/17 01:23:32	6 C, 233 U	0.00234	0.00239	0.000468	
NOMA 4	11	6004	6/17 19:05:32	6/17 19:52:32	37 U	0.00366	0.00526	0.00377	
NOMA 4	42	60002	6/15 02:10:02	6/15 11:13:02	57 C	0.00278	0.00278	0.0000685	
NOMA 4	42	60003	6/16 00:30:02	6/16 11:11:02	61 C	0.00341	0.00342	−0.000240	
NOMA 4	42	60004	6/17 01:36:32	6/17 11:12:32	222 U	0.00460	0.00483	−0.00146	
NOMA 4	61	60001	6/15 11:25:32	6/15 19:22:32	58 C	0.00511	0.00537	0.00166	
NOMA 4	61	60002	6/16 11:28:32	6/16 19:13:32	47 C	0.00501	0.00510	0.000925	
NOMA 4	61	60003	6/17 12:01:32	6/17 18:36:32	207 U	0.00749	0.00751	−0.000646	

Table 1 (contd)

Orbit identification[a]	DSIF station	Data type	Begin data, date / h:min:s	End data, date / h:min:s	No. of points	Standard deviation, units: deg for HA and DEC; Hz for CC3	Rms, units: deg for HA and DEC; Hz for CC3	Mean error, units: deg for HA and DEC; Hz for CC3	Remarks
NOMA 7	51	10001	6/14 07:04:22	6/14 07:04:22	1 *U*	0.000	0.0371	0.0371	
NOMA 7	51	05001	6/14 07:13:11	6/14 07:18:11	6 *U*	0.00826	0.00857	−0.00228	
NOMA 7	51	60001	6/14 07:20:32	6/14 18:25:32	273 *U*	0.0158	0.0159	−0.00116	
NOMA 7	61	60001	6/14 11:40:32	6/14 17:09:32	149 *U*	0.0157	0.0159	−0.00234	
NOMA 7	61	60002	6/15 11:25:32	6/15 19:22:32	58 C	0.00570	0.00595	0.00168	
NOMA 7	61	60003	6/16 11:28:32	6/17 12:03:32	47 C	0.00493	0.00493	0.000135	
NOMA 7	61	60004	6/17 12:14:02	6/17 18:34:02	42 C	0.00206	0.00254	−0.00149	
NOMA 7	61	60005	6/18 11:57:02	6/18 18:33:02	23 C	0.00300	0.00354	0.00189	
LAMC 1	11	60001	6/14 22:55:02	6/15 01:53:02	19 C	0.00403	0.00443	−0.00185	Post roll
LAMC 1	11	60002	6/15 19:38:02	6/15 21:37:02	13 C	0.00161	0.00190	−0.00101	
LAMC 1	11	60003	6/16 19:39:02	6/17 01:21:32	51 C	0.00248	0.00292	0.00154	
LAMC 1	11	60004	6/17 19:10:02	6/18 02:01:02	44 C	0.00167	0.00170	0.000344	
LAMC 1	11	60005	6/18 18:56:02	6/18 22:31:32	2 C, 182 *U*	0.00347	0.00351	−0.000539	
LAMC 1	42	60002	6/15 02:10:02	6/15 11:13:02	57 C	0.00283	0.00283	0.000188	
LAMC 1	42	60003	6/16 00:30:02	6/16 11:11:02	61 C	0.00347	0.00358	0.000856	
LAMC 1	42	60004	6/17 01:41:02	6/17 11:12:02	26 C	0.00272	0.00327	−0.00182	
LAMC 1	42	60005	6/18 02:24:02	6/18 11:08:02	53 C	0.00239	0.00259	−0.00100	
LAMC 1	61	60002	6/15 11:25:32	6/15 19:22:32	58 C	0.00529	0.00585	0.00248	
LAMC 1	61	60003	6/16 11:28:32	6/17 12:03:32	47 C	0.00493	0.00518	0.00161	
LAMC 1	61	60004	6/17 12:14:02	6/17 18:34:02	42 C	0.00225	0.00281	−0.00169	
LAMC 1	61	60005	6/18 11:57:02	6/18 18:33:02	23 C	0.00287	0.00315	−0.00132	
LAPM	11	60001	6/14 22:00:32	6/15 01:53:02	36 *U*, 19 C	0.00789	0.00794	−0.000897	Includes some roll data from DSS 11
LAPM	11	60002	6/15 19:38:02	6/15 21:37:02	13 C	0.00164	0.00164	−0.000338	
LAPM	11	60003	6/16 19:39:02	6/17 01:21:32	51 C	0.00258	0.00305	0.00162	
LAPM	11	60004	6/17 19:10:02	6/18 02:07:02	44 C	0.00162	0.00169	−0.000488	
LAPM	11	60005	6/18 18:56:02	6/19 02:53:32	23 C, 189 *U*	0.00292	0.00304	0.000849	
LAPM	11	60006	6/19 18:53:32	6/19 22:17:32	198 *U*	0.00396	0.00398	0.000343	
LAPM	42	60002	6/15 02:10:02	6/15 11:13:02	57 C	0.00277	0.00301	0.00117	
LAPM	42	60003	6/16 00:30:02	6/16 11:11:02	69 C	0.00331	0.00356	0.00130	
LAPM	42	60004	6/17 01:41:02	6/17 11:12:02	59 C	0.00261	0.00286	−0.00115	
LAPM	42	60005	6/18 02:24:02	6/18 11:08:02	53 C	0.00269	0.00367	−0.00249	
LAPM	42	60006	6/19 01:05:32	6/19 11:03:32	412 *U*	0.00463	0.00475	−0.00105	
LAPM	42	60006	6/19 11:04:32	6/19 11:11:32	8 *U*	0.00346	0.00117	0.0112	
LAPM	61	60002	6/15 11:25:32	6/15 19:14:32	55 C	0.00389	0.00453	0.00232	
LAPM	61	60003	6/16 11:28:32	6/17 12:03:32	46 C	0.00403	0.00413	0.000934	
LAPM	61	60004	6/17 12:14:02	6/17 18:34:02	42 C	0.00216	0.00360	−0.00288	
LAPM	61	60005	6/18 11:57:02	6/18 18:33:02	29 C	0.00214	0.00398	−0.00335	
LAPM	61	60006	6/19 11:31:32	6/19 18:36:32	389 *U*	0.00839	0.00851	−0.00146	

of eliminating counter truncation error. It is shown in Table 1, for example, that with this system, DSS 11 doppler cycles reached a standard deviation of 0.00234 Hz for 6 doppler points lasting 600 s and 233 doppler points lasting 60 s in pass 3 of orbit *NOMA 4*. This compares favorably with pass 4 of DSS 42 doppler cycles in the same orbit, for which the standard deviation was 0.00460 Hz for 222 sample doppler points lasting 60 s. Only DSS 11 used a time resolver device in the premaneuver phase of the mission.

B. Premaneuver Orbit Determination Results

1. Orbit state vector. The JPL Single Precision Orbit Determination Program (SPODP) (Ref. 2) utilizes a weighted least squares technique for estimating up to 20 parameters and forming up to a 20 by 20 covariance matrix. The first 12 premaneuver orbits, through 1938 GMT, June 15, estimated only the geocentric equatorial position and velocity of the probe, with a corresponding 6 by 6 covariance matrix. Of these early orbits, *PROR XA*, *PROR YA*, and *ICEV XA* were degraded by biased angles, as previously mentioned. Table 2 shows the state vector solutions and associated standard deviations from the premaneuver orbits. Note that two epochs were used for starting the trajectory integration. Orbits using an epoch of $06^h\,24^m\,37^s.100$ include data during the controlled roll period, whereas orbits with an epoch of $22^h\,00^m\,00^s.000$ did not include this data in the least squares fit.

2. Target point. The SPODP has the capability of mapping the covariance matrix from epoch to the target planet at the time of closest approach. These target parameters are expressed in the B plane system (see Appendix A). Target parameters and statistics are tabulated for each orbit in Table 3. The parameter t is the time of flight linearized along the incoming asymptote of the planet-centered flight hyperbola (Ref. 1). The semiminor axis is SMIA and SMAA is the semimajor axis of the 1σ dispersion ellipse of the orbit determination uncertainty in the B plane. The angle θ gives the orientation of the SMAA, measured counterclockwise from T. The vector **S** lies along the incoming asymptote and is normal to the R–T plane. The target points of each orbit, except for *PROR XA*, and *PROR YA*, are plotted in the **R**–**T** plane in Figs. 3 and 4.

3. Solar radiation pressure. The perturbative spacecraft acceleration resulting from solar radiation pressure is modeled by:

$$\Delta\ddot{R} = \frac{kA}{mR^2}(1 + \gamma_B)$$

where

R is the probe–sun distance, in km

$k = 1.031 \times 10^8$, a solar radiation constant

A is the spacecraft effective area normal to R, nominally 6.60519 m^2

m is the spacecraft mass, nominally 245.71 kg

γ_B is the reflectivity coefficient of the spacecraft, nominally 0.40123054

The premaneuver and postmaneuver solutions for γ_B are compared in Table 4. It is apparent that the span of tracking data available in the premaneuver solution is not adequate for a strong solution, as the standard deviation has not significantly improved over the *a priori* standard deviation assigned to the nominal value. By contrast, the postmaneuver solution contains nearly a month's tracking data, including ranging data. Moreover, the ranging data are particularly effective in this type of solution.

4. Station locations. The SPODP is capable of estimating tracking station locations to a high degree of precision where sufficient doppler tracking data have been obtained. In the premaneuver phase of the mission, solutions were obtained for the locations of DSS 11, 42, and 61. The stations are tabulated and compared with nominal values and postmaneuver solutions in Table 4. The geocentric radius of the station is r, ϕ is the geocentric latitude, and λ is the longitude. The systematic differences in longitude of about 0.0003 deg between the premaneuver and postmaneuver solutions are probably caused by the two orbits being gravitationally tied to earth and the sun, where neither body is a strong longitude source. An insignificant error at target is produced, however. The cause of the systematic differences in r cos ϕ, the distance from earth's spin axis, is unknown; however, these differences are also very small (4.3 to 8.8 m).

5. Mass of earth solution. The five days of premidcourse tracking data provided the opportunity for obtaining a least squares estimate of the gravitational mass of earth ($GM_\oplus$). This was done for *Mariner V*, yielding a value of $GM_\oplus = 398601.49 \pm 0.4$ km^3/s^2. This compares

Table 2. Initial conditions of *Mariner* Venus 67 premaneuver orbits

Orbit identification	Epoch, GMT, June 14, 1967, h:min:s	Geocentric space: fixed position			Geocentric space: fixed velocity			Uncertainties, position, 1σ			Uncertainties, velocity, 1σ		
		X, km	Y, km	Z, km	DX, km/s	DY, km/s	DZ, km/s	σ X, m	σ Y, m	σ Z, m	σ DX, m/s	σ DY, m/s	σ DZ, m/s
PROR XA	06:24:37.100	6416.6756	−1230.8562	−731.91162	1.6219889	9.7114220	−5.7422701	21435.0	45206.0	81177.0	23.42	30.59	38.50
PROR YA	06:24:37.100	6430.7816	−1160.2529	−533.85299	1.7051417	9.6648580	−5.7670747	9743.4	13897.0	5453.8	18.64	51.66	22.34
ICEV XA	06:24:37.100	6435.0075	−1166.9439	−523.24137	1.6985057	9.7519772	−5.6694543	2938.0	7898.0	14923.0	9.853	6.898	7.800
ICEV YA	06:24:37.100	6437.6896	−1191.5500	−534.17180	1.7101299	9.7199947	−5.7073967	3147.0	9568.0	18419.0	11.75	10.15	12.09
ICEV XB	06:24:37.100	6439.0375	−1187.4443	−537.59330	1.7017812	9.7221273	−5.7049827	1056.8	3563.0	3497.0	0.9456	6.728	9.384
MDPR YA	06:24:37.100	6438.9529	−1186.4890	−537.72921	1.7007203	9.7219321	−5.7060349	2489.7	15015.0	7689.9	11.73	19.15	28.60
PREL YA	06:24:37.100	6438.9480	−1186.5558	−537.74087	1.7007838	9.7218896	−5.7060745	2489.5	15026.0	7672.8	11.73	19.16	28.61
PREL YB	06:24:37.100	6439.0166	−1187.2355	−537.37487	1.7017861	9.7230284	−5.7040332	761.3	518.5	629.2	0.6666	1.446	31.13
DACO YA	06:24:37.100	6439.2577	−1187.2355	−537.37486	1.7017861	9.7225636	−5.7043627	518.0	397.5	693.7	0.5347	0.7014	2.051
GLPR YA	06:24:37.100	6439.2120	−1187.3930	−537.00825	1.7020798	9.7229566	−5.7032949	1196.3	865.0	1505.0	1.046	1.612	4.645
DACO YB	06:24:37.100	6438.9782	−1187.1913	−537.40764	1.7017661	9.7224742	−5.7045916	287.9	373.7	428.2	0.3509	0.7723	1.055
NOMA 1	06:24:37.100	6439.0098	−1187.2602	−537.51488	1.7017203	9.7222863	−5.7048408	68.76	108.5	130.3	0.0902	0.2164	0.2620
NOMA 2	06:24:37.100	6438.3870	−1188.8097	−536.31939	1.7035321	9.7224200	−5.7047653	885.7	1526.7	922.5	1.623	0.5181	0.6515
NOMA 3	06:24:37.100	6439.0485	−1187.3274	−537.50841	1.7017447	9.7222307	−5.7048470	30.23	46.54	33.63	0.0472	0.0529	0.0880
NOMA 4	22:00:00.000	−162050.57	155937.37	−56185.187	−2.6362289	2.1369942	−0.69217914	1817.0	2135.0	2897.0	0.0203	0.0206	0.0433
NOMA 5	06:24:37.100	6439.0489	−1187.3289	−537.50879	1.7017450	9.7222283	−5.7048498	75.56	96.44	90.70	0.0803	0.1610	0.2012
NOMA 6	22:00:00.000	−162050.61	155937.28	−56185.251	−2.6362273	2.1369958	−0.69218034	1611.0	1939.0	2779.0	0.0156	0.0170	0.0395
NOMA 7	06:24:37.100	6439.0505	−1187.3315	−537.51215	1.7017435	9.7222240	−5.7048541	74.91	94.08	88.51	0.0788	0.1568	0.1951
LAMC	22:00:00.000	−162050.21	155937.31	−56185.189	−2.6362305	2.1369918	−0.069218217	1611.0	1920.0	2772.0	0.0155	0.0168	0.0394
LAPM	22:00:00.000	−162050.22	155937.32	−56185.164	−2.6362309	2.1369915	−0.69218127	1537.0	1795.0	2706.0	0.0143	0.0154	0.0397

Table 3. Target parameters of *Mariner* Venus 67 premaneuver orbits

Orbit identification	Time on computer (GMT) day:h:min:s	Target statistics											Type solution	Encounter time date:h:min:s
		B, km	$\mathbf{B} \cdot \mathbf{T}$, km	$\mathbf{B} \cdot \mathbf{R}$, km	t_L, days	SMIA, km	SMAA, km	θ, deg	$\sigma\, \mathbf{B} \cdot \mathbf{R}$, km	$\sigma\, \mathbf{B} \cdot \mathbf{T}$, km	σ t, s	σ S, km		
PROR YA	165:08:42:00	553321.70	452429.88	−318546.85	123.09	24123.0	209921.0	27.15	98185.0	187114.0	106300.0	350763.0	6 × 6	10/15 15:57:36.641
PROR XA	07:41:00	8608.9830	722810.36	467644.18	139.28	10351.4	3081917.0	162.72	915498.0	2942819.0	1675672.0	4628031.0	6 × 6	11/01 01:58:43.431
ICEV XA	08:56:00	92462.993	63398.130	−67305.878	126.7	6991.0	26896.0	46.01	19951.0	19344.0	25658.0	27790.0	6 × 6	11/01 02:27:56.082
ICEV YA	10:08:00	103665.06	86031.496	−57836.193	126.8	7445.0	29746.0	46.79	22274.0	21075.0	28906.0	88905.0	6 × 6	11/01 06:32:28.629
ICEV XB	11:49:00	104715.86	81712.672	−65486.255	126.7	2288.6	3398.8	178.63	2289.4	3398.2	2811.4	8670.3	6 × 6	11/01 03:50:01.188
MDPR YA	12:38:00	103031.03	79941.151	−64998.496	126.7	8585.9	21500.0	162.70	10395.0	20686.0	12917.0	39834.0	6 × 6	11/01 03:57:40.176
PREL YA	14:01:00	103100.66	80043.522	−64982.922	126.7	8583.7	21522.0	162.75	10389.0	20711.0	12899.0	39778.0	6 × 6	11/01 03:58:06.020
PREL YB	14:36:00	104640.21	81534.246	−65587.639	126.7	579.1	1902.0	73.68	1832.6	771.1	2246.0	6928.0	6 × 6	11/01 03:47:45.320
DACO YA	18:51:00	104922.83	81680.620	−65856.484	126.7	183.0	564.8	68.67	530.3	267.0	604.9	1865.6	6 × 6	11/01 03:43:10.051
GLPR YA	19:44:00	104885.54	81661.791	−65820.505	126.7	377.8	1347.0	70.77	1278.6	569.4	1465.0	4518.0	6 × 6	11/01 03:43:46.342
DACO YB	165:22:18:00	104511.22	81482.685	−65445.908	126.7	317.5	406.9	39.62	356.5	373.1	431.8	1131.5	6 × 6	11/01 03:50:20.814
NOMA 1	166:19:38:00	104540.10	81532.887	−65429.504	126.7	81.53	157.0	39.48	118.0	131.8	164.8	508.3	6 × 6	11/01 03:50:41.614
NOMA 2	167:23:07:00	104422.43	81494.182	−65289.677	126.7	171.2	192.3	96.49	192.0	171.5	221.7	683.7	14 × 14	11/01 03:53:54.728
NOMA 3	168:00:33:00	104398.75	81459.476	−65295.114	126.7	142.0	175.8	125.8	165.0	154.4	179.1	552.2	16 × 16	11/01 03:55:00.697
NOMA 4	168:21:54:00	104382.47	81456.020	−65273.405	126.1	131.5	196.3	59.75	182.0	150.6	253.0	780.3	14 × 14	11/01 03:55:27.943
NOMA 5	168:23:00:00	104382.32	81450.270	−65280.322	126.7	75.6	152.7	56.01	133.5	106.0	201.8	622.2	16 × 16	11/01 03:55:27.280
NOMA 6	169:20:36:00	104395.13	81470.350	−65275.753	126.1	178.2	202.8	94.80	202.7	178.4	235.1	724.9	14 × 14	11/01 03:55:19.402
NOMA 7	169:22:20:00	104388.91	81454.418	−65285.684	126.7	155.3	180.8	117.01	175.8	160.9	194.6	600.0	16 × 16	11/01 03:55:18.761
LAMC	169:23:51:00	104447.01	81483.270	−65342.590	126.1	176.7	203.0	94.97	202.9	176.9	235.5	726.1	14 × 14	11/01 03:53:14.919
LAPM	178:22:30:00	104455.70	81486.744	−65352.149	126.1	162.9	194.1	107.71	191.4	166.1	213.1	657.2	16 × 16	11/01 03:53:00.547

Table 4. Preliminary *Mariner* Venus 67 solutions[a]

Parameter	Estimated premidcourse, σ	Nominal postmidcourse, σ	Estimated postmidcourse, σ	Observed postmidcourse and premidcourse, σ
$G\gamma_B$	0.40864007 ±0.0288	0.40123054 ±0.0400	0.37740661 ±0.0112	−0.03123346
$r_{11} \cos \phi_{11}$ (m)	5206331.4 ±6.3	5206353.3 ±20.0	5206327.1 ±3.5	−4.3
λ_{11}, deg	243.15101 ±0.00015	243.15091 ±0.00050	243.15070 ±0.00018	−0.00031
$r_{42} \cos \phi_{42}$ (m)	5205353.5 ±6.0	5205341.6 ±20.0	5205347.3 ±2.7	−6.2
λ_{42}, deg	148.98174 ±0.00015	148.98148 ±0.00050	148.98141 ±0.00018	−0.00033
$r_{61} \cos \phi_{61}$ (m)	4862606.4 ±6.0	4862604.5 ±18.7	4862597.6 ±4.3	−8.8
λ_{61}, deg	355.75146 ±0.00015	355.75113 ±0.00050	355.75114 ±0.00018	−0.00032
x, km[b]	−1194554.1 ±4.8	−1194559 ±3.2	−1194555.9 ±1.3	−1.8
y, km[b]	986076.85 ±5.28	986069.1 ±3.3	986075.40 ±1.11	−1.45
z, km[b]	−319684.35 ±12.06	−3196927 ±8.5	−319682.47 ±4.59	1.88
$\dot{x}$, m/s	−2280.1899 ±0.0065	−2280.931 ±0.13	−2280.8194 ±0.0067	−0.6295
$\dot{y}$, m/s	1849.3605 ±0.0067	1842.512 ±0.13	1842.7422 ±0.0071	−6.6183
$\dot{z}$, m/s	−574.33642 ±0.01668	−588.9205 ±0.13	−588.24114 ±0.00567	−14.90472

[a]For solar radiation pressure, station locations, and geocentric equatorial state vector at $23^h08^m20^s.650$, June 19, 1967.

[b]Estimated positions were obtained independently from the other tabulated results. The midcourse position results use the standard deviations as a priori uncertainties. This is not true in the case of the other parameters because of the corrupting influence of the maneuver.

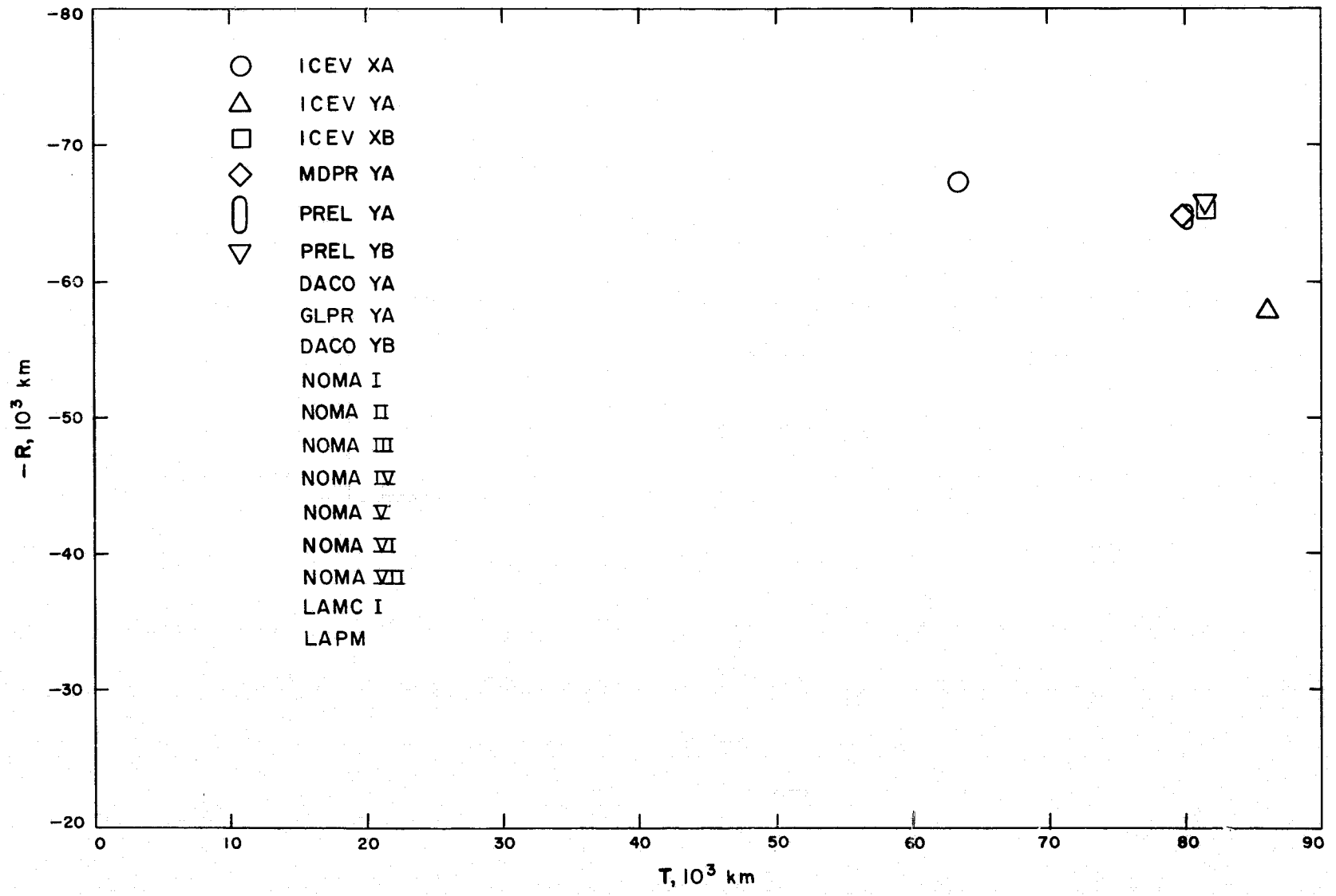

Fig. 3. B-plane target area from premidcourse orbit determination

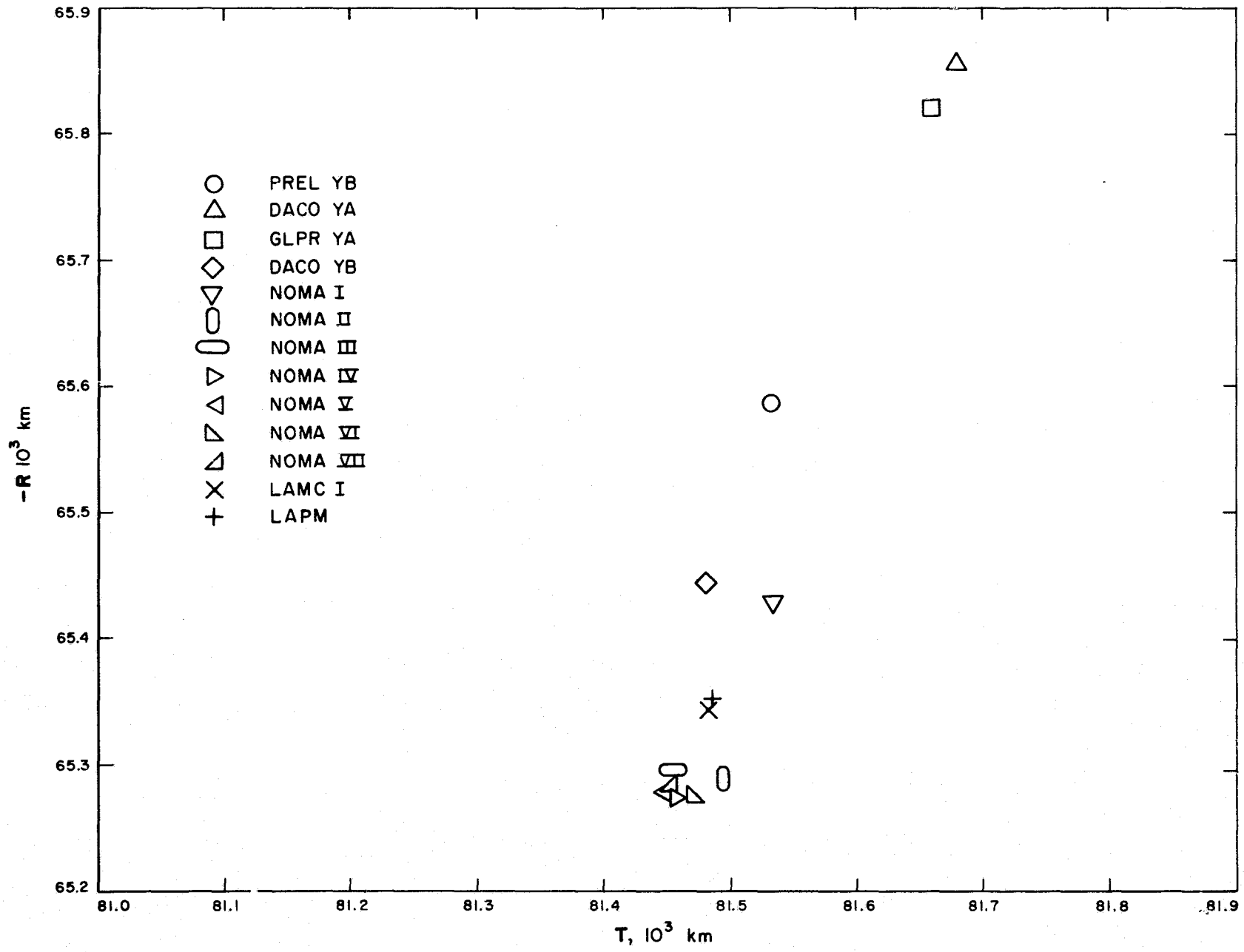

Fig. 4. Detailed view of premidcourse orbit determination target area

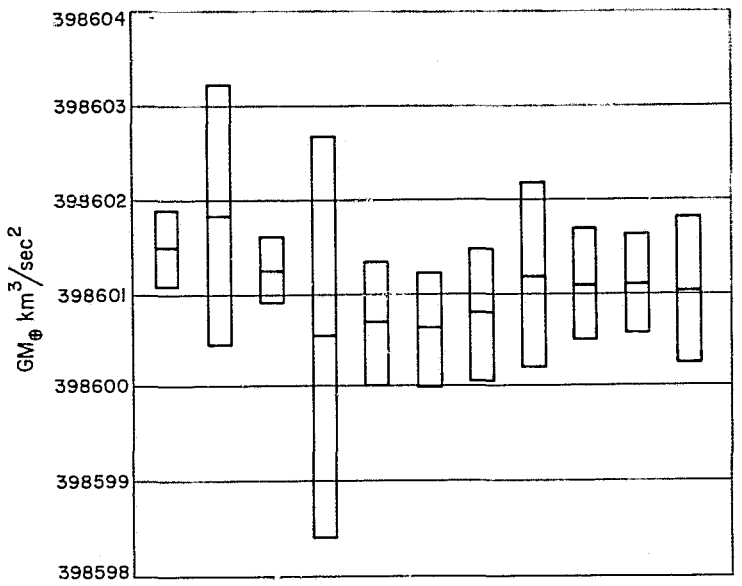

Fig. 5. Gravitational mass of earth estimates from lunar and planetary spacecraft

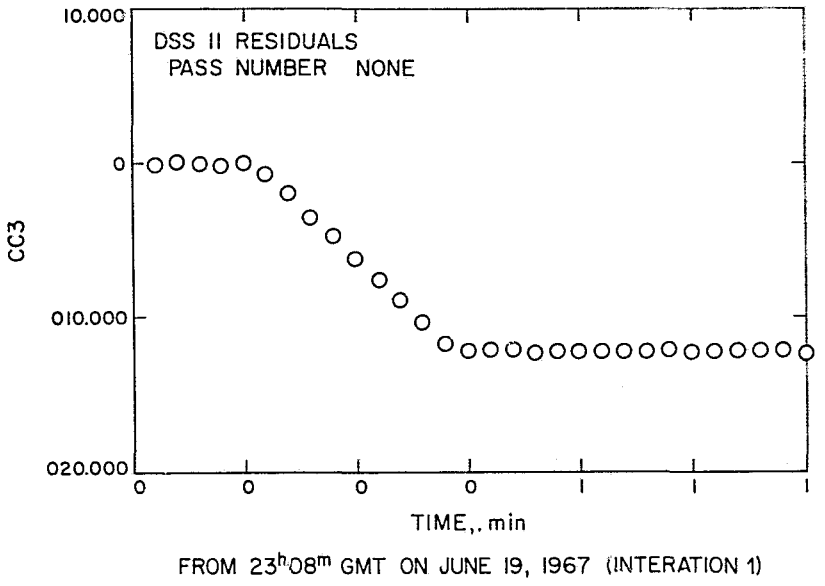

Fig. 6. Two-way doppler residuals during *Mariner V* midcourse maneuver

favorably with the *Ranger*, *Surveyor*, *Lunar Orbiter*, and *Mariner IV* estimates, shown in Fig. 5. The standard deviations overlap in the various missions.

C. Analysis of the *Mariner V* Midcourse Maneuver from Radio Tracking Data

The *Mariner V* spacecraft was injected into its earth-Venus trajectory at $6^h24^m19^s.2$ UT, June 14, 1967. The nominal aiming point was to bring the spacecraft 8,165 km from the center of Venus on October 19, 1967; however, at injection, this aiming point was deliberately biased out to 75,000 km from Venus center to avoid impacting the planet. Hence, a midcourse maneuver was planned at the outset to achieve the nominal aiming point. The spacecraft actually has the capability for two maneuvers, but the second maneuver capability was considered to be in the category of a backup procedure; i.e., to be used only in case primary mission objectives were not achieved by the first maneuver. The second maneuver capability was not, in fact, exercised during the *Mariner* mission.

Subsequent orbit determination after injection showed that the spacecraft would fly just within 76,000 km of Venus center in the absence of a maneuver. Accordingly, a midcourse maneuver was planned and executed at $23^h08^m06^s$ UT, June 19, 1967. The motor burn was planned to last 17.66 s and to impart an additional velocity of 16.1272 m/s to the spacecraft. This was to have put the spacecraft within 8,200 km of Venus center at closest approach on October 19. Telemetry and tracking data proved the duration of the motor burn to have been of approximately nominal duration (see Fig. 6) and the direction of the impulse to have been within ½° of the nominal pointing angle. Yet, orbit determination soon indicated that the probe would fly by Venus at a closest approach distance of not less than 10,000 km from the planet center, and that the velocity imparted to the spacecraft by the motor burn was 15.4123 ±0.0163 m/s rather than the planned 16.1272 ±0.13 m/s. Because primary mission objectives were not jeopardized by the new arrival point, no second maneuver was required. The following analysis shows how orbit determination can be used to analyze the magnitude and direction of the midcourse maneuver.

D. Comparison of Premaneuver and Postmaneuver Velocities at Midcourse Epoch

The orbit determination procedure used involves a weighted least squares fit of approximately 1,200 points of 600-s count-interval two-way coherent doppler tracking data in the 5 days from injection to midcourse maneuver. In the 28-day period from midcourse to July 17, approximately 2,000 points of 600-s doppler data and 900 points of ranging data were included in the least squares fit. Table 4 shows the premidcourse least squares solution for the spacecraft velocity at $23^h08^m20^s.650$ UT, June 19, if no maneuver had been performed. Actually, this time occurs, during the motor burn interval; however, only premidcourse tracking data were used in the solution. This solution is labeled *Estimated premidcourse* in Table 1. The *Nominal postmidcourse* column indicates the velocity which would have been achieved at this time had a nominal maneuver been executed before. The *Estimated postmidcourse*

column tabulates the least squares solution for velocity based on postmidcourse tracking data to July 17 (SPODP cruise run 16). This is considered an adequate data arc for the solution; a longer arc allows the corrupting effect of small forces in the orbit fit.

It is now possible to compare the nominal maneuver with that actually achieved. Table 5 compares the velocity components and magnitudes of the nominal and achieved maneuvers.

Table 5. Comparison of nominal and achieved maneuver velocity increments for *Mariner V* at $23^h03^m20^s.650$ UT, June 19, 1967

Velocity component, m/s	Nominal[a] postmidcourse and premidcourse, σ	Achieved postmidcourse and premidcourse, σ
$\Delta\dot{x}$	-0.73797 ± 0.13	-0.6295 ± 0.0093
$\Delta\dot{y}$	-6.84993 ± 0.13	-6.6183 ± 0.0098
$\Delta\dot{z}$	-14.5815 ± 0.13	-13.90472 ± 0.0176
Δv	16.1272 ± 0.13	15.4123 ± 0.0163

[a]Based on earlier premidcourse orbit than tabulated in Table 1.

It appears, therefore, that an error of 0.715 ± 0.016 m/s was committed in the magnitude of the maneuver velocity increment. If no pointing error was made, this would nearly account for the achieved closest approach distance of 10,151 km, compared to the nominal value of 8,165 km from Venus center. Furthermore, the pointing error of the maneuver thrust axis is easily calculated. The pitch and roll turns may be calculated as follows:

$$\text{pitch turn} = \arctan\left(\frac{\mathbf{V}\cdot\mathbf{j}}{\mathbf{V}\cdot\mathbf{k}}\right) + \arccos\left(\frac{-\cos\xi}{\sqrt{1-\left(\frac{\mathbf{V}\cdot\mathbf{i}}{\mathbf{V}}\right)^2}}\right)$$

$$= 55.453 \pm 0.062 \text{ deg},$$

$$\text{roll turn} = -\gamma - \arccos\left(\frac{-\mathbf{V}\cdot\mathbf{i}}{\mathbf{V}\sin\xi}\right)$$

$$= 70.660 \pm 0.004 \text{ deg},$$

where

$\mathbf{V}$ = maneuver velocity

$\mathbf{i}, \mathbf{j}, \mathbf{k}$ = unit vectors of premaneuver pitch, yaw, and roll axes

ξ = orientation of maneuver thrust axis to roll axis = 88.5 deg

γ = orientation of projection of maneuver thrust axis on pitch-yaw plane from pitch axis = 45 deg

The pitch and roll uncertainties were obtained from a computer program which makes use of the 3×3 velocity covariance matrix of Δx, Δy, and Δz. The unit vectors used in the above calculations assume the attitude control error to be zero. Table 6 shows the corrections indicated by limit cycle telemetry and the commanded values of the turns.

Thus, errors of about 0.3 deg were made in execution of the turns; however, the actual errors must include the effects of attitude control displacement. It is readily seen that the execution and displacement errors partially cancel. An additional limitation on the system is imposed by the command pulse system used to fire the gas jets. This system limits the time duration of gas jet firing to an integral number of seconds. Thus, the commanded turns differ from the nominal turns. Table 7 shows the nominal turns and the total achieved minus nominal pointing error, including attitude control contribution. This result is directly measured to a high degree of accuracy by orbit determination.

If subscripts denote achieved and nominal velocities and if ψ is the total angle of the achieved thrust axis from the nominal thrust axis, then

$$\sin\psi = \frac{\mathbf{V}_A \times \mathbf{V}_N}{V_A V_N \hat{\psi}}$$

$$= 0.007062989$$

$$\psi = 0.405 \text{ deg}$$

Table 6. Execution errors

Turn	Premaneuver telemetry corrections, attitude control limit cycle information, deg	Corrected turns, achieved, deg	Commanded turns, deg	Achieved-commanded turns, deg
Pitch	$+0.333 \pm 0.020$	55.120 ± 0.065	55.267	-0.147 ± 0.065
Roll	$+0.028 \pm 0.014$	90.632 ± 0.015	70.946	-0.314 ± 0.015

Table 7. Summary of measured pointing error

Turn	Nominal turn, s	Achieved turn, deg	Commanded turn duration, s	Total achieved minus nominal pointing error, deg
Pitch	304.46	55.453 ±0.062	304.0	0.103 ±0.062
Roll	380.43	70.660 ±0.004	380.0	0.365 ±0.004

This pointing error can contribute only about 300 km in closest approach distance. The remaining 1700-km error is entirely due to the magnitude of the velocity error of 0.715 ±0.016 m/s.

III. Cruise Orbit Determination Results

A. Tracking Data Types

1. Ranging data. In addition to angular and doppler data described in Section I, two types of ranging measurement were performed during cruise. These were performed with the Mark IA system at the DSS sites shown in Table 5 and with the planetary ranging system at DSS 14 (Goldstone-Mars). Mark IA range units (RU) are defined as follows:

$$\rho_{DSIF} = \left[\frac{15\,(\Delta t + \epsilon)}{221}\,96 f_q\right] \bmod 785762208$$

where

ρ_{DSIF} = measured round-trip interval, in RU

Δt = round trip light time, in UTC s

f_q = transmitter reference frequency $\simeq$ 22 MHz

ϵ = time delay in seconds from station equipment, spacecraft transponder, and intervening space plasma-ionospheric medium

785762208 RU = code length of system

The Mark IA ranging system is limited to an effective one-way range of about 5.8×10^6 km, attained July 6, 1967 (see Table 8).

Table 8. Mark IA ranging data obtained during *Mariner V* mission

DSS	Location	Start month, day, 1967	Stop month, day, 1967	No. of points, sampling interval 60 s
62	Cebreros	July 6	July 6	48
11	Goldstone-Pioneer	June 20	June 29	2390
42	Tidbinbilla	June 24	July 6	3031
41	Woomera	June 21	June 22	714
12	Goldstone-Echo	June 30	July 2	1503
61	Robledo	June 20	June 29	2720

Table 9. Planetary range units (PRU) residuals (standard deviation)

Day	Date	σ_{PRU}	σ_ρ(m)	ρ(m)	σ_ρ/ρ
Station 14 residuals					
172	6/21	103	15	0.18E10	0.83E-8
191	7/10	492	74	0.68E10	1.09E-8
203	7/22	628	94	1.00E10	0.94E-8
204	7/23	654	98	1.03E10	0.95E-8
209	7/28	730	110	1.19E10	0.92E-8
279	10/06	3580	537	6.25E10	0.86E-8
203	10/10	5600	840	6.78E10	1.23E-8
Station 11 and 12 RU residuals					
172	6/21		20	0.18E10	1.11E-8
173	6/22		26	0.21E10	1.24E-8
174	6/23		30	0.24E10	1.25E-8
175	6/24		36	0.27E10	1.33E-8
177	6/26		37	0.30E10	1.23E-8
178	6/27		40	0.33E10	1.21E-8
179	6/28		41	0.36E10	1.14E-8
180	6/29		62	0.39E10	1.59E-8
182	7/1		43	0.42E10	1.02E-8
183	7/2		45	0.45E10	1.00E-8
Station 42 last RU data					
187	7/6		53	0.58E10	0.91E-8
Station 62 last RU data					
187	7/6		61	0.58E10	1.05E-8

The *Mark II* (planetary) ranging system at DSS 14 (Goldstone-Mars) measures the round trip delay directly in nanoseconds. The code length of the equipment is 1.00947/1.0002 s, hence

$$\rho_{\text{planetary}} = [10^9\,(\Delta t + \epsilon)] \bmod \frac{1.00947 \times 10^9}{1.0002}$$

With the use of the Mark II equipment and the 210-ft antenna at the Mars site, Mark II ranging measurements may be made to planetary distances, as the name of the data type implies. During the *Mariner V* mission, approximately 7000 points of 60-s sampled planetary ranging were obtained between July 21 and November 20, 1967.

2. *Tracking data statistics.* Table 9, shows the manner in which ranging data noise increases as a function of range when processed by the SPODP. Statistics are given for individual passes of tracking data on the days shown, where ρ is the one-way spacecraft range in meters, and standard deviations on PRU and RU have been converted to $\sigma\rho$. The last column shows that 8-place accuracy is retained in the computations, which is all that may be expected of a single precision program with a floating-point word length of 27 binary bits.

Doppler residuals do not display large numerical truncation and round-off as a function of range, but are, nevertheless, limited by single precision and by the stability of the reference frequency standard over the light–time interval. Table 10 shows a sample of cruise doppler residual statistics reduced by the SPODP. These data have been averaged over 10-min intervals to reduce the total number of points to a manageable level. The statistics reflect the precision of the least squares fit over a long arc (3 months). Table 10 also gives combined ranging statistics through July 28, 1967. The degradation from fitting a long arc is more apparent here than in the individual pass statistics in Table 9. This, of course, means that individual passes are biased differently, partly from single precision truncation and partly from the nature of the least squares fitting process.

Table 10. CC3 residuals by station (cruise data, T_c = 600 s)

DSS	No. of points	Rms, Hz	First moment, Hz	σ, Hz	Rms, mm/s	μ, mm/s	σ, mm/s
11	422	0.00348	−0.000395	0.00346	0.227	−0.0258	0.226
12	255	0.00400	−0.000356	0.00398	0.261	−0.0233	0.260
14	165	0.00433	−0.000976	0.00421	0.283	−0.0638	0.275
41	311	0.00368	−0.000452	0.00365	0.241	−0.0295	0.239
42	770	0.00312	−0.000762	0.00302	0.204	−0.0498	0.197
61	831	0.00411	−0.000682	0.00405	0.269	−0.0446	0.265
62	172	0.00473	−0.000158	0.00473	0.309	−0.0103	0.309
TOTAL CC3	2926	0.00378	−0.000595	0.00373	0.247	−0.0389	0.244
PRU residuals through July 29, 1967							
14	847	868.9	−433.4	753.1	130	−65	113
RU residuals							
11	240	45.4	0.251	45.4	47	0.3	47
12	65	52.6	−30.1	43.1	55	−31	45
41	74	59.4	54.1	24.4	62	57	26
42	298	55.3	−17.5	52.4	58	−18	55
61	285	49.9	0.255	49.9	52	0.3	52
62	6	59.5	−10.5	58.6	62	−11	61
TOTAL RU	968	51.6	−3.2	51.5	54	−3	54

B. Cruise Solutions for Physical Constants

1. Solar radiation pressure. During cruise, continuous least squares estimates were made of γ_B, the solar radiation pressure coefficient defined in Section I, Early Mission Performance and Results. The time history of these solutions is shown in Fig. 7. The solutions are consecutively identified by orbit number. There appears to be a distinct trend towards lower pressure with increasing time. The physical interpretation of this phenomenon could be that an actual degradation of the total reflectance of the spacecraft took place during cruise. For instance, temperature monitoring of the bus indicates that the absorptance of the bus radiation shield may have increased by 30 percent through UV darkening.* This would cause a corresponding decrease in reflectivity of the shield which could account for a decrease in γ_B of up to 0.007. There is, in addition, the possibility of a decrease in specularity of the shield which L. Dumas* has estimated could cause a decrease in γ_B of as much as 0.028. As seen in Fig. 7, the observed change in γ_B is on the order of 0.06 which is nearly twice as much as the maximum combined effect of the above explanations. Since the standard deviations on the orbit solutions for γ_B are typically less than 0.01, it seems likely that the effect is real. The use of ranging data, in particular, adds great strength to the cruise solutions. The possibility remains, however, that the observed effect is at least partially due to a small force other than solar radiation pressure. This could result from a systematic decoupling of the attitude control gas jet torques which could, in

*L. Dumas, Jet Propulsion Laboratory, personal communication.

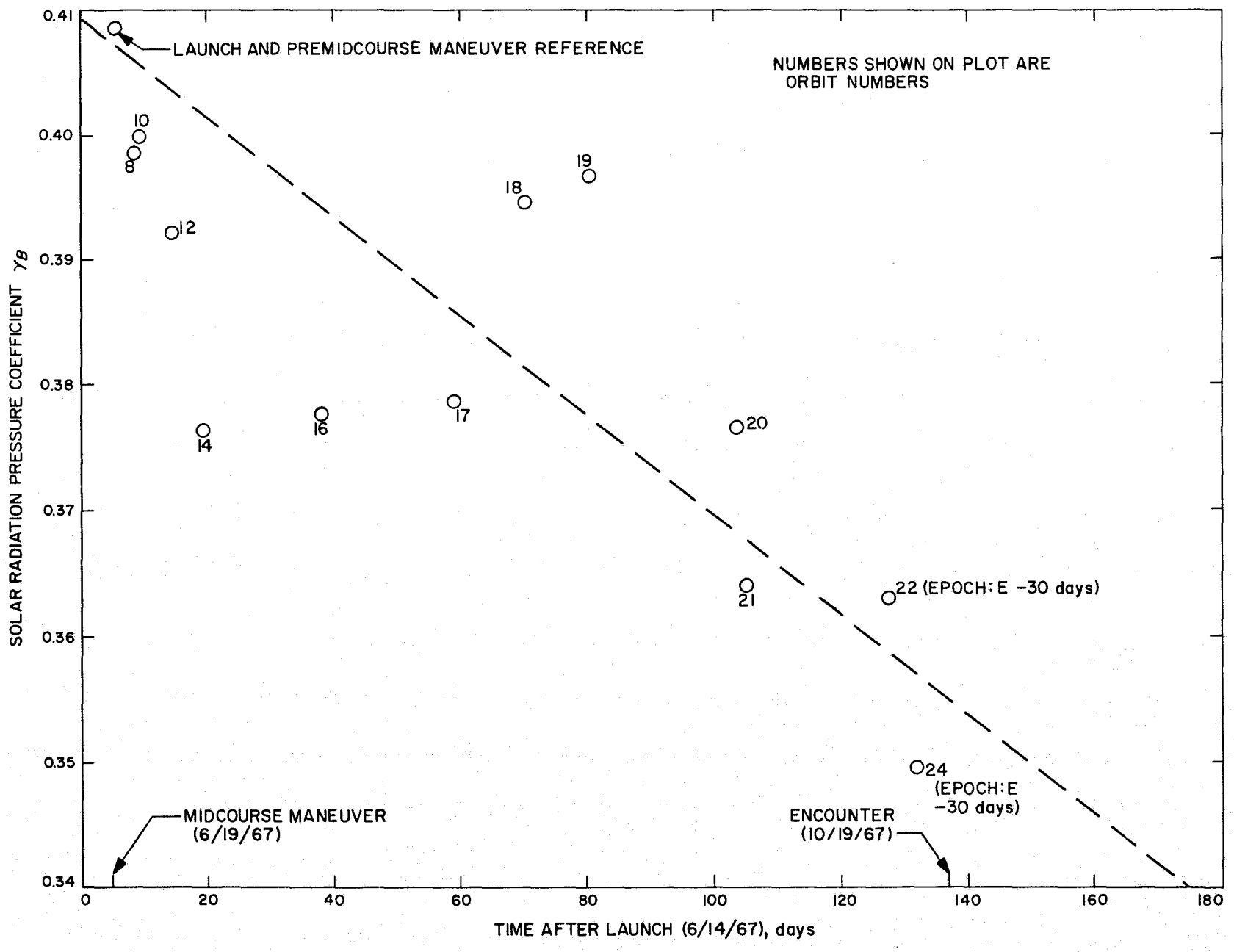

Fig. 7 *Mariner V* cruise solutions for solar pressure coefficient γ_B by orbit number

turn, result from problems such as temperature differential between the sunlit jets and the shaded jets. A discussion of the attitude control torques is in Section II which describes nongravitational forces.

2. *Station locations.* Least squares estimates of station locations based on postmidcourse maneuver tracking data are shown in Figs. 8 through 21. The *a priori* standard deviations for spin axis distance γ_s and longitude λ are $\tilde{\sigma}\gamma_s = 24$ m, $\tilde{\sigma}\lambda = 50$ m. The estimates were reduced to the mean pole of 1900–1905 and plotted by N. Mottinger of JPL. The solutions for perpendicular distance off the earth's spin axis, reduced to the mean pole of 1900–1905, and the associated standard deviations (plotted as vertical bars) are shown in Figs. 10 through 14. In general, the solutions are consistent to ±5 m.

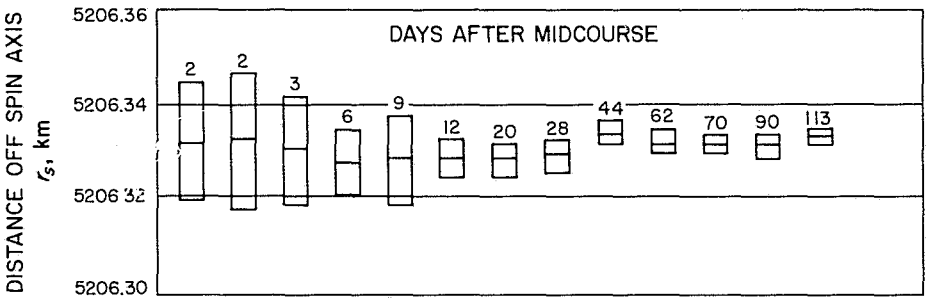

Fig. 8. Distance off spin axis, DSS 11

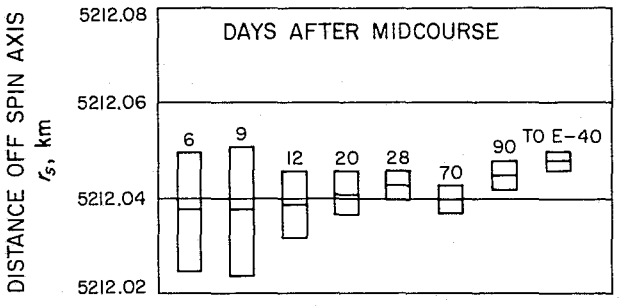

Fig. 9. Distance off spin axis, DSS 12

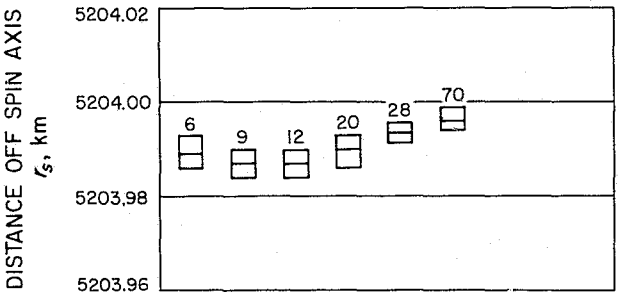

Fig. 10. Distance off spin axis, DSS 14

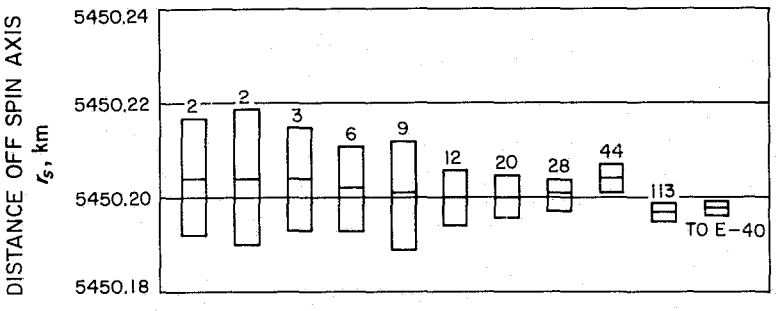

Fig. 11. Distance off spin axis, DSS 41

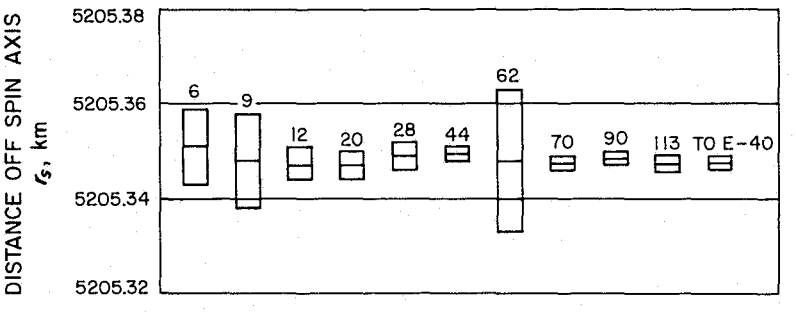

Fig. 12. Distance off spin axis, DSS 42

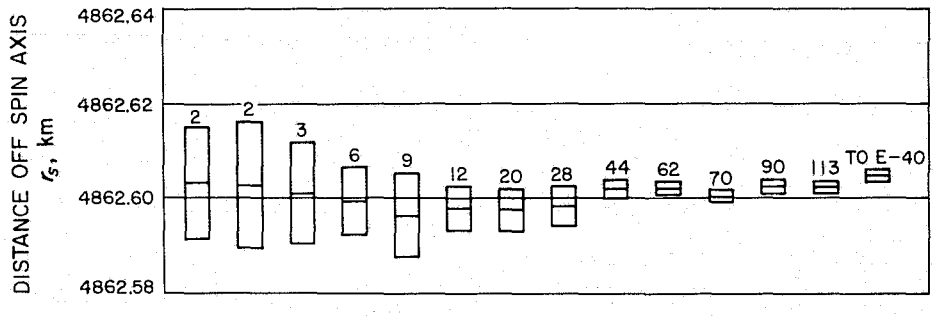

Fig. 13. Distance off spin axis, DSS 61

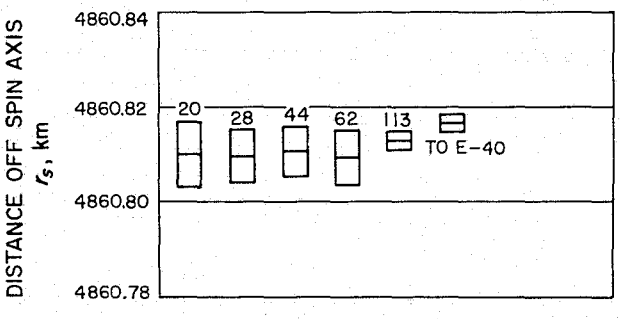

Fig. 14. Distance off spin axis, DSS 62

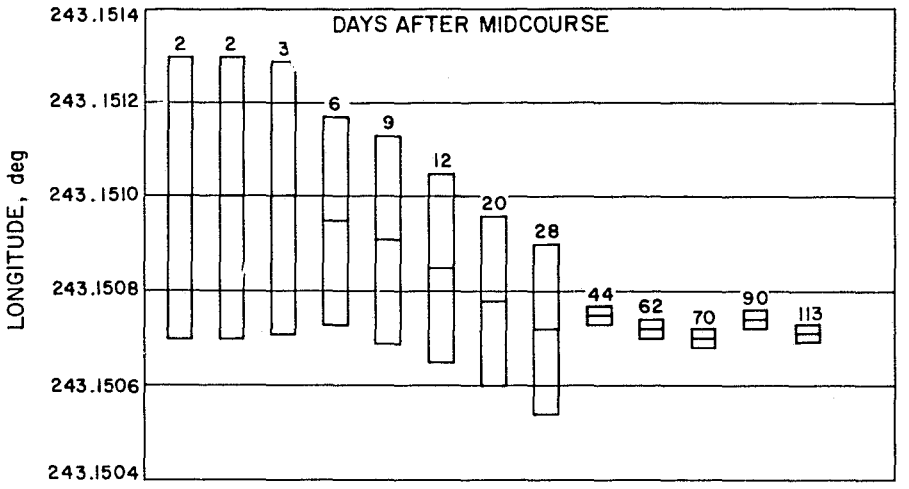

Fig. 15. Geocentric longitude, DSS 11

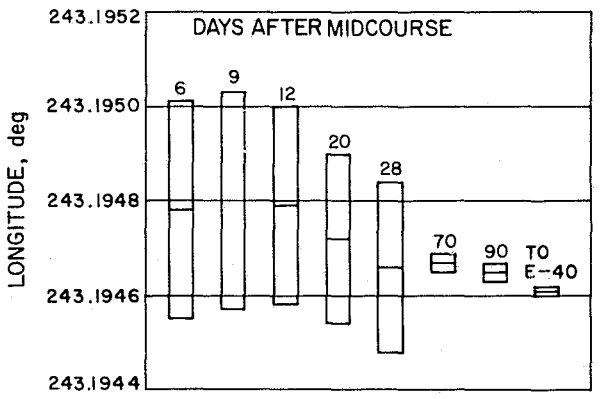

Fig. 16. Geocentric longitude, DSS 12

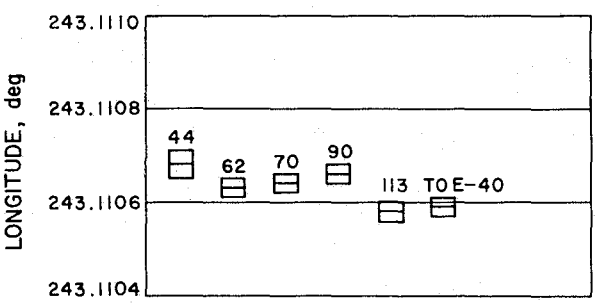

Fig. 17. Geocentric longitude, DSS 14

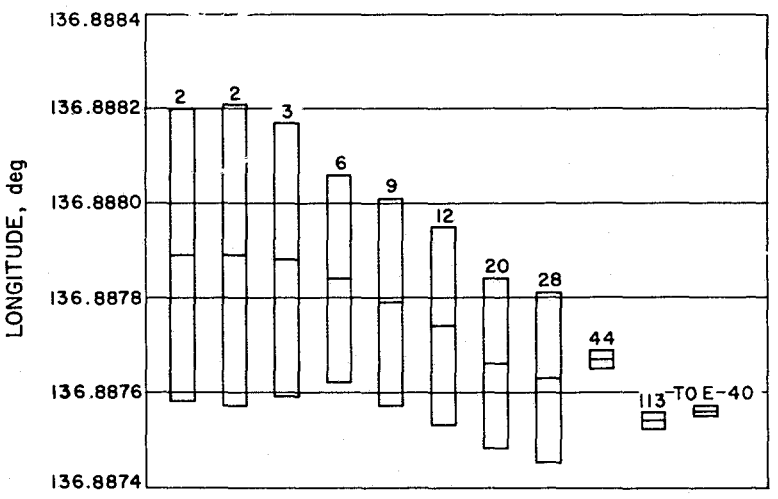

Fig. 18. Geocentric longitude, DSS 41

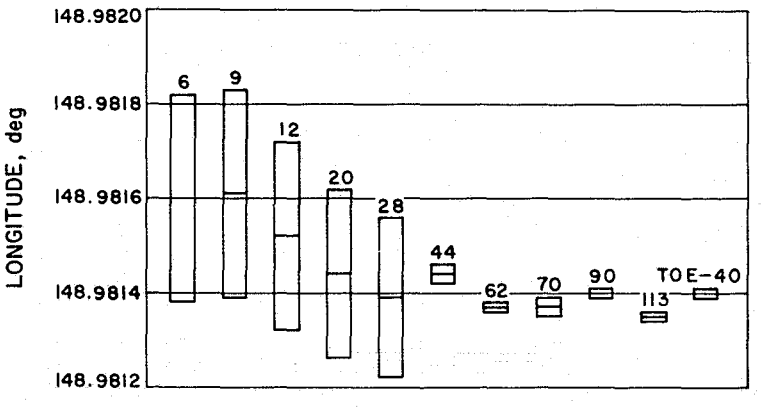

Fig. 19. Geocentric longitude, DSS 42

The *Mariner* cruise longitude solutions reduced to the pole of 1900–1905 are plotted in Figs. 16 through 21. The salient feature of these solutions is the 25- to 30-m difference between early and late cruise solutions. The high values obtained shortly after midcourse maneuver tend to be in good agreement with the longitudes obtained before the maneuver, whereas the late cruise solutions tend to be close to those obtained during encounter. Runs up to Post 14 did not represent WWV − UT timing differences, whereas later runs used a polynomial representation of these differences. The timing error caused by making WWV − UT = 0 is about 10 ms on June 19, or 4 m in longitude. The remaining differences are probably due to earth ephemeris errors.

3. Cruise solutions for mass of moon. Figure 22 shows the lunar gravitational constant solutions based on the

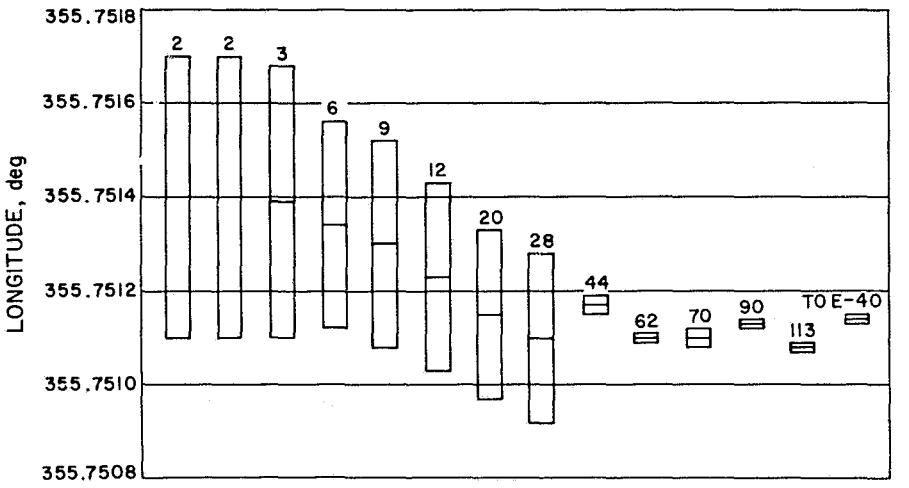

Fig. 20. Geocentric longitude, DSS 61

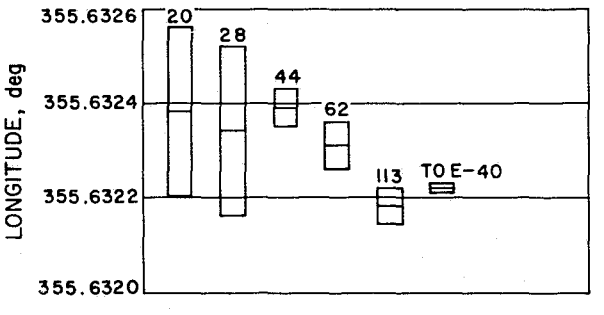

Fig. 21. Geocentric longitude, DSS 62

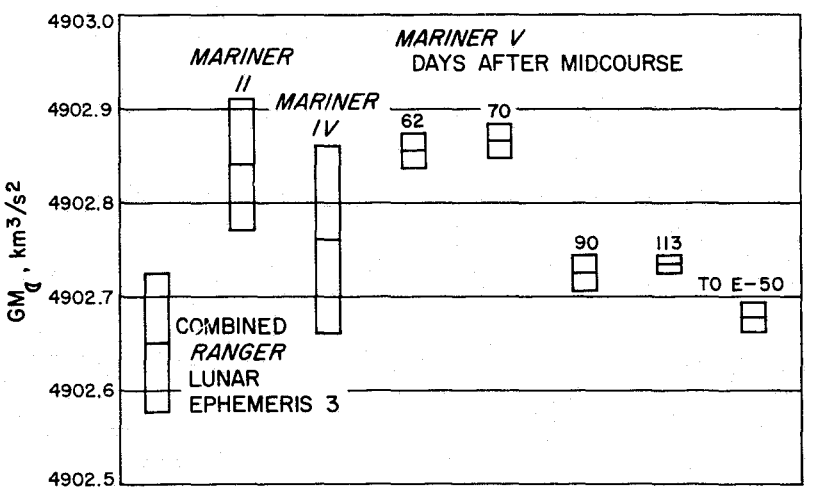

Fig. 22. Gravitational mass of the moon from combined *Ranger* and *Mariners II, IV,* and *V* data

combined *Ranger* missions. (Ref. 3), *Mariner II* (Ref. 4) and *IV*, (Ref. 5), and *Mariner V* in real time. The low *Ranger* result, $GM_{☾} = 4902.6493$ km³/s², was obtained by measuring the effect of the lunar gravity field on the probe acceleration. The *Mariner* results, on the other hand, measure the barycentric motion of the tracking station over the long cruise interval; therefore, the results, in reality, are a determination of the earth–moon mass ratio, assuming a known value for the earth-moon distance from optical and radar observations. The *Mariner II* result of $GM_{☾} = 4902.8442$ km³/s² is based on the *Ranger* earth gravitational constant, $GM_{⊕} = 398601.27$ km³/s², yielding a mass ratio $\mu^{-1} = 81.3000 \pm 0.0011$. The *Mariner IV* value also uses the *Ranger* $GM_{⊕}$ to obtain $\mu^{-1} = 81.30147 \pm 0.0016$ from $GM_{☾} = 4902.756 \pm 0.1$ km³/s². The real-time *Mariner V* solutions shown in Fig. 22 display a sharp break between data spans incorporating a 2- and 3-month accumulation of data, respectively. The explanation of this phenomenon is not known at this time but is probably related to ephemeris errors of the earth-moon barycenter. Over the cruise interval, three relatively uncorrelated parameters showed a marked decrease: solar radiation pressure, tracking station longitudes, and the moon–earth mass ratio μ. Although correlations are low between these parameters, they are probably significant. If a representative value were to be given for the real-time cruise solutions for $GM_{☾}$ it would have to be between the two extremes of 4902.86 km³/s² and 4902.68 km³/s². A realistic evaluation of the real-time results yields $GM_{☾} = 4902.77 \pm 0.1$ km³/s². Since all *Mariner V* solutions assume a value $GM_{⊕} = 398601.33$, the corresponding real-time estimate of μ^{-1} is 81.30125 ± 0.00166.

The gravitational constant values given in Fig. 23 reflect the result of an effort to estimate physical constants. The values included $GM_{☾}$, by careful post-processing of the cruise data for the *Mariner* celestial mechanics experiment, conducted by the principal investigator, J. D. Anderson of JPL. These results seem to indicate a value of $GM_{☾} = 4902.81 \pm 0.5$ km³/s² which yield $\mu^{-1} = 81.30059 \pm 0.00083$. This value is remarkably close to the *Mariner II* mass ratio, and is in good agreement with the *Mariner IV* value. In these runs, ranging data have been weighted more heavily than in the real

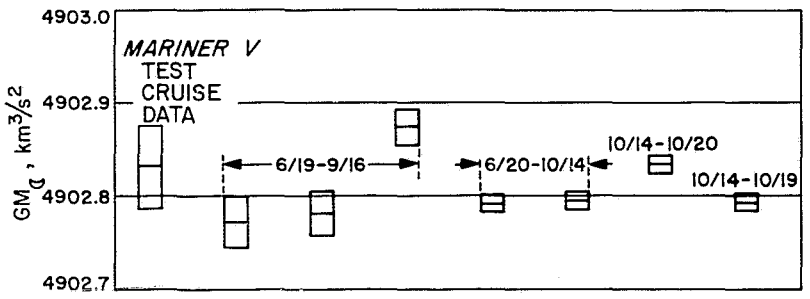

Fig. 23. Gravitational mass of the moon from *Mariner V* post cruise analysis

time runs, and less late-cruise data is used than in the late real time solutions.

C. Target Parameters from Cruise Solutions

1. Time of closest approach. Cruise orbit estimates of time of closest approach to Venus are shown in Fig. 24. As in Fig. 7, these are labeled by orbit number in order of increasing time. It is seen that the solutions cluster around 1735 UT on October 19, 1967. The actual encounter time was $17^h34^m54^s.937$ UT, demonstrating that the cruise solutions were not affected by detectable systematic errors in the flight time parameter.

2. B-plane target point. A standard measurement of the trajectory aiming point is the position of the incoming asymptote in the **B**-plane; i.e., in the plane normal to the asymptote and passing through the center of the target planet. Figure 25 shows the predicted aiming points from cruise orbit determination in planet-centered **B**-plane components $\mathbf{B}\cdot\mathbf{R}$ and $\mathbf{B}\cdot\mathbf{T}$, where **T** is in the ecliptic plane and **R** is normal to **T**. The solutions appear to randomly cluster about $\mathbf{B}\cdot\mathbf{R} = -14830$ km and $\mathbf{B}\cdot\mathbf{T} = 24270$ km. They are noticeably offset on the plot from the *posteriori* solution of $\mathbf{B}\cdot\mathbf{R} = -14761.9 \pm 1$ km, $\mathbf{B}\cdot\mathbf{T} = 24334.3 \pm 1$ km. This offset of about 100 km is probably attributable to earth-Venus ephemeris errors, station locations errors, and timing errors.

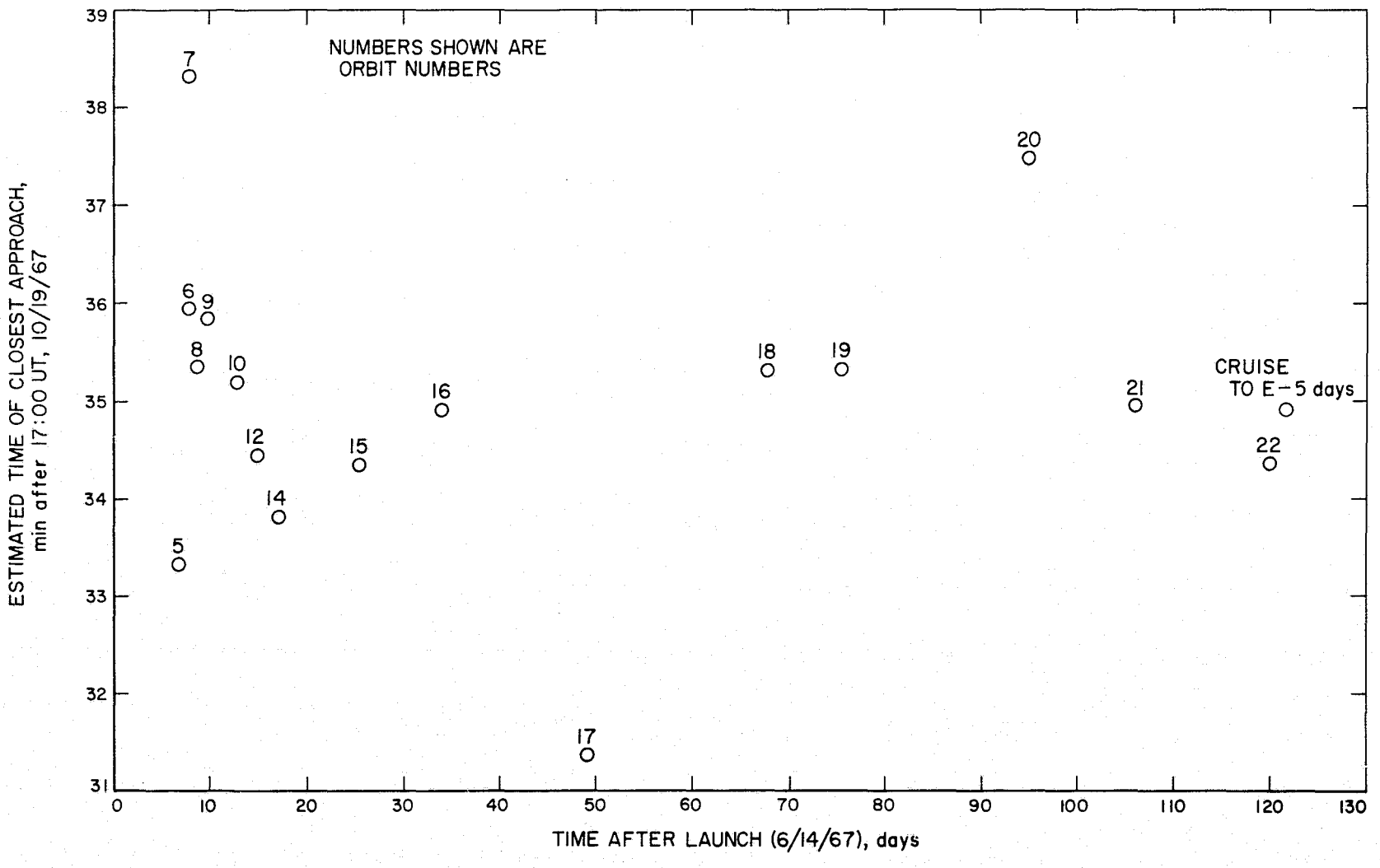

Fig. 24. Cruise orbit estimates of time of closest approach to Venus

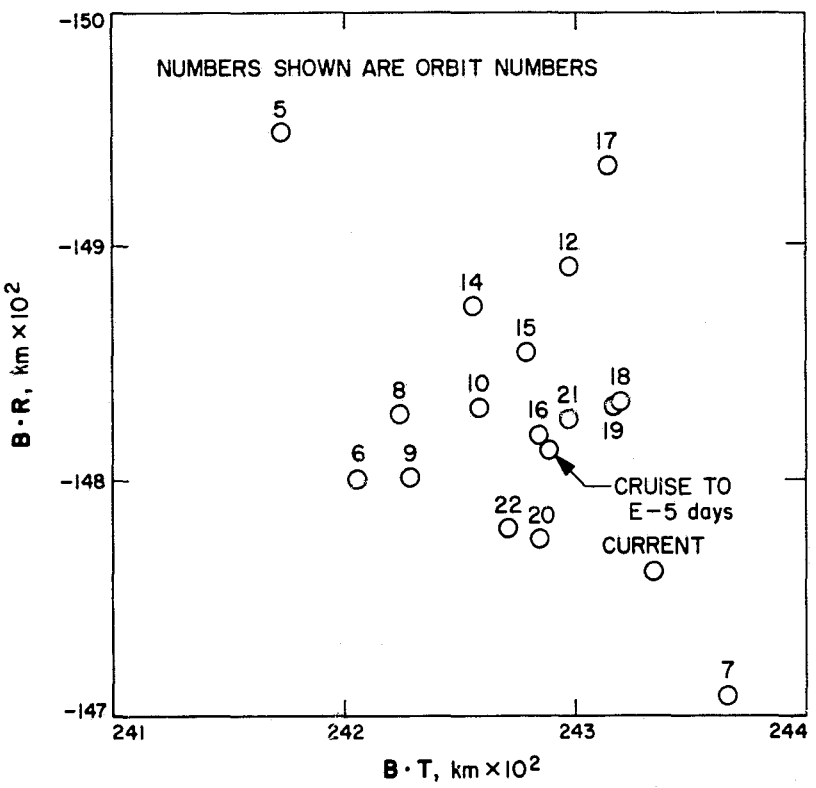

Fig. 25. Ecliptic B-plane aiming point from cruise orbit determination

IV. Real-Time Encounter Orbit Determination Results

A. Real-Time Encounter Orbit Estimation Procedures

1. Tracking data acquisition. During the period $E - 12$ h to $E + 3$ h, where E is encounter, 11 orbits were run on two IBM 7044-7094 computer strings as tracking data were acquired in real time by the Deep Space Network (DSN). Figure 26 shows the tracking data distribution from E − 5 days to E + 5 days. The real-time encounter orbits utlized data from E − 5 days to E + 1 h, while the postencounter analyses made use of the full 10 days.

2. Orbit estimation procedure. Orbits run on the prime computer string were labeled with a "10" prefix, while those run as backup support were given a 20 prefix. The prime runs estimated spacecraft trajectory, the astronomical unit, and station locations. The backup runs estimated various combinations of parameters, including Venus ephemeris elements.

3. Real-time encounter aiming point estimates. The primary excursions noted in the real-time encounter orbits were in the direction normal to the **B** vector. Thus the solutions line up very nearly along a line normal to **B** in the **R**-**T** plane (see Fig. 27). The total variation amounts to 900 km, or 1.8 deg measured from planet center. This is in good agreement with uncertainties predicted in Ref. 2. The major error source seems to be numerical instability in the station location astronomical unit, and Venus ephemeris solutions. The current best estimate based upon 10 days of encounter tracking data is also shown in Fig. 27. The systematic offset of the solutions from the current value is about 100 km, which is much smaller than the total scatter. Interestingly, this offset is in the opposite direction from the cruise solutions. The current values of $\mathbf{B}\cdot\mathbf{R} = -14761.9$ km, $\mathbf{B}\cdot\mathbf{T} = 2433.3$ km are known to ±1 km.

4. Solution for astronomical unit. The radar value of 149597900 ±100 km was adopted as an *a priori* starting value in the encounter runs. The solutions showed no tendency to significantly deviate from this value within the limitations of single precision; three possibilities therefore, are indicated: (1) the radar value is correct within ±100 km, (2) ephemeris errors in the range direction are within ±100 km, and (3) the strength of the single precision solution is not great enough to detect errors on the order of 100 km. The latter possibility may be ruled out, as the ranging data are sufficiently precise to establish the earth-Venus distance to better than ±10 km even in single precision, although the program cannot effectively separate Venus ephemeris error in the range direction from error in the astronomical unit. The current best *Mariner V* astronomical unit solution yields 149597904 ±44 km.

5. Target ephemeris error. Preencounter estimates of Venus ephemeris errors were hampered by low numerical stability and unfavorable partial derivatives. In particular, ephemeris errors are highly correlated with tracking station longitudes and the astronomical unit. Thus, these solutions were not accurate to the requisite of ≅50 km needed to define ephemeris errors. The planetary ephemeris used successfully for the mission was the highly accurate JPL Development Ephemeris (DE) No. 24, utilizing radar corrections to the older optical ephemeris. The current *Mariner V* encounter solution for corrections to the DE 24 position of Venus at $17^h35^m33^s.138$ UT, October 19, is in earth equatorial coordinates, $x = -14.6$ ±0.8 km, $y = -14.7$ ±14.8 km, $z = -23.2$ ±44.3 km for the DE 24 AU of 149597877 km. The ability to detect such relatively small corrections to the astronomical unit and planetary ephemeris must be credited in large part to the planetary ranging system used with *Mariner V*.

6. Encounter station location solutions. Figures 28 through 37 show the *Mariner V* encounter solutions for

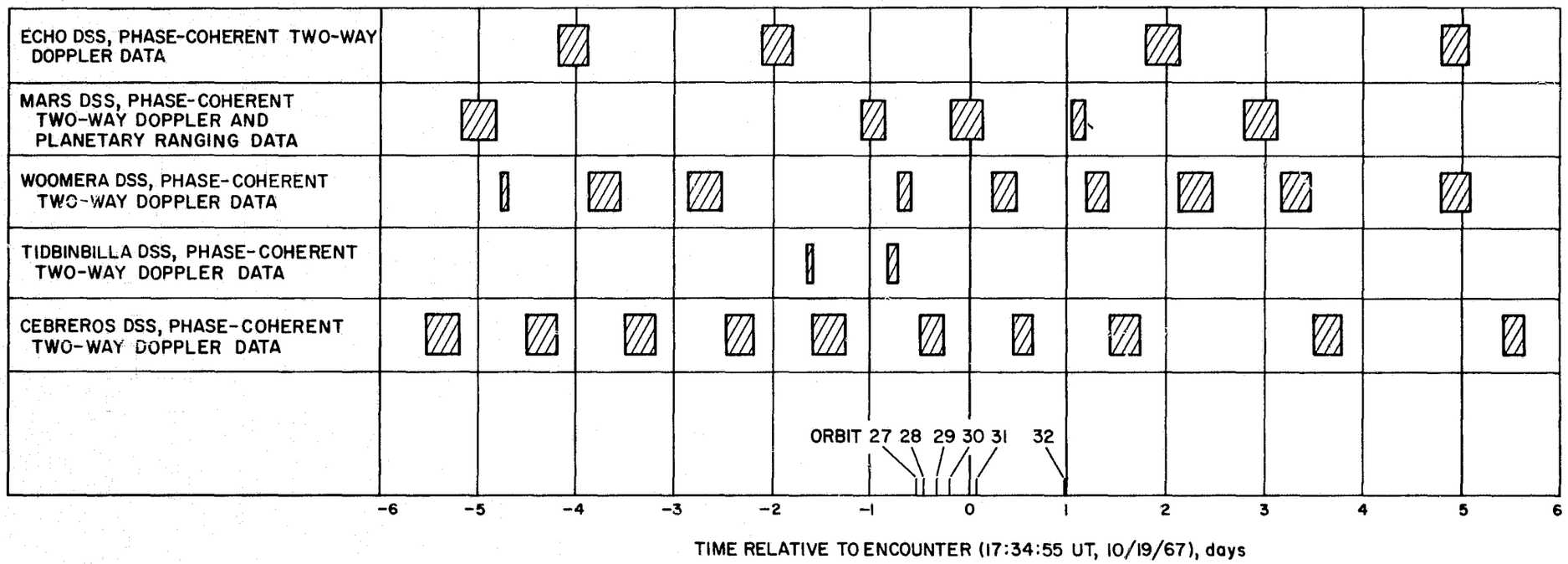

Fig. 26. Near encounter station view periods

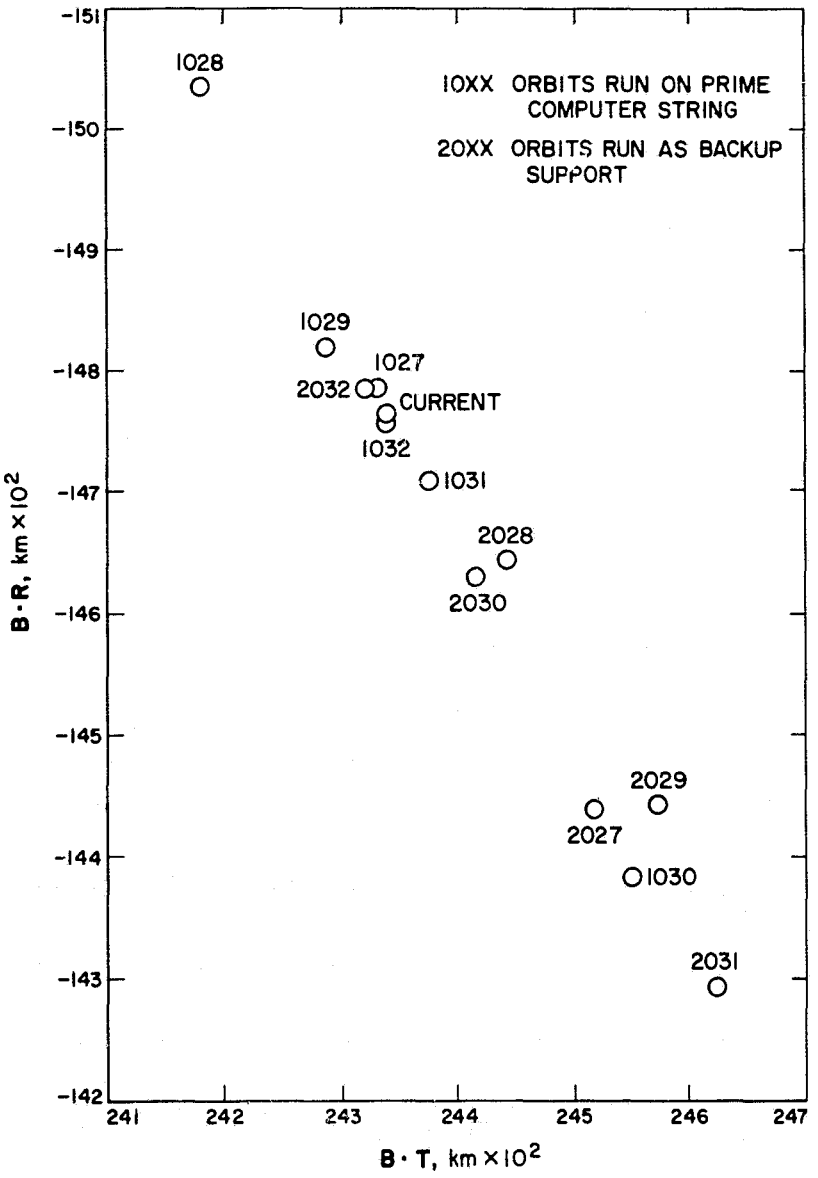

Fig. 27. Real-time *Mariner* Venus 67 encounter B-plane estimates

station locations reduced to the pole of 1903.0. Solutions for the distatnce off the earth's spin axis r_s are plotted by station number with associated standard deviations in Figs. 28–32, while station longitudes λ are plotted with their standard deviations in Figs. 33–37. Assumed *a priori* standard deviations were the same as for cruise; $\tilde{\sigma}r_s = 24$ m, $\tilde{\sigma}\lambda = 50$ m. The r_s solutions exhibit very little systematic trends except for orbit 1026. This orbit was run with an earlier data span which did not estimate the astronomical unit and did not include ranging data in the fit. Comparing the other solutions with Figs. 9 through 12 and Fig. 14, it is seen that the cruise and encounter spin-axis distance solutions are in good agreement.

Although considerably noisier than the spin-axis estimates, the encounter solutions for station longitude shown in Figs. 27–31 are in good agreement with the cruise longitude solutions of Figs. 16–19 and Fig. 21. The high-frequency random noise is due to numerical instability in the single precision orbit program. Note the trend toward increasing longitude with increasing data in the real-time solutions, in contrast to the opposite trend in the cruise solutions. The longitudes deduced from tracking data from $E-5$ day to $E+5$ day (best encounter solution) were reduced using JPL Development Ephemeris 40, which incorporates Venus radar bounce data past *Mariner* encounter.

7. Mass of Venus. The mass of Venus is the astrodynamical quantity most precisely determined by *Mariner V* encounter tracking data. This is because (1) the Venus-centered hyperbolic encounter trajectory is curved nearly 90 deg by the gravitational influence of the planet, and (2) this trajectory bending is very accurately measured by doppler tracking data. The *Mariner II* spacecraft, utilizing L-band doppler data and an ephemeris based on optical data only yielded a sun–Venus mass ratio of 408505 ± 6 (Ref. 4). This value was used a *a priori* information in the *Mariner* encounter solutions, but the *a priori* standard deviation was enlarged to 150 to avoid possible biasing of the solution towards the *Mariner II* result. The current *Mariner V* estimate of the sun–Venus mass ratio is 408522.66 ± 3. This is based on doppler and ranging tracking data from $E-5$ day to $E+5$ day, assuming $GM_\odot = 13271251 \times 10^4$ km^3/s^2 and an astronomical unit of 145957904 km, so that $GM_\varphi = 324859.6 \pm 3$ km^3/s^2.

V. Tracking Data System

Primary DSIF tracking data is two-way phase-coherent doppler data. A functional block diagram of the standard DSIF doppler system is shown in Fig. 1. In the course of the *Mariner V* mission the DSIF recorded two-way data in the quantities given in Table 11.

Table 11. DSIF tracking data

DSS	Two-way data points, as taken at various sampling rates
11	10,704
12	15,354
14	24,210
61	18,832
62	19,487
51	770
41	19,209
42	19,450

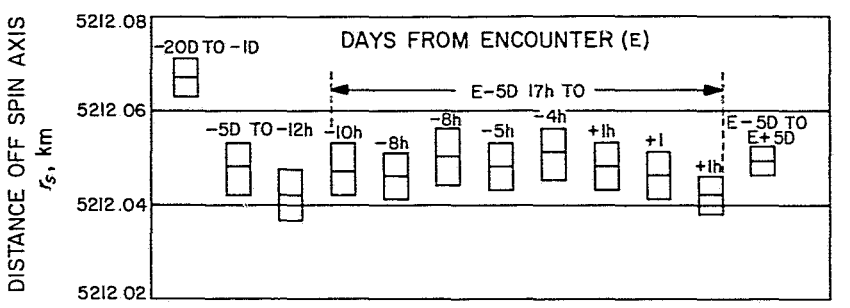

Fig. 28. Encounter solutions for DSS 12

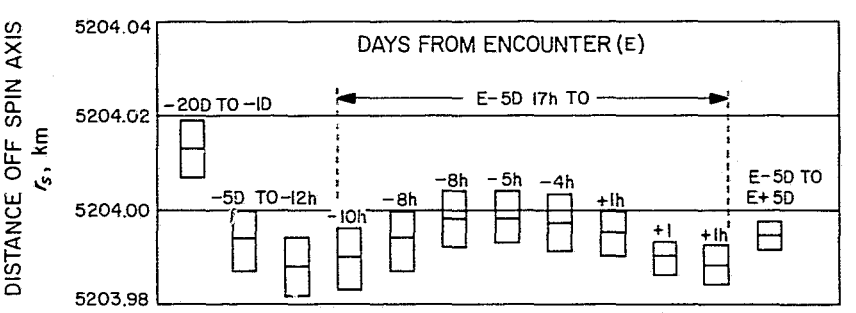

Fig. 29. Encounter solutions for DSS 14

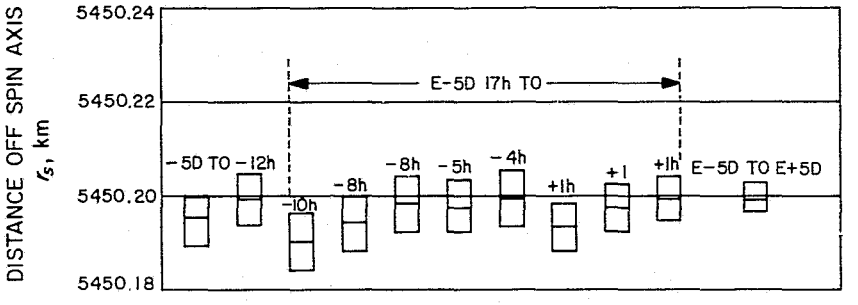

Fig. 30. Encounter solutions for DSS 41

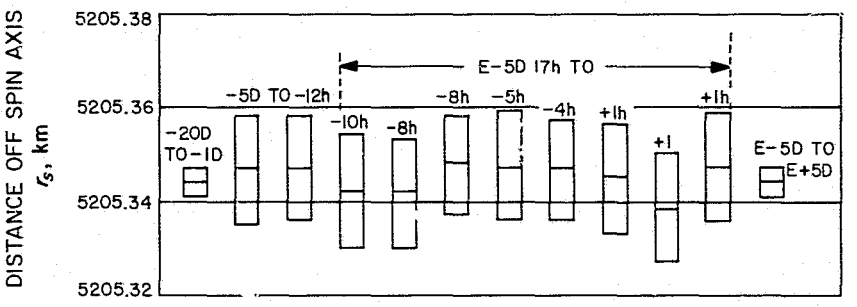

Fig. 31. Encounter solutions for DSS 42

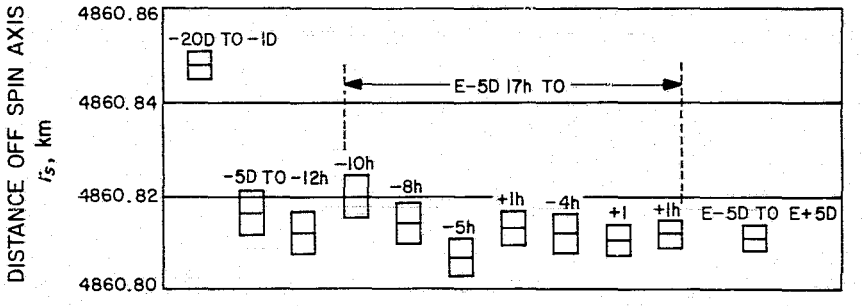

Fig. 32. Encounter solutions for DSS 62

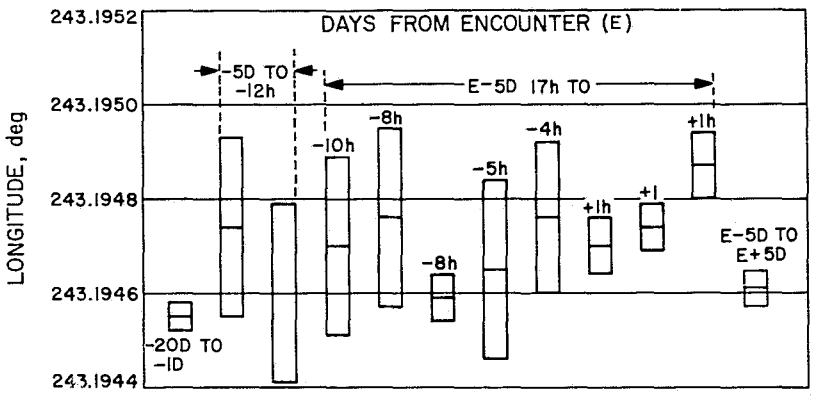

Fig. 33. Geocentric longitude, DSS 12

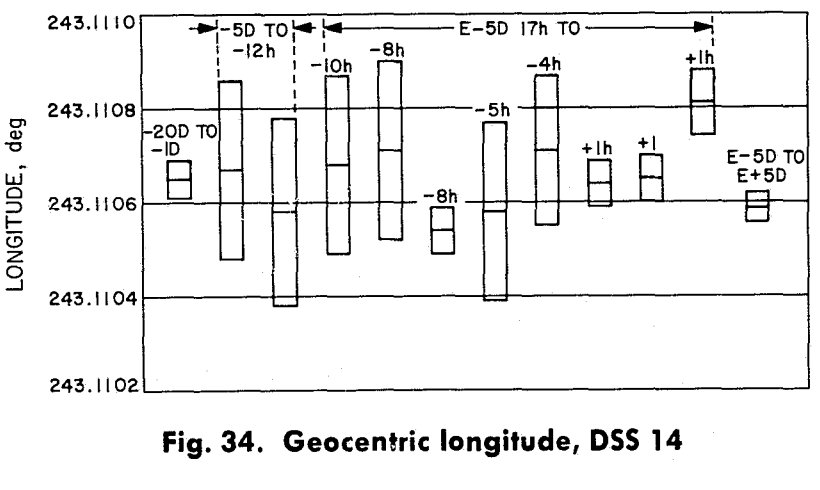

Fig. 34. Geocentric longitude, DSS 14

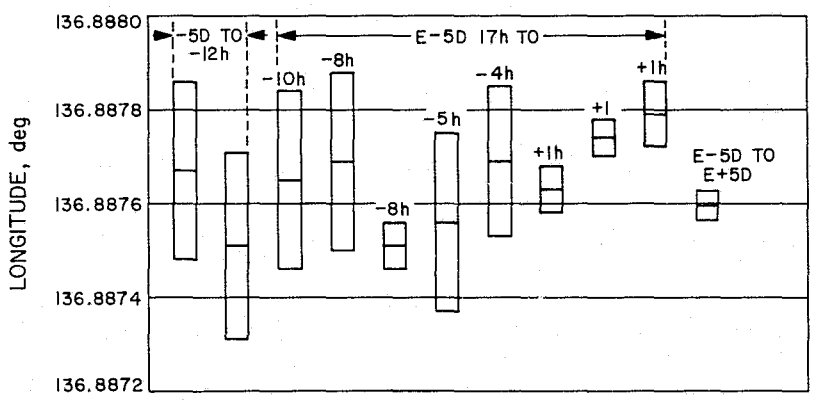

Fig. 35. Geocentric longitude, DSS 41

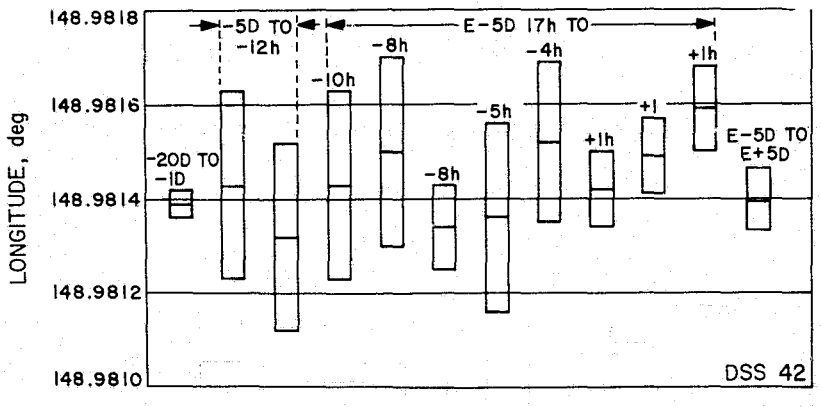

Fig. 36. Geocentric longitude, DSS 42

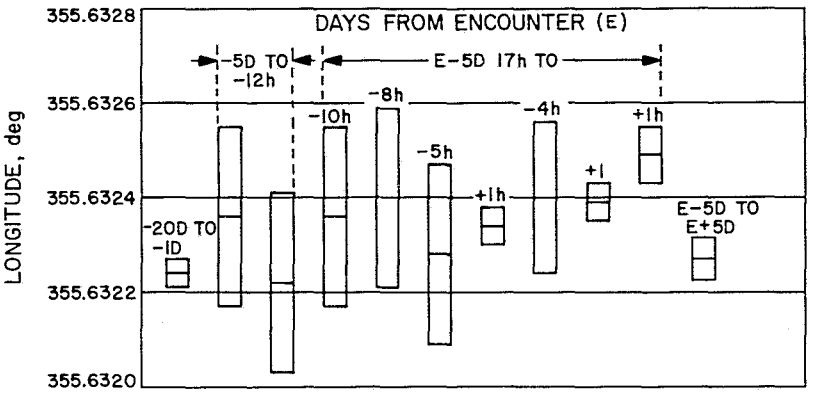

Fig. 37. Geocentric longitude, DSS 62

During the mission, the doppler digital resolver became fully operational throughout most of the net (except DSS 51). This subsystem provides a means of correcting the doppler count for the noninteger number of cycles between sampling times. It has demonstrated its effectiveness by reducing the high-frequency noise on the doppler data by more than an order of magnitude.

The *Mariner V* mission provided the first opportunity to employ the mark IA ranging system at ranges substantially greater than the distance of the moon. Mark IA ranging data was taken from just after midcourse on June 19 until system threshhold was reached on July 6 at a distance of 5,800,000 km. A total of 10,406 ranging points were taken. The mark IA ranging system was used to provide time correlations between DSIF stations via both the *Mariner V* spacecraft and the operational *Lunar Orbiter* spacecraft.

During this mission, the planetary ranging subsystem (PRS) became operative at DSS 14. PRS data was taken during the approach phase to the planet and in close proximity to Venus on either side of the closest approach time. After encounter, PRS measurements were made to distances in excess of 110,000,000 km.

Another innovation, introduced during *Mariner V*, was the use of the pseudoresidual program for real-time tracking data monitoring. This is an IBM 7044 program which compares any of the various tracking data-types with their corresponding computed values from the PRDX Program, the DSN predict program, and outputs observed-minus-predicted quantities and noise estimates. Although a number of program bugs invalidated much of the noise computation, the program proved itself a valuable aid in detecting and diagnosing DSIF hardware problems quickly. A modification of the program was used to provide real-time plots of the atmospheric effects for the occultation experiment.

APPENDIX A
Definition of the miss parameter B

The miss parameter **B** is used at JPL to measure miss distances for lunar and interplanetary trajectories and is described in Ref. 10. The desirable feature of **B** is its being nearly a linear function of changes in injection conditions.

The osculating conic at closest approach to the target body is used in defining **B**. The vector from the target's center of mass perpendicular to the incoming asymptote is **B**. Let $\mathbf{S}_I$ be a unit vector in the direction of the incoming asymptote. The orientation of **B** in the plane normal to $\mathbf{S}_I$ is described in terms of two unit vectors **R** and **T**, normal to $\mathbf{S}_I$. **T** is taken parallel to a fixed *reference plane* and **R** completes a right-handed orthogonal system.

The *Mariner V* work has used the ecliptic plane as the reference plane. Figure A-1 illustrates the situation.

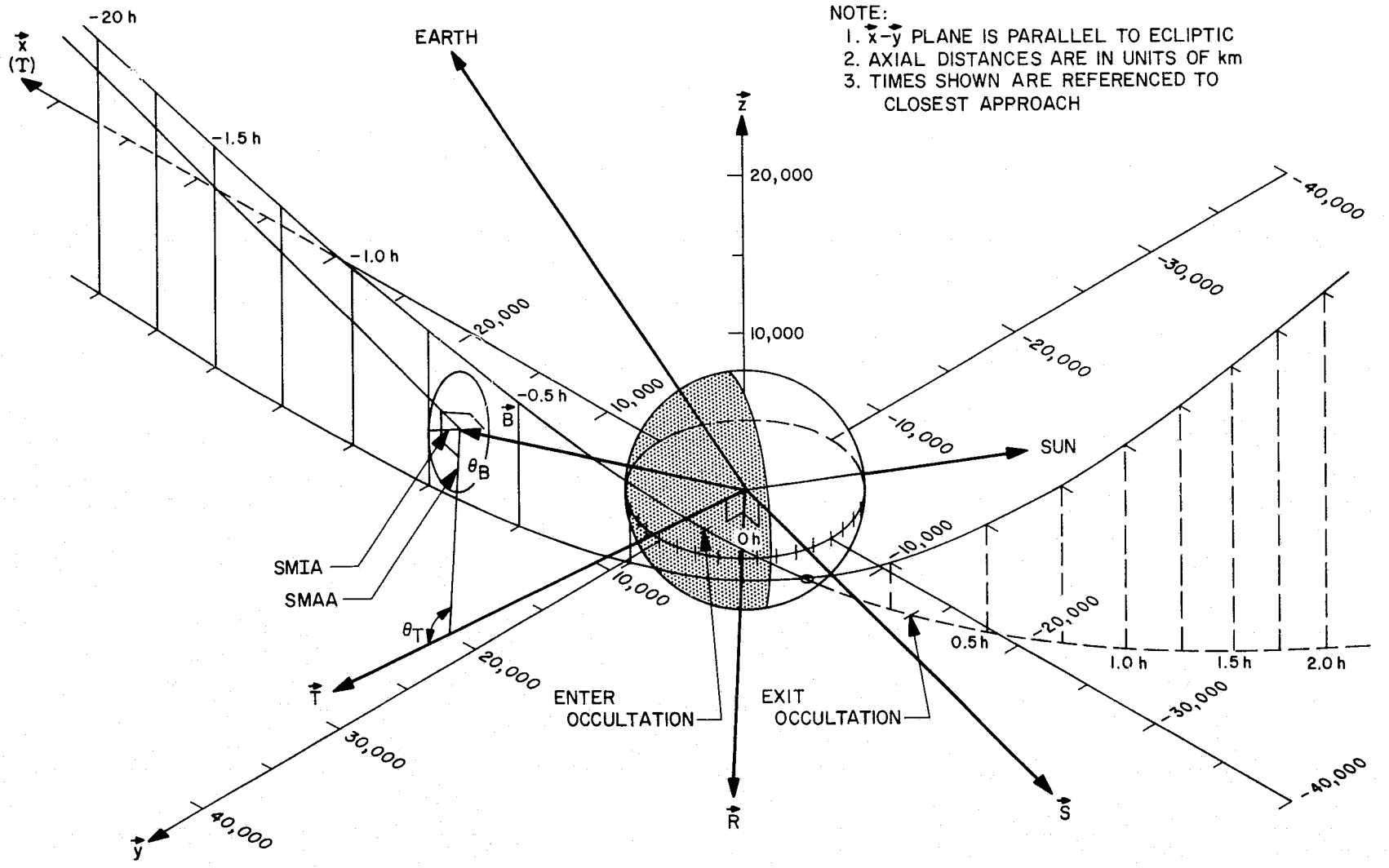

Fig. A-1. Isometric view of near-Venus trajectory

The *Mariner V* Flight Path and its Determination from Tracking Data

Part II. Nongravitational Forces

R. D. Bourke, S. R. McReynolds, and K. L. Thuleen

I. Introduction

Nongravitational forces on the *Mariner V* spacecraft were studied through their effects on attitude motion. The most significant forces were those due to solar radiation pressure and attitude control system thrusters. Since radiation pressure is adequately represented and solved for in the orbit determination process, concentration was on the attitude control-produced forces. The fundamental result is that these forces had a negligible effect on the trajectory; furthermore, the anomolous behavior of the spacecraft reflection coefficient cannot be attributed to control system thrusters.

II. Attitude Control System

Design of the *Mariner V* attitude control system is essentially the same as that of *Mariner IV* described in Ref. 6. Essential components operating during the cruise phase (the majority of the mission) are shown in Fig. 38. The spacecraft is nominally oriented with the $+z$ axis along the sunline and the Canopus sensor (midway between the $+x$ and $-y$ axes) in the sun–spacecraft–Canopus plane. Angular deviations from this orientation are detected by the sun sensors in pitch and yaw (see Fig. 38) and the Canopus sensor in roll. When the angular deviation in any of the axes reaches a certain level, the gas jets at the ends of the solar panels are momentarily actuated to drive the orientation back to nominal.

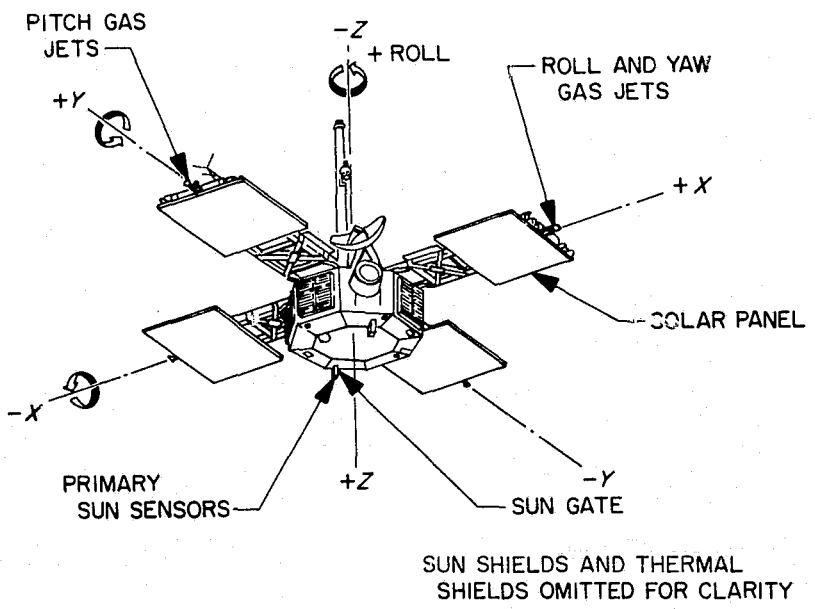

Fig. 38. *Mariner* Venus 67 spacecraft

Outputs of the three sensors are telemetered to earth with other engineering data so that spacecraft orientation vs time may be reconstructed. A typical history of spacecraft motion is shown in Fig. 39 where pitch, yaw, and roll motion is plotted vs time on July 25, 1967. Slope

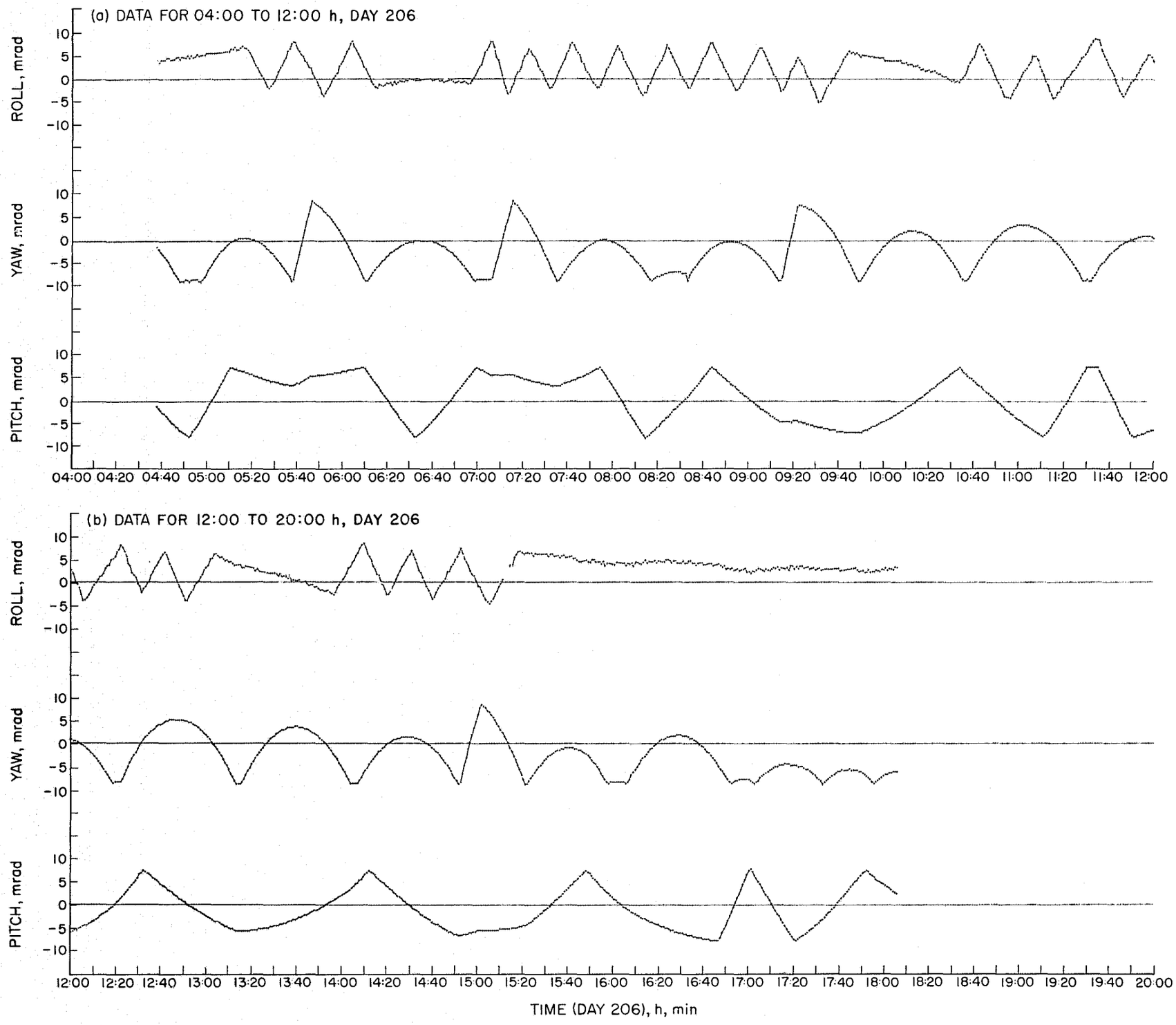

Fig. 39. Attitude angles vs time

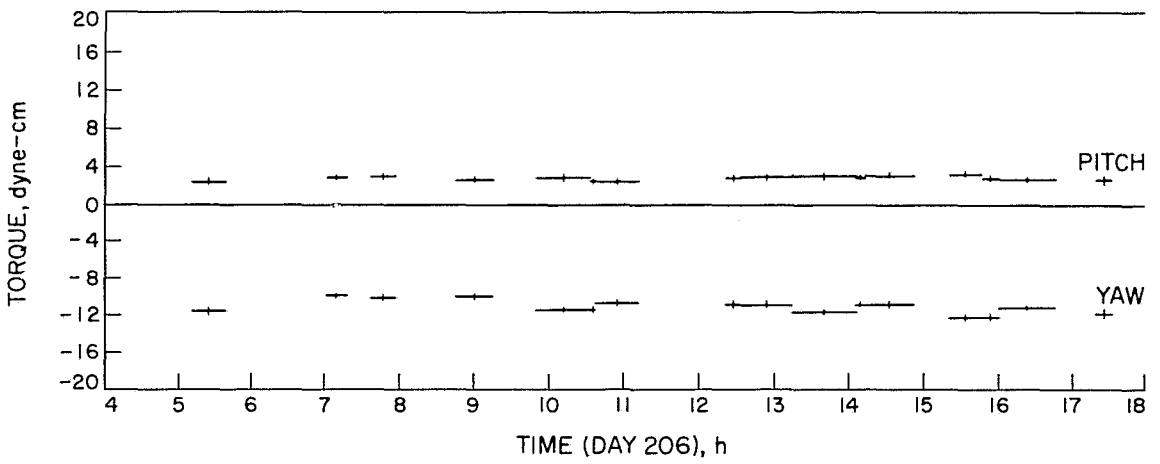

Fig. 40. Pitch and yaw torque vs time

discontinuities which occur at the edge of the dead band are due to thruster firings.

III. Spacecraft Torques

From analysis of the attitude data it is possible to deduce the torque history of the spacecraft by the method given in Ref. 7. This was done for the pitch and yaw axes for 25 days through the mission (roll was omitted because the data was more noisy than that in pitch and yaw, and the telemetry resolution more coarse). A plot of the total pitch and yaw torque vs time for several hours is shown in Fig. 40. Note that error flags, calculated by a method described in Ref. 8, are plotted on top of the torque levels to give an idea of the confidence in the results. Where the torque uncertainty was greater than ± 1 dyn-cm, the plot has been omitted; an example of this is between 14 h 50 min and 15 h 20 min where the relatively short segments between thruster firings in yaw preclude accurate torque calculations (Fig. 40).

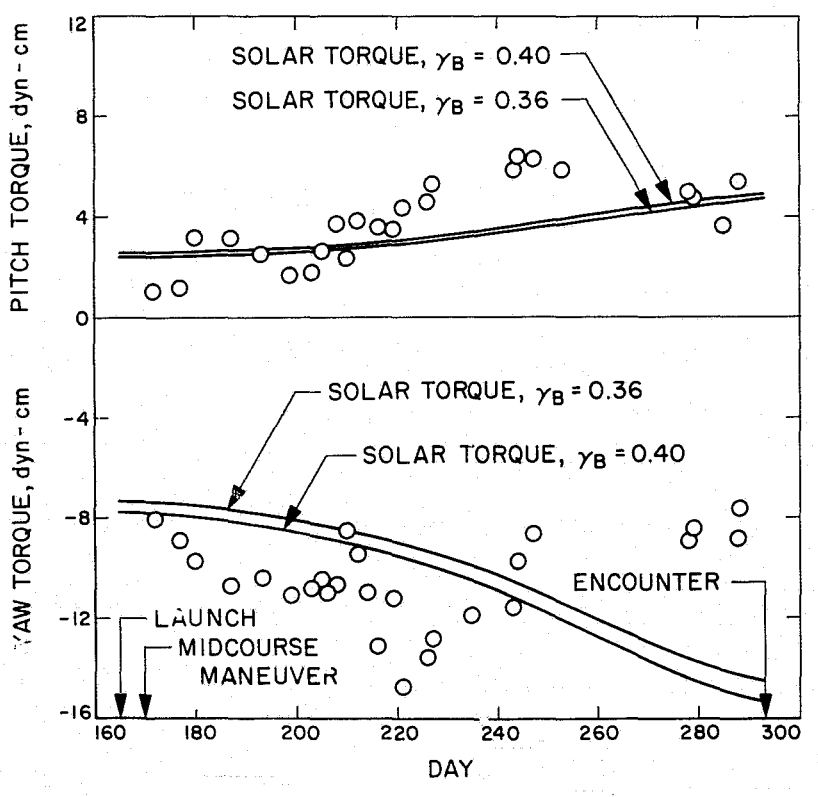

Fig. 41. Daily torque averages for pitch and yaw

It may be seen from Fig. 40 that the torques on both axes are relatively constant over the length of a day. This is in marked contrast to *Mariner IV* results as reported in Ref. 9, where substantial changes (on the order of 5 dyn-cm) were found to take place from thruster firing to firing. These high-frequency torque variations on *Mariner V* are found to be on the order of 1 to 2 dyn-cm; however, long term variations of several dyn-cm are apparent. These are illustrated in Fig. 41 in which pitch and yaw torque are averaged over one day and are plotted as single points for several representative days throughout the mission.

IV. Spacecraft Forces

To separate the translational forces due to solar pressure from the forces due to the attitude control systems, it is necessary to separate the associated torques. Solar torques arise from a displacement of the spacecraft center of mass from the solar center of pressure. The post-maneuver spacecraft center of mass is located at $x = 1.83$ cm, $y = 0.58$ cm, and $z = -30.9$ cm; although these values are calculated, the performance of the autopilot during the midcourse maneuver indicated that they are quite accurate.[1] The solar center of pressure was assumed

[1]E. H. Kopf, Jr., Jet Propulsion Laboratory, Spacecraft Control Section, personal communication.

to be along the roll axis since the sun side of the spacecraft is almost reflectively symmetric (Fig. 38). The solar force acts nominally in the $-z$ direction, and is described in Part I as

$$F_{solar\ pressure} = \frac{kA}{R^2}(1 + \gamma_B)$$

where k is the solar radiation constant, A is the spacecraft effective area, R is the sun–spacecraft distance, and γ_B is the overall reflection coefficient. Using these values, the solar torque in pitch and yaw has been plotted as a function of time as the smooth curves in Fig. 41. Two values of γ_B are used corresponding to the extremes in this quantity obtained in the SPODP solutions.

It is evident from Fig. 41 that the total spacecraft torque is not due simply to solar pressure. The difference between the solar torque curves and the daily averaged torques is thought to be caused by thruster leakage. Indeed, tests performed recently on thruster leaks indicate that torques of this magnitude are consistent with valve leak specifications (Ref. 10). Accordingly, the difference between the curves and points in Fig. 42 is interpreted as due to leakage of one or more thrusters. If the leakage in the four thrusters controlling pitch is random, then the variance of the force they produce equals the variance in the torque they produce divided by the center of mass to thruster distance ℓ. Hence, the translational forces can be inferred statistically by examining the quantity

$$\frac{M_i}{\ell}$$

where M_i is the leakage torque, in either pitch or yaw, and ℓ equal 248 cm. Figs. 42 and 43 show this ratio as a function of time.

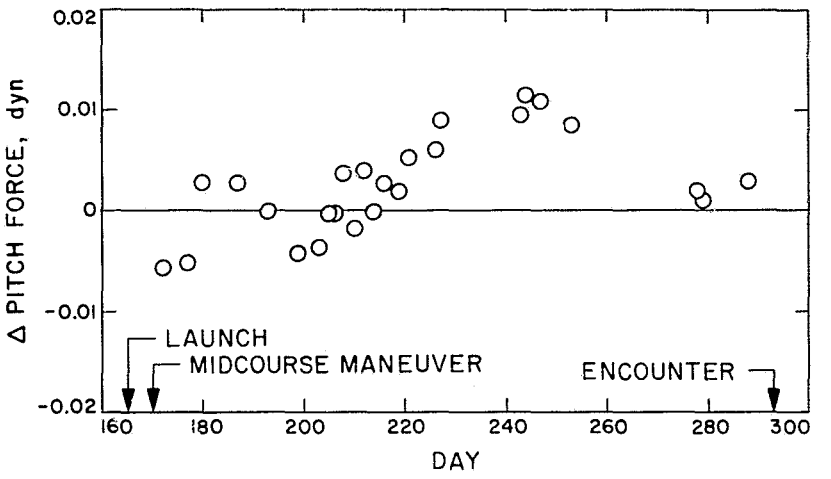

Fig. 42. Pitch torque/ℓ vs time

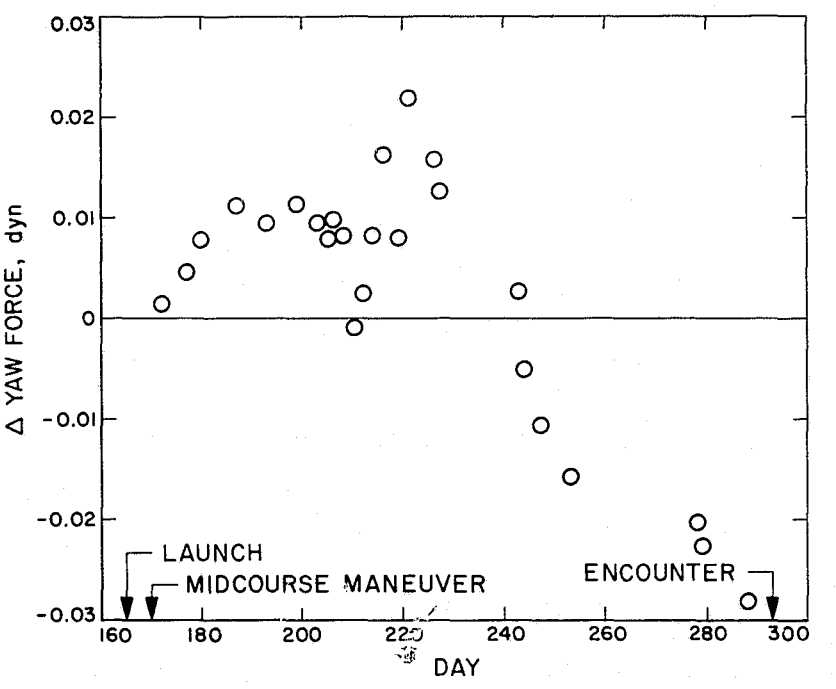

Fig. 43. Yaw torque/ℓ vs time

V. Conclusions

The forces produced by the attitude control system are on the order of 0.02 dyne corresponding to leaks of about 1 std cm³/h. These are 0.3 to 0.5% of the solar force and, therefore, approximately the same as its uncertainty. Furthermore, the variation in γ_B between 0.40 and 0.36 over the life of the mission corresponds to a 3% variation in solar force, or about 0.15 dyne. Hence, the changes in the spacecraft force, which are interpreted by SPODP to be a variation in γ_B, cannot be caused by the attitude control system. The basic conclusion is that attitude control system forces had a negligible effect on the *Mariner V* trajectory in comparison to other unknowns.

The *Mariner V* Flight Path and its Determination from Tracking Data

Part III. Mission Trajectory

J. A. Borras

I. Launch Phase

The *Mariner V* spacecraft was launched from Launch Complex 13 at the Air Force Eastern Test Range (AFETR), Cape Kennedy, Florida, on Wednesday, June 14, 1967. The launch vehicle consisted of an *Atlas D*/*Agena D* combination. Liftoff occurred at $06^h01^m00^s.176$ GMT, with an inertial launch azimuth of 101.1 deg east of north. After liftoff, the booster rolled to an azimuth of 102.3 deg and performed a programmed pitch maneuver until booster cutoff. During the sustainer and vernier stages, adjustments in vehicle attitude and engine cutoff times were commanded, as required, to adjust the altitude and velocity at the *Atlas* vernier cutoff. Vernier engine cutoff occurred as anticipated at 317.75 s into the mission. Following *Atlas* cutoff the shroud protecting the spacecraft during the ascent through the atmosphere was jettisoned and the *Atlas* booster separated from the *Agena* stage. The *Agena* engine was then burned for 142.5 s, injecting itself and the spacecraft into a near circular parking orbit at $06^h09^m45^s.360$ GMT at an altitude of 185.04 km (see Figs. 44 and 45).

After a parking orbit coast time of 13.28 min, determined by the ground guidance computer and transmitted to the *Agena* during the *Atlas* vernier stage, a second ignition of the *Agena* engines occurred. The burn duration was 94.40 s after which the *Agena* and the spacecraft were traveling in a geocentric escape hyperbola at 11.40 km/s. The *Agena* and spacecraft then separated after which the *Agena* performed a maneuver to place

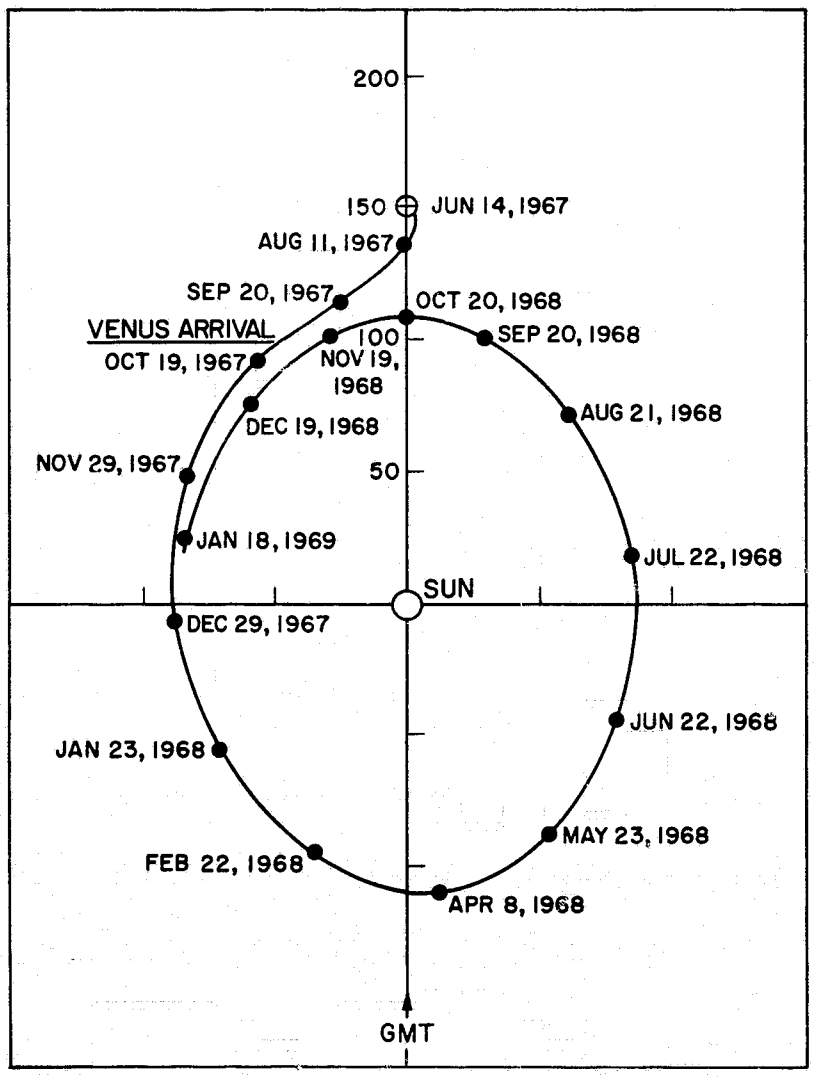

Fig. 44. Sun-earth line plot, *Mariner V*, from June 1967 to January 1969

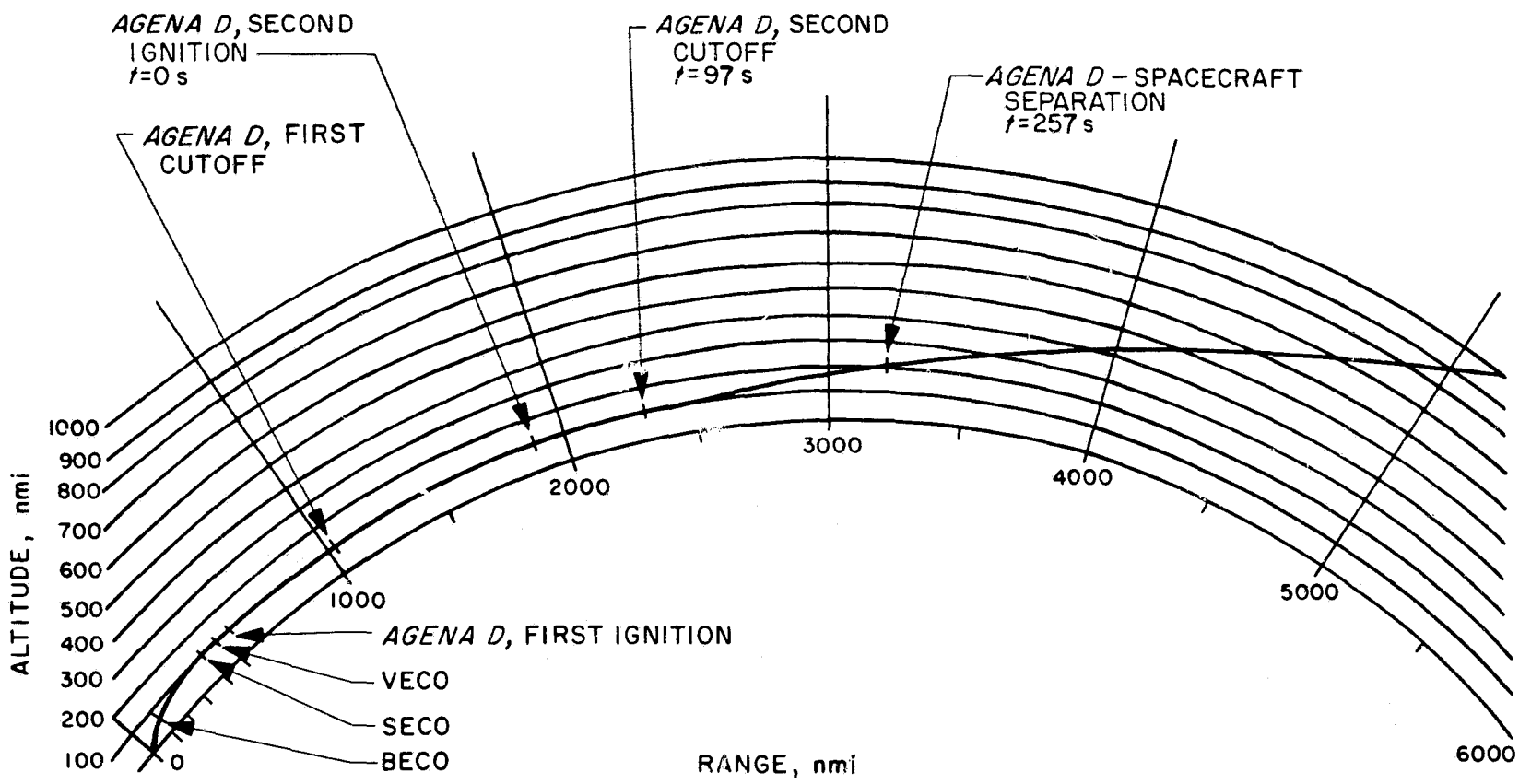

Fig. 45. Ascent trajectory profile

Table 12. Geocentric characteristics of *Mariner V* trajectory

Characteristics	Preencounter, injection	Preencounter, postmidcourse	Encounter
Parameter			
Radius R, km	6569.6304	1,581,614.7	79,764,369
Inertial speed V, km/s	11.400128	2.9906291	25.350066
Earth-fixed speed v, km/s	10.989368	112.96141	5767.1726
Geocentric latitude ϕ, deg	−4.6930562	−11.661170	6.0399302
Longitude θ, deg	351.53082	245.89289	230.61465
Right ascension Θ, deg	349.55227	140.46105	161.85034
Path angle of inertial velocity Γ, deg	1.8980037	89.329033	40.868340
Azimuth of inertial velocity Σ, deg	119.97742	61.817187	117.01311
Path angle of Earth-fixed velocity γ, deg	1.9689745	1.5169653	0.16479112
Azimuth of Earth-fixed velocity σ deg	121.22208	270.00839	269.91349
Time of event T, GMT	06:24:37.100 (June 14, 1967)	23:08:20.650 (June 19, 1967)	17:34:55.841 (October 19, 1967)
Hyberbolic orbital element			
Semimajor axis a, km	−46,261.501	−47228.659	
Eccentricity e	1.1418646	1.0783954	
Inclination to Earth's equator i, deg	30.308785	30.315918	
Longitude of ascending node Ω, deg	161.47921	161.12906	
Argument of perigee ω, deg	185.77009	179.05761	
Perigee distance p, km	6562.8713	3702.5079	
Time of perigee passage T, GMT	06:24:01.322 (June 14, 1967)	06:14:55.037 (June 14, 1967)	

it in a separate orbit from that of the spacecraft so as to reduce the probability of the *Agena* impacting Venus and, hence, contaminating its surface.

II. Premaneuver Phase

Injection (second *Agena* cutoff) occurred at $06^h24^m35^s.500$ GMT over the Atlantic Ocean at a geocentric latitude of −4.67 deg and longitude of 351.54 deg. At that time, the *Agena*/spacecraft combination was at an altitude of 192.65 km and traveling at an inertial speed of 11.40 km/s. The geocentric characteristics of the *Mariner V* trajectory are listed in Table 12.

The spacecraft/*Agena* combination was in earth's shadow from launch to 19.27 min after launch. *Agena*/spacecraft separation occurred 161.3 s after transfer orbit injection. Within an hour after injection, the spacecraft was receding from the earth in an almost radial direction, with decreasing speed. This reduced the geocentric angular rate of the spacecraft, in inertial coordinates, until the angular rate of the earth's rotation exceeded that of the spacecraft. This phenomenon is illustrated (Fig. 46) on a map showing the earth track of the spacecraft reversing its direction from increasing to decreasing longitude. Also shown is the tracking station coverage and location of the various boost vehicle and spacecraft events.

Due to the low sensitivities of the transfer orbits of both the spacecraft and the *Agena* to changes in the injection (the second *Agena* cutoff) conditions, it was necessary to bias the targeted aiming point away from the target Venus. This was done to ensure a probability of less than 3×10^{-5} of the *Agena* or spacecraft impacting and contaminating Venus. After several days of continuous tracking, it was estimated that, without a midcourse correction, the spacecraft was on a nominal biased trajectory that would pass the leading edge of Venus at a

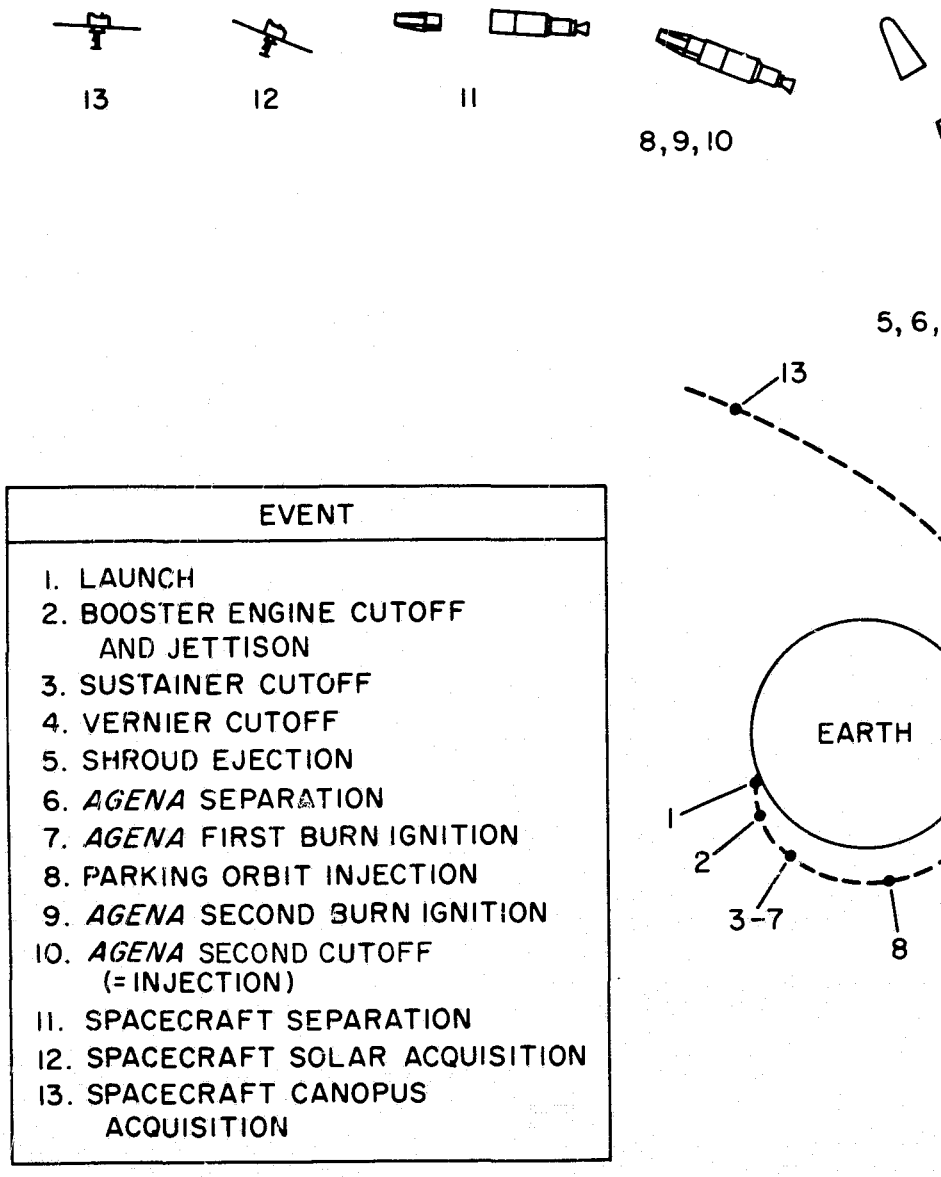

Fig. 46. Sequence of events to Canopus acquisition

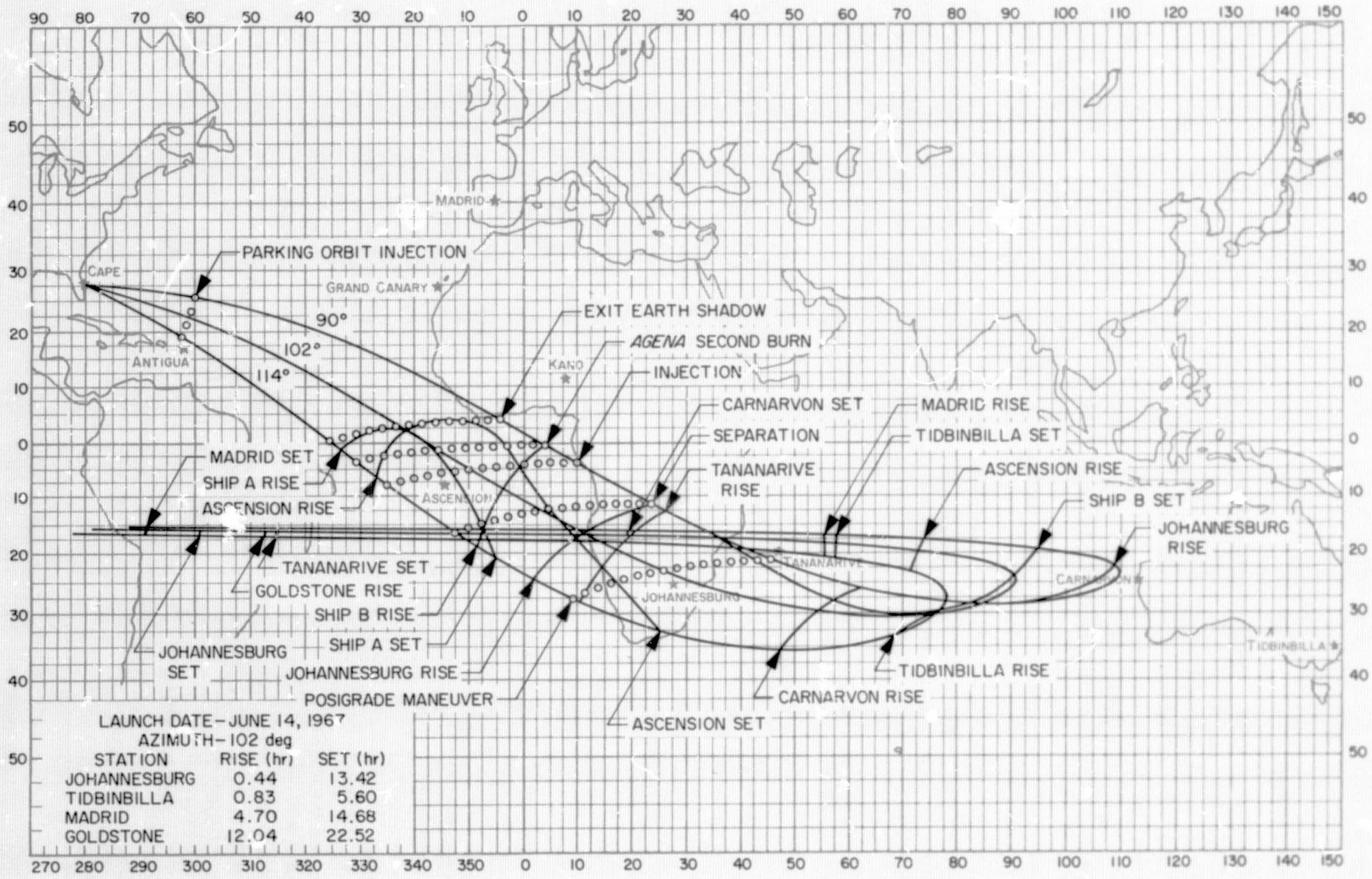

Fig. 47. Earth tracks for June 14, 1967

closest approach altitude of 69,693 km. Closest approach would have occurred at $03^h52^m45^s.155$ (GMT) on October 19, 1967.

The trajectory was altered by the midcourse maneuver so that the spacecraft would pass approximately 10,200 km from the center of Venus (4000 km from the surface), at closest approach. In addition to altering the miss distance at Venus, this correction changed the arrival time to $17^h35^m00^s$ GMT, October 19, 1967, and thus allowed the spacecraft's CC&S to activate various subsystems at the correct times near encounter and for closest approach to occur over the prime tracking station, Goldstone, California. The midcourse motor was ignited at 23:08:06 GMT, June 19, 1967, at which time the spacecraft was at a geocentric range of 1,581,570.3 km and traveling at an inertial speed of 2.9915344 km/s relative to earth.

III. Cruise Phase

Following the midcourse maneuver, the spacecraft reacquired the sun and Canopus and returned to the cruise mode. At this time, the spacecraft was moving primarily under the gravitational influence of the sun in an ellipse with the sun at the focus. During the early portion of the cruise phase, the spacecraft's heliocentric velocity was less than that of the earth's; this caused the spacecraft to trail the earth for several days around the sun. This phenomenon is illustrated in Fig. 47 which contains a heliocentric plan view of the trajectory of *Mariner V* holding a fixed sun–earth line. However, *Mariner V* began moving closer to the sun thus picking up speed, catching up to the earth, and eventually passing it.

Earth–probe distance curves, celestial latitude, celestial longitude, heliocentric distance, Venus/probe distance, and cone and clock angle of earth as functions of time from launch to end of 1967 are shown in Figs. 48–53. The heliocentric characteristics of the *Mariner V* trajectory are shown in Table 13.

Table 13. Heliocentric orbital elements of *Mariner V* trajectory

Elliptical orbital element	Preencounter orbit	Postencounter orbit
Semimajor axis, a, km	129,733,170	98,313,649
Eccentricity e	0.17436497	0.11849217
Inclination to the ecliptic i, deg	2.6968311	1.3733747
Longitude of ascending node Ω, deg	81.968201	114.58310
Argument of perihelion ω, deg	350.65626	91.603240
Perihelion distance p, km	107,112,250	86,664,251
Time of perihelion passage T, GMT	10:45:37.572 (Oct 28, 1967)	08:59:27.189 (Jan 4, 1968)
Period P, days	294.97604	194.59467

During the interplanetary phase of the flight, several orbital computations were made covering the period from June 19, 1967 when the midcourse maneuver was performed, to October 19, 1967 when encounter with Venus occurred. These computations stabilized very early in the flight of *Mariner V* and the predicted near-Venus orbit did not change by any considerable amounts.

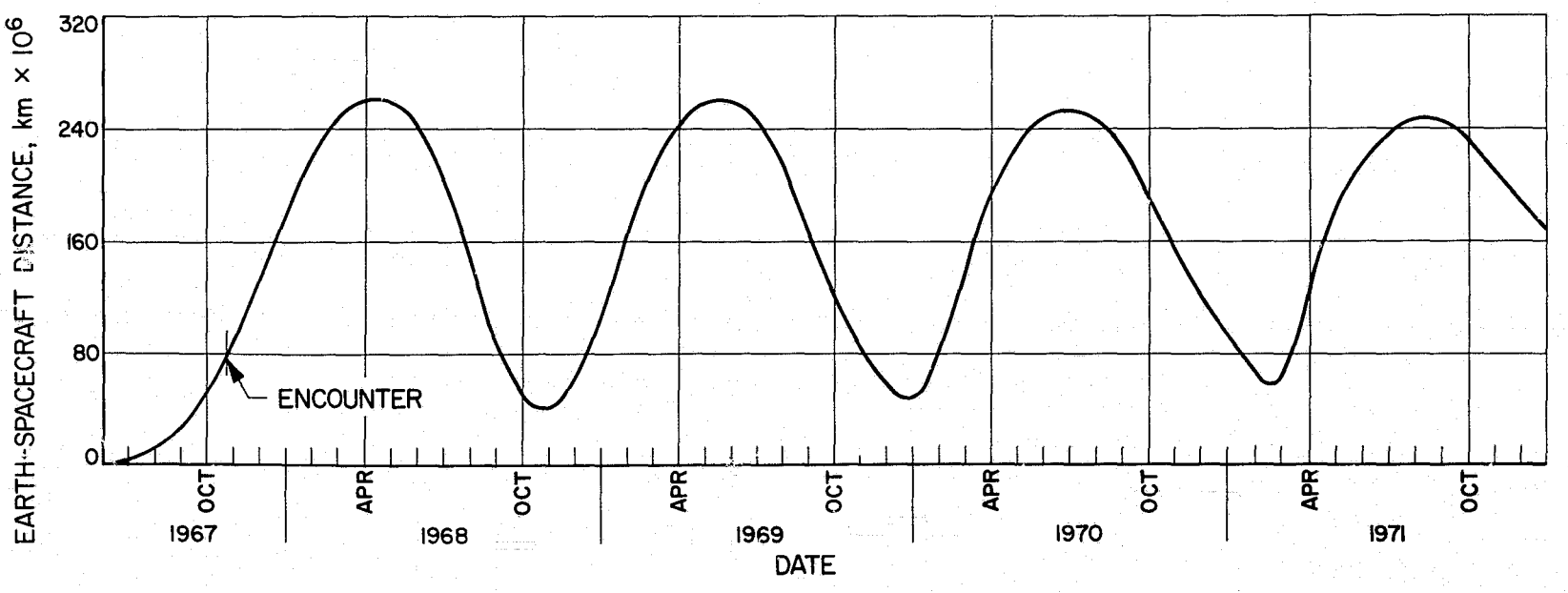

Fig. 48. Spacecraft distance from earth, launch through 1971

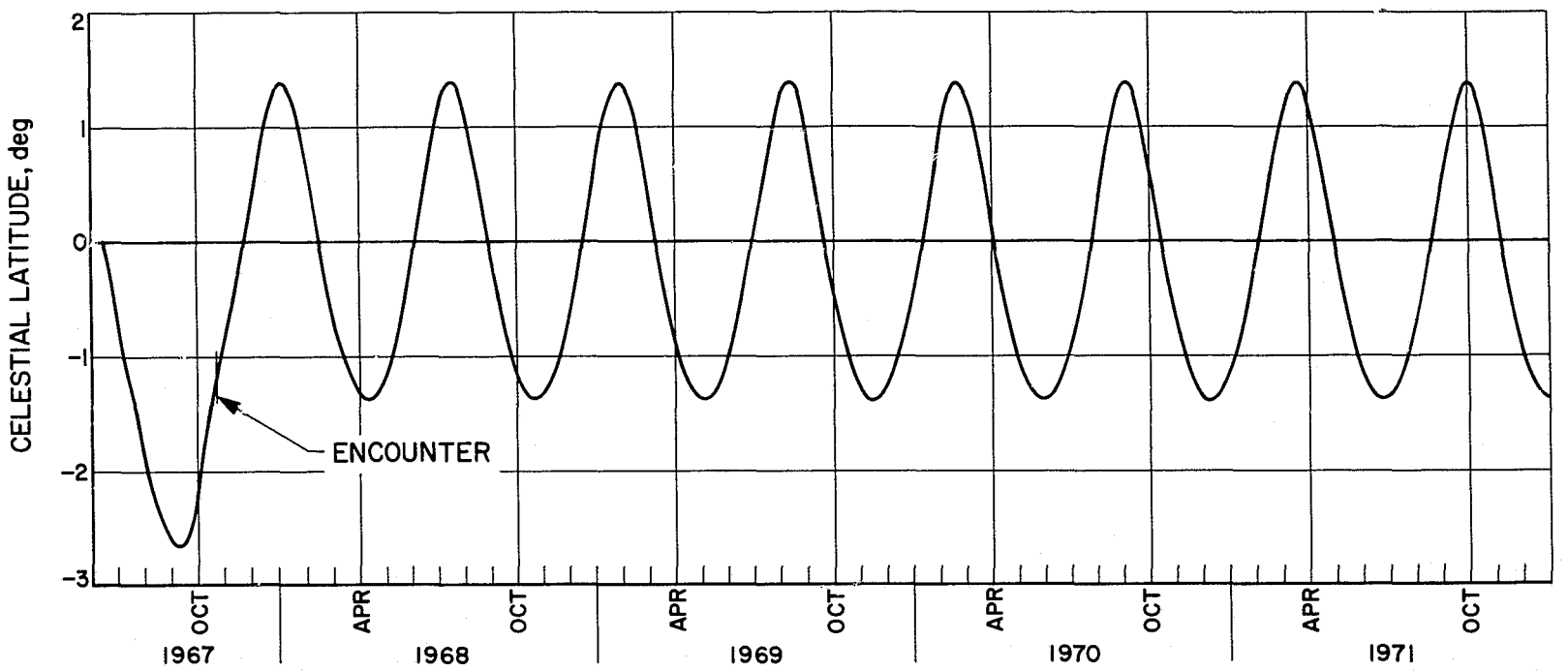

Fig. 49. Spacecraft celestial latitude, launch through 1971

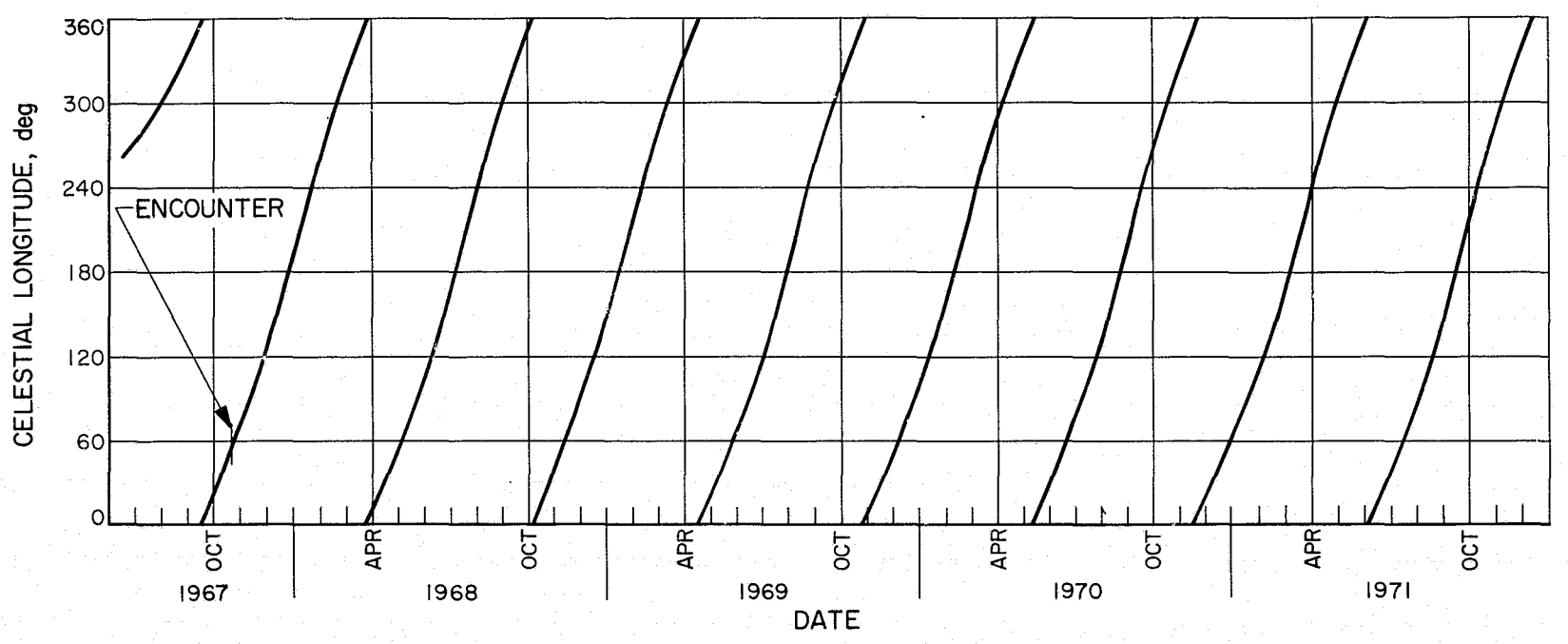

Fig. 50. Spacecraft celestial longitude, launch through 1971

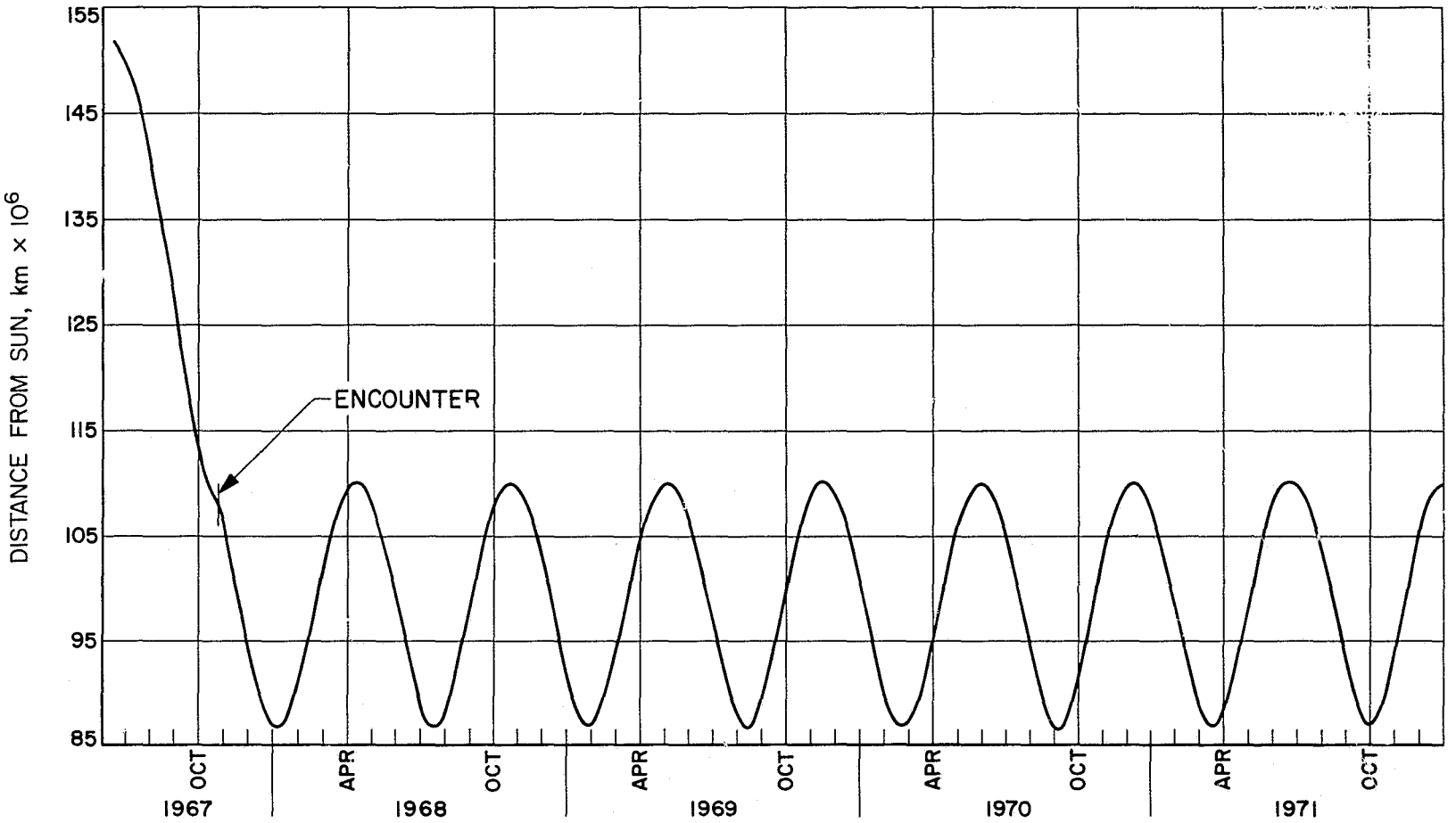

Fig. 51. Spacecraft distance from sun, launch through 1971

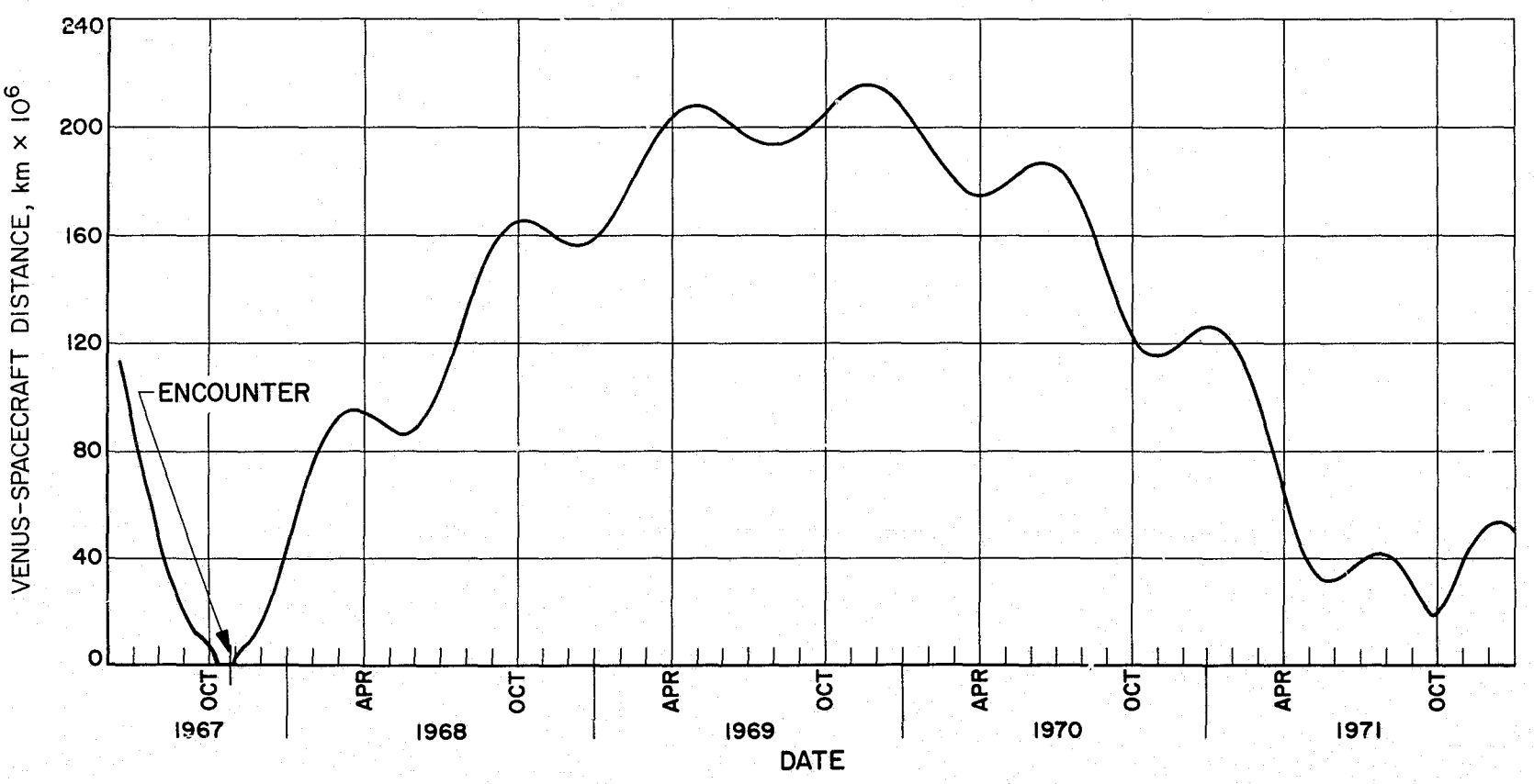

Fig. 52. Spacecraft distance from Venus, launch through 1971

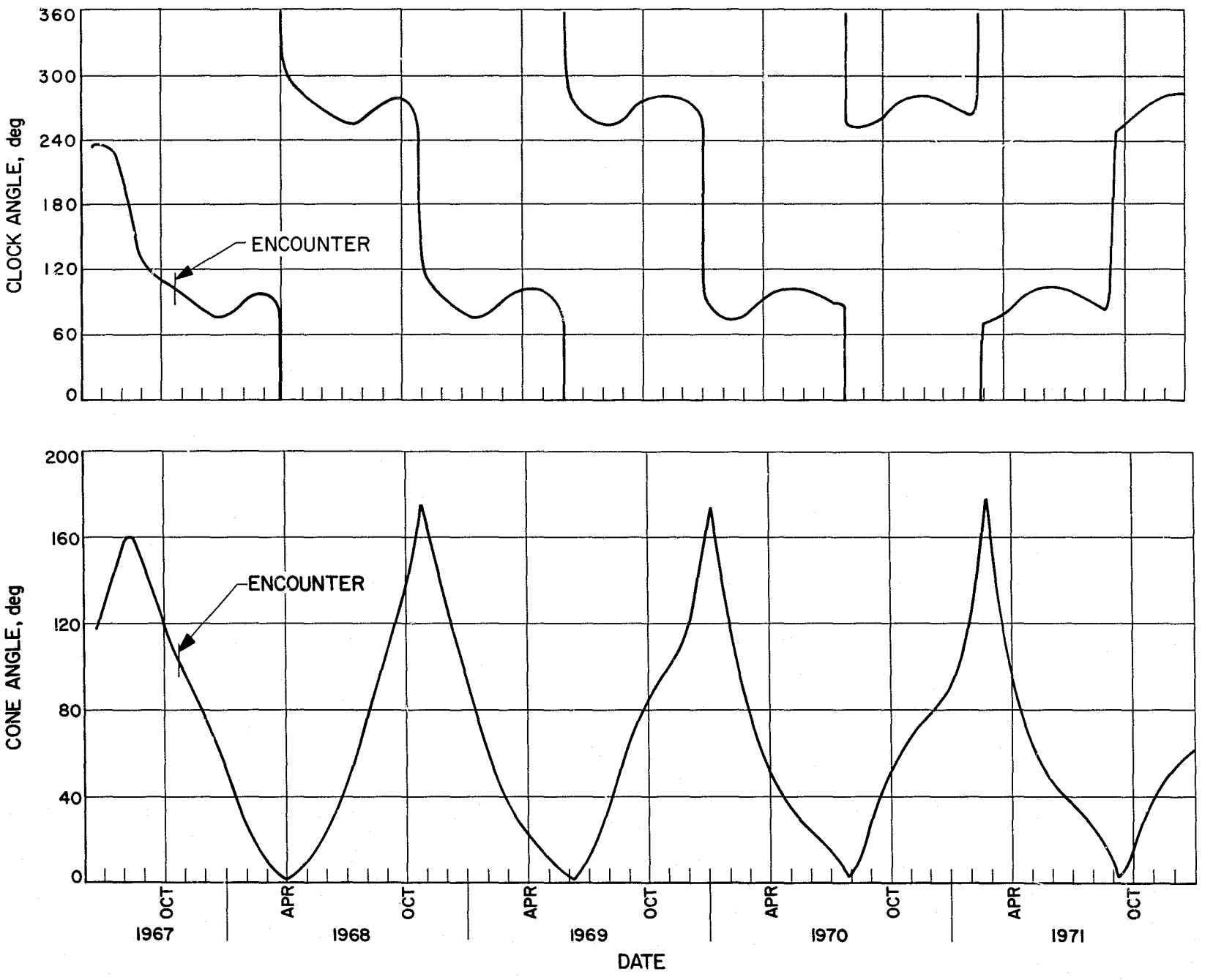

Fig. 53. Clock and cone angles of earth, launch through 1971

The Aphrodiocentric characteristics of the *Mariner V* trajectory as predicted during the interplanetary portion of the flight are listed in Table 14.

IV. Encounter Phase

Mariner V approached Venus along the leading edge and from outside the planet's orbit. At about 3.3 min before closest approach, the radio signal was lost as the spacecraft occulted Venus. While the spacecraft was behind the planet, the antenna position was switched automatically from its original position by a sensor which triggered the mechanism when it saw the planet terminator approximately half-way through the occultation. The new

Table 14. Aphrodiocentric orbital elements of *Mariner V* trajectory

Hyperbolic orbital element	Preencounter prediction	Actual Venus encounter orbit
Semimajor axis a, km	−34,825.175	−34,824.285
Eccentricity e	1.2917091	1.2914715
Inclination to the ecliptic i, deg	32.001963	31.700211
Longitude of ascending node Ω, deg	341.30976	341.19472
Argument of periapsis ω, deg	152.82175	152.92873
Periapsis distance p, km	10,158.819	10,150.288
Time of periapsis passage T, GMT	17:34:22.823 (Oct 19, 1967)	17:34:55.841 (Oct 19, 1967)

antenna position compensated for the trajectory bending near the planet; this would have displaced the antenna beam from its ideal position during emergence from occultation, thus enhancing the chances of a rapid reacquisition of the signal as it passed through the atmosphere of Venus coming out of occultation.

Tracking data gathered and analyzed during the encounter sequence indicated that the Venus encounter trajectory predicted during the cruise portion of the flight did not differ significantly from the observed encounter trajectory. The Aphrodiocentric characteristics of the *Mariner V* trajectory determined from encounter data are given in Table 14. A plot of the encounter velocities and altitude is shown in Fig. 54, which describes the closest approach epoch of October 19, 1967, at $17^h34^m55^s.8$.

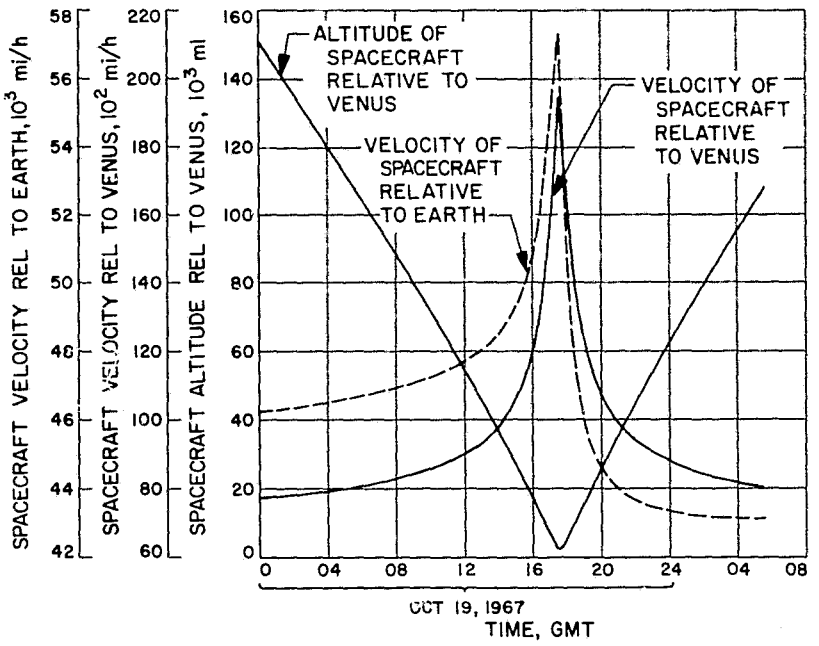

Fig. 54. Encounter velocities and altitude

V. Postencounter Phase

The planet's gravitational pull altered the spacecraft's heliocentric orbit, as it left the vicinity of Venus, to the extent of changing the perihelion distance from 107,112,250 km to 86,664,251 km. The change in other elements of the trajectory are shown in Table 2.

Mariner V returned for a close pass at earth on October 27, 1968, when it was within 38,995,000 km. It will return to the vicinity of earth approximately every 14 months.

The next time *Mariner V* will be near Venus will be at the end of October 1975. The closest approach distance to Venus will be 4,300,000 km. The heliocentric characteristics of the *Mariner V* postencounter trajectory are shown in Table 13. The trajectories of *Mariner V* and *Mariner IV* are illustrated in a heliocentric plan view of the ecliptic in Fig. 55. The cone angle and clock angle of earth during the near-Venus portion of the trajectory are shown in Figs. 56 and 57, respectively. Plots of the postencounter celestial latitude, celestial longitude, heliocentric distance, earth–probe distance, Venus–probe distance, cone angle of Canopus, cone angle of earth, and clock angle of Earth are presented in Figs. 58–65.

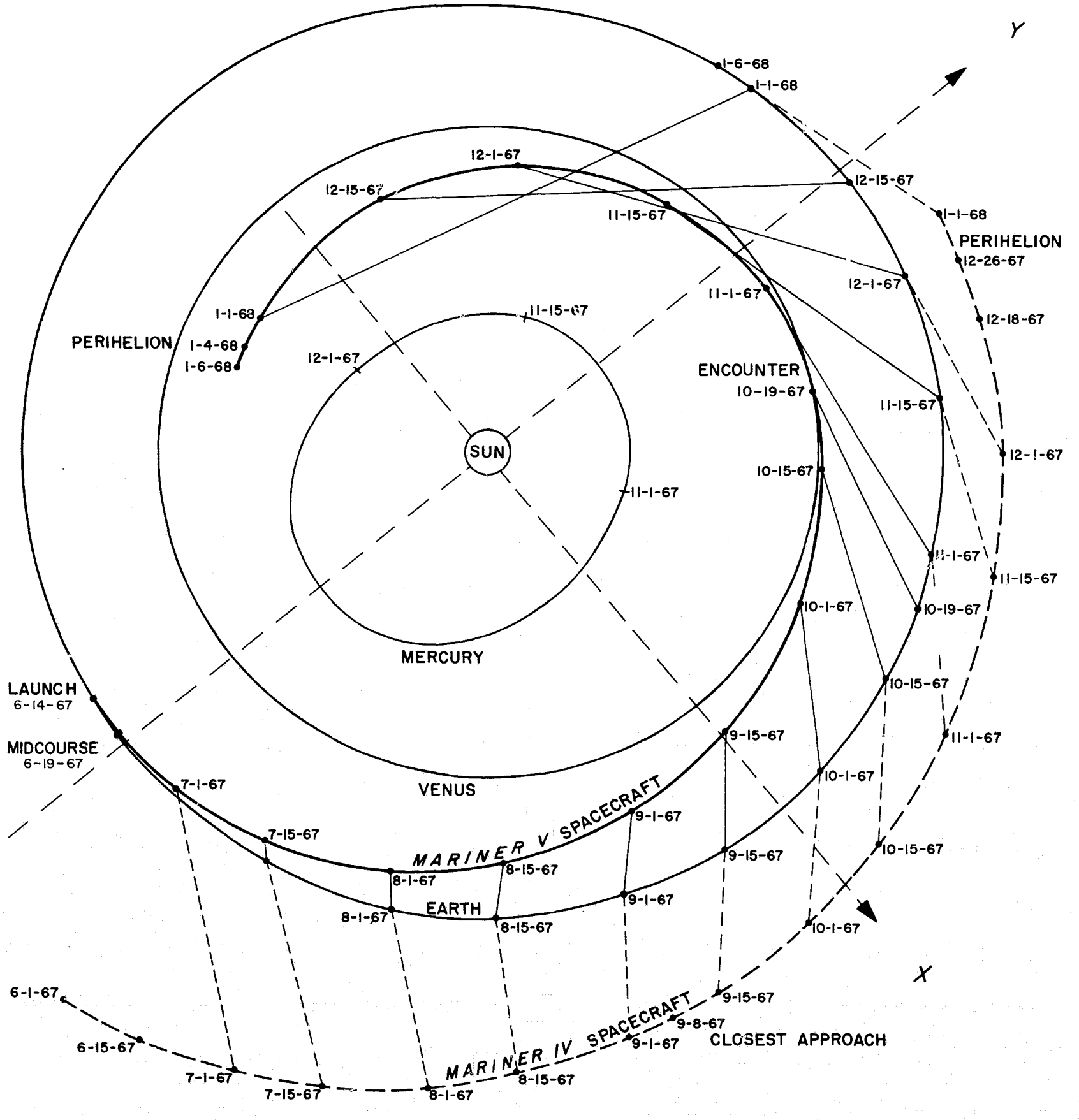

Fig. 55. Heliocentric plan view of *Mariner IV* and *Mariner V*

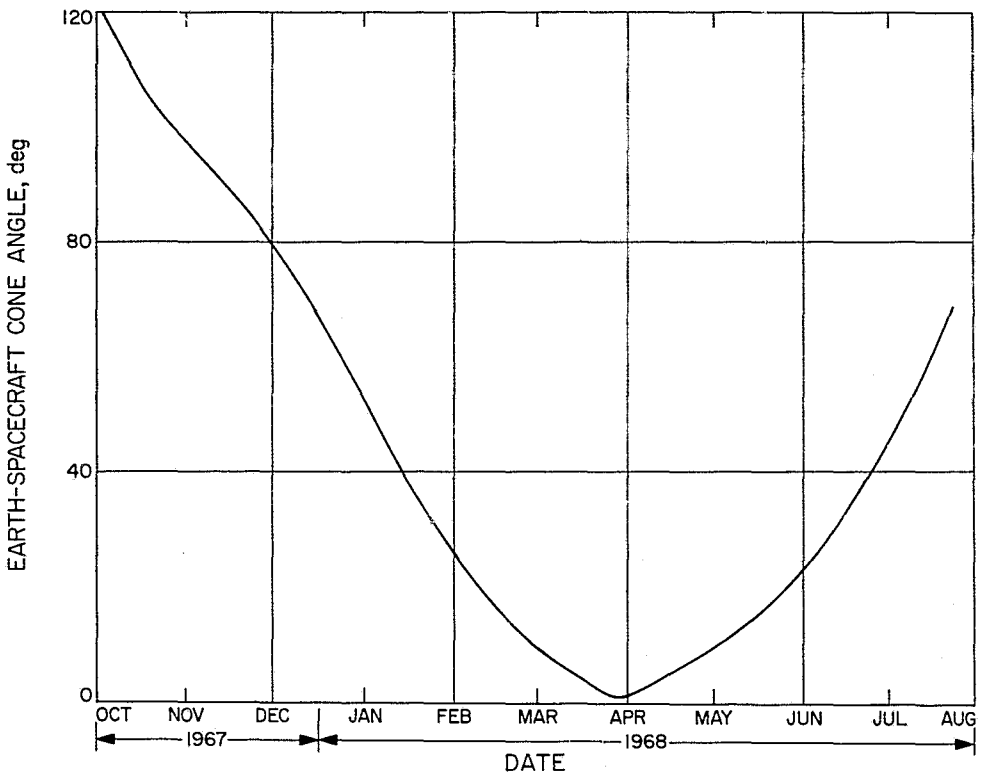

Fig. 56. *Mariner V* earth cone angle, deg

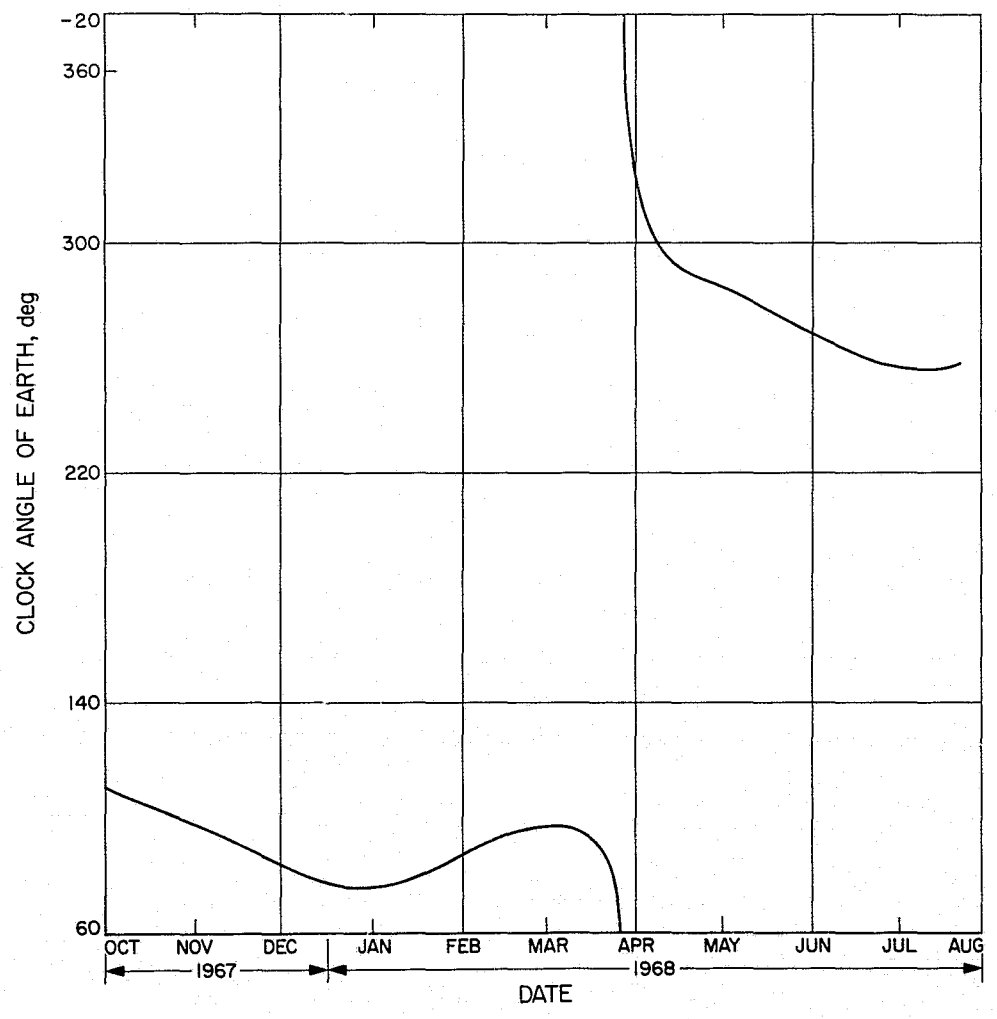

Fig. 57. *Mariner V* earth clock angle, deg

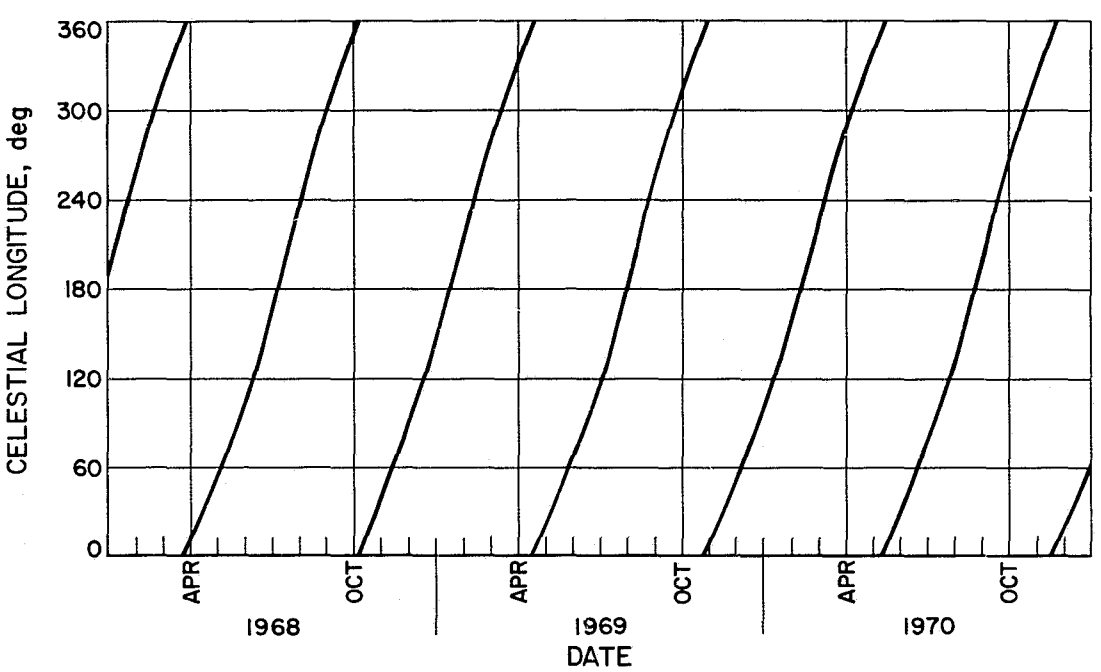

Fig. 58. Celestial longitude, 1968 through 1970

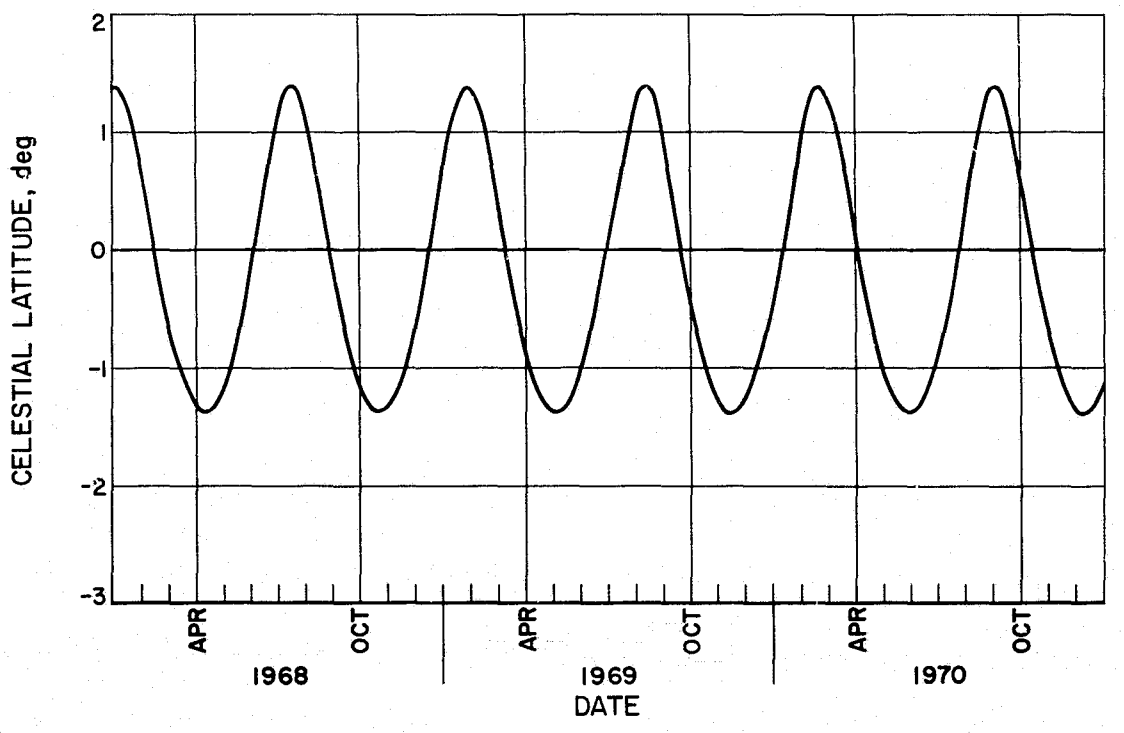

Fig. 59. Celestial latitude, 1968 through 1970

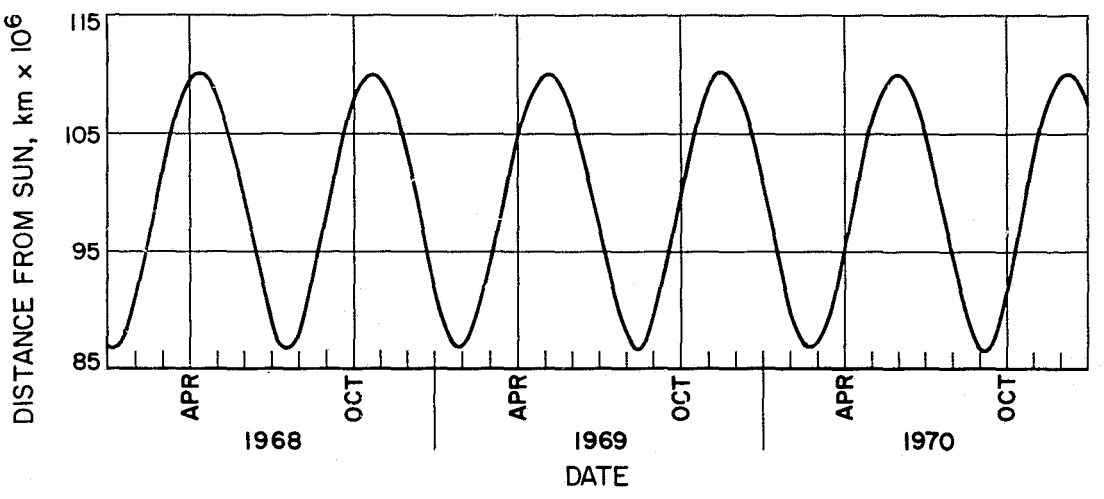

Fig. 60. Spacecraft distance from sun, 1968 through 1970

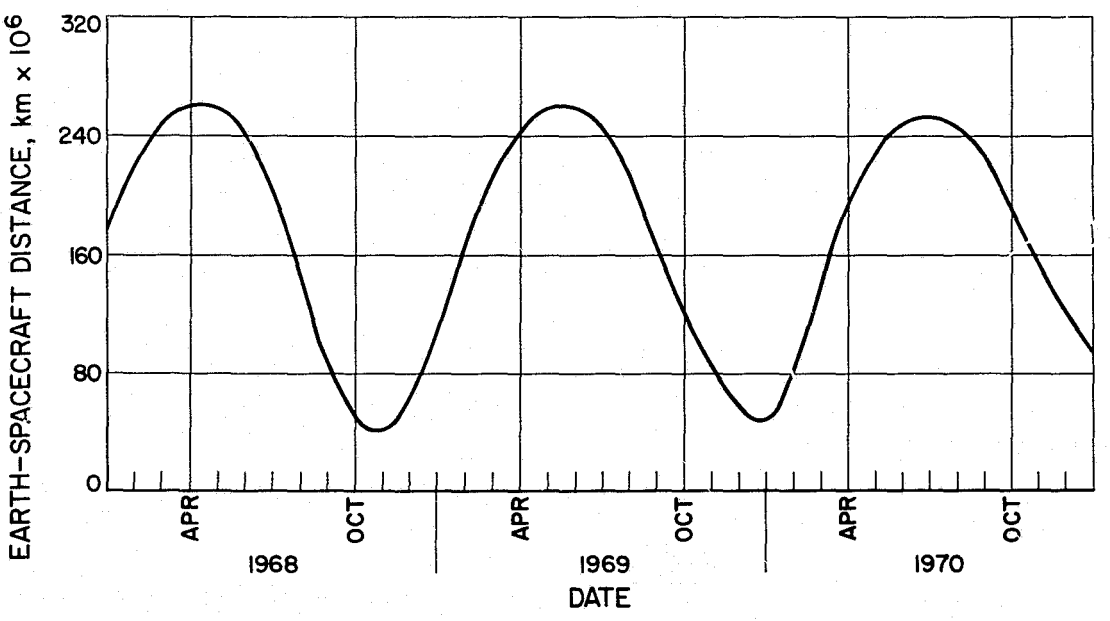

Fig. 61. Spacecraft distance from earth, 1968 through 1970

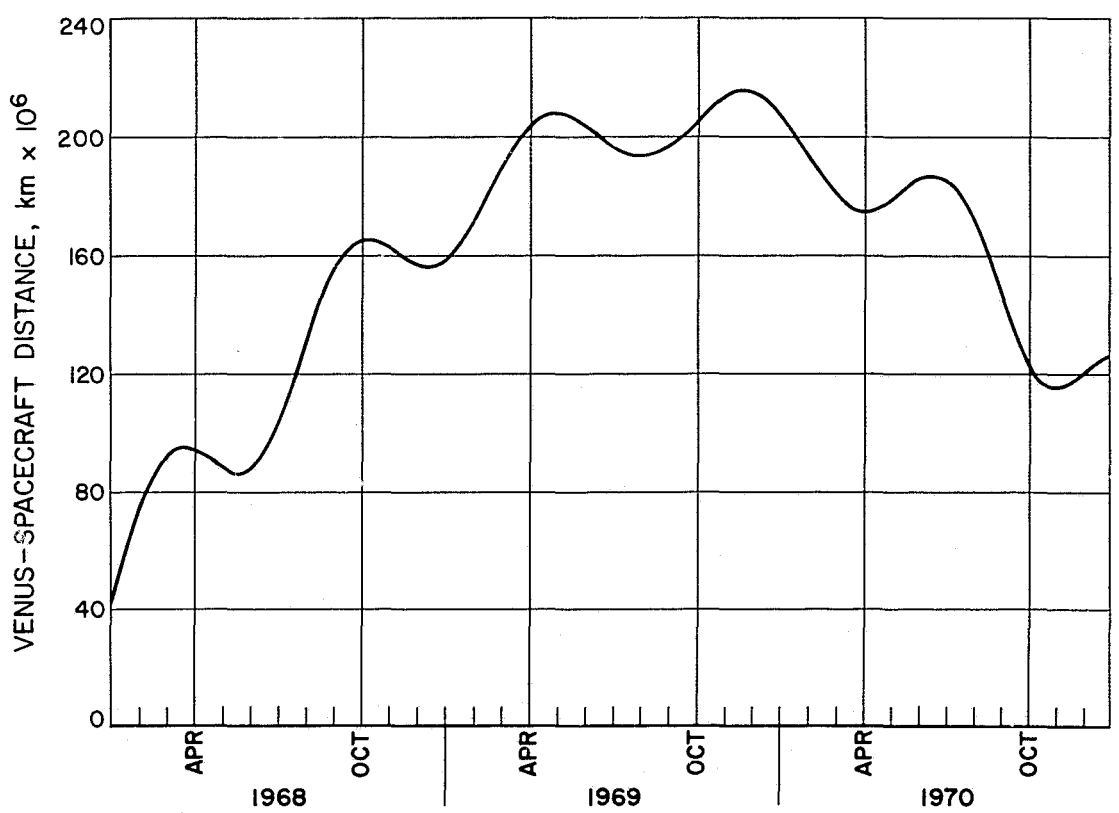

Fig. 62. Spacecraft distance from Venus, 1968 through 1970

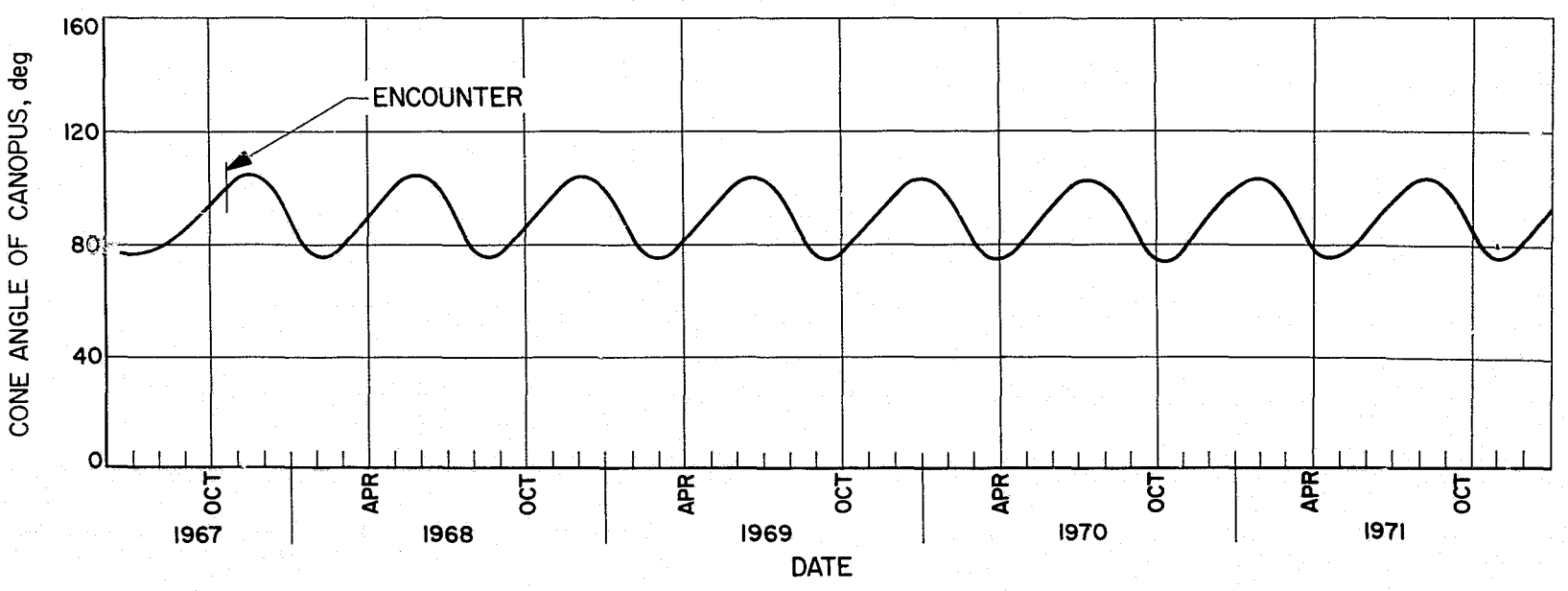

Fig. 63. Cone angle of Canopus, launch through 1971

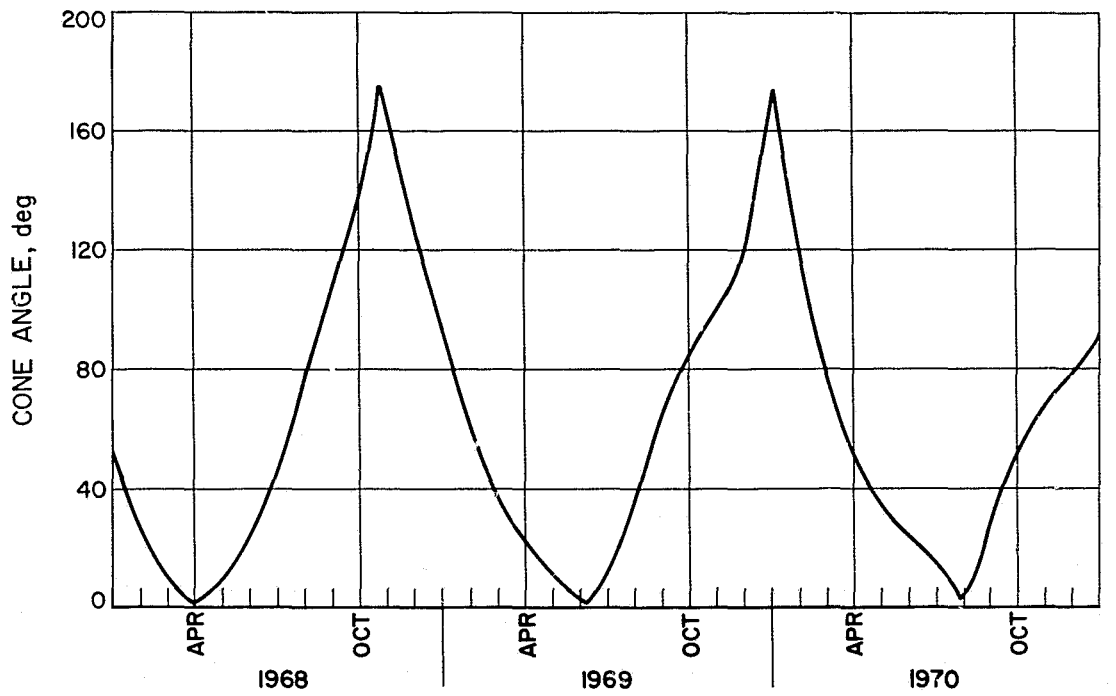

Fig. 64. Cone angle of earth, 1968 through 1970

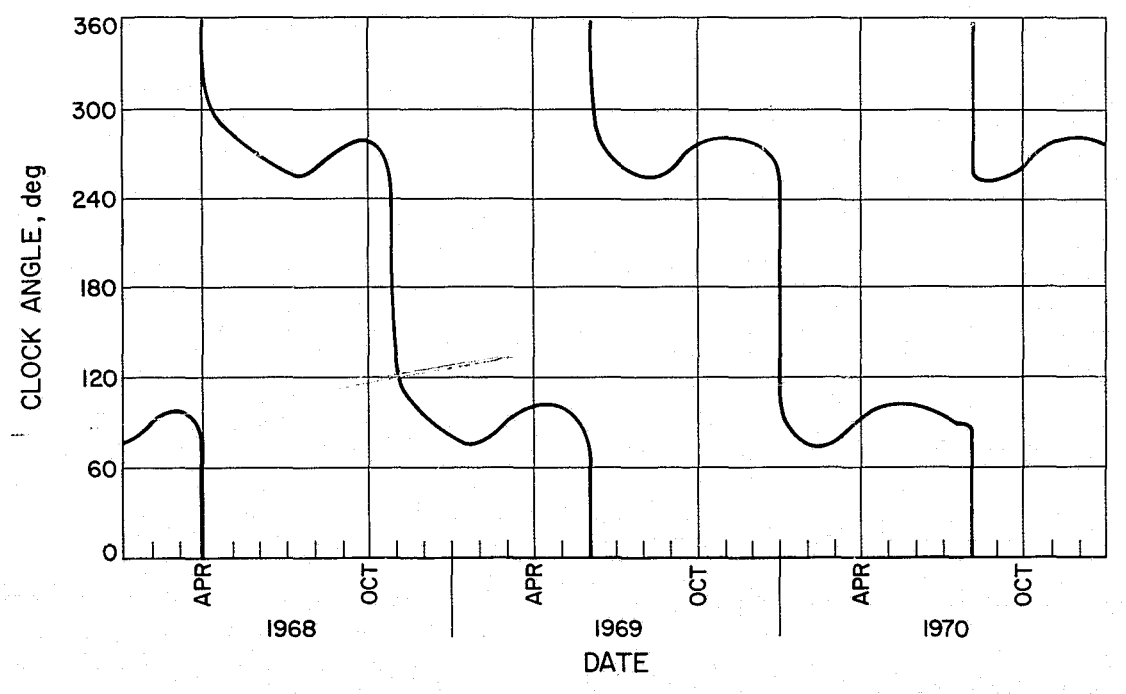

Fig. 65. Clock angle of earth, 1968 through 1970

The *Mariner V* Flight Path and its Determination from Tracking Data

Part IV. Midcourse Maneuver Program

R. T. Mitchell

The computer program used in real-time operations to determine the maneuver parameters, known as the Midcourse Maneuver Operations Program (MMOP), consists of five independent operational blocks. A functional block diagram of the program, indicating a typical logic flow for standard operations is shown in Fig. 66. Control from link to link is manual, and in each case, after completion of the last requested link, control is returned to the Introductory Printout. The five operational blocks of the MMOP are:

(1) Introductory Printout (INTRO). The INTRO link accepts input from cards and disk, performs preliminary calculations, and provides the printout for all input. The control of all other links is handled through INTRO.

(2) Midcourse Decision Program (DECPR). The purpose of the DECPR is to compute the maneuver parameters (velocity increment, pitch turn, roll turn) and test for violation of three constraints; i.e., propulsion, time of flight, and low-gain antenna. The propulsion and the time of flight constraints are hard constraints. If it is not possible to reach the $\mathbf{B}\cdot\mathbf{R}$, $\mathbf{B}\cdot\mathbf{T}$ location requested without violating one of these constraints, DECPR will print a message to that effect and return to INTRO. If it is possible to satisfy the propulsion and time of flight constraints for a different $\mathbf{B}\cdot\mathbf{R}$ and $\mathbf{B}\cdot\mathbf{T}$ than that requested, DECPR will exit through the residual miss subprogram and compute the minimum associated miss. When the low-gain antenna constraint is violated, a message to this effect will be printed, and DECPR will attempt to find an acceptable modified maneuver. If none exists, this constraint may be violated at the expense of some telemetry data during the maneuver.

(3) Command Generation Program (COMGN). The purpose of COMGN is to convert the maneuver parameters into three commands expressed in binary form and adjusted to a form which is usable by the CC&S. The propulsion subprogram (PRPLS) is used to compute the burn time. Additional quantities of interest during the execution of the maneuver are computed in COMGN.

(4) Plotting Program (PLOTZ). The PLOTZ shows the expected dispersion ellipse at encounter due to maneuver execution and orbit estimation errors, and also plots angular information of interest during the maneuver turns.

(5) Capability Ellipse Generator (CAPEL). The CAPEL will generate the maximum capability ellipse in the **R–T** plane assuming the maximum maneuver is applied in the critical plane.

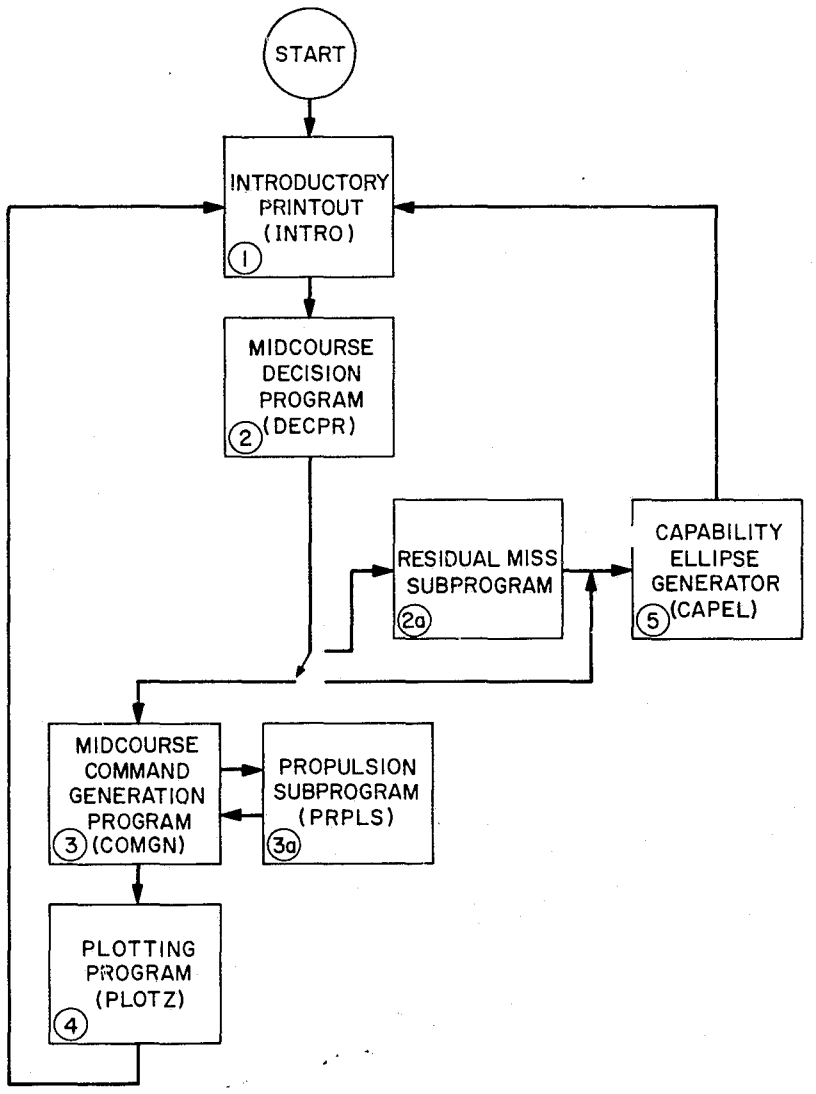

Fig. 66. Functional block diagram

References

1. Hudson, R. H., Nead, M. W., Warner, M. R., *The Orbit Determination Program of The Jet Propulsion Laboratory,* Technical Memorandum 33-168. Jet Propulsion Laboratory, Pasadena, Calif., Dec. 1, 1963.

2. Pease, G. E., *Mariner Venus 67 Orbit Determination Characteristics and Accuracy,* June 9, 1967 (Internal communication).

3. Vegos, C. J. and Trask, D. W., "Ranger Combined Analysis, Part II: Determination of the Masses of the Earth and Moon from Radio Tracking Data," *The Deep Space Network,* Space Programs Summary 37-44, Vol. III, pp. 11-28, Jet Propulsion Laboratory, Pasadena, Calif., March 31, 1967.

4. Anderson, J. D., *Determination of the Masses of the Moon and Venus and the Astronomical Unit from Radio Tracking Data of the Mariner II Spacecraft,* Technical Report 32-816. Jet Propulsion Laboratory, Pasadena, Calif., July 1, 1967.

References (contd)

5. Null, G. W., *The Mariner IV Flight Path and Its Determination From Radio Tracking Data,* Technical Report 32-1108. Jet Propulsion Laboratory, Pasadena, Calif., August 1, 1967.

6. *Mariner Mars 1964 Project Report: Mission and Spacecraft Development Vol. I. From Project Inception Through Midcourse Maneuver,* Technical Report 32-740, pp. 255-264. Jet Propulsion Laboratory, Pasadena, Calif., March 1, 1965.

7. McReynolds, S. R., Bourke, R. D., and Thuleen, K. L., *Nongravitational Forces on Spacecraft,* Vol. II, pp. 21-27, SPS 37-47. Jet Propulsion Laboratory, Pasadena, Calif., Sept. 30, 1967.

8. McReynolds, S. R., *Estimation Techniques for Truncated Data,* Vol. III, SPS 37-50. Jet Propulsion Laboratory, Pasadena, Calif., June 30, 1968.

9. Null, G. W., Gordon, H. J., and Tito, D. A., *The Mariner IV Flight Path and Its Determination From Tracking Data,* Technical Report 32-1108. Jet Propulsion Laboratory, Pasadena, Calif., Aug. 1, 1967, pp. 11–17.

10. Dobrotin, B. M., Prelewicz, D. A., and Laumann, E. A., *Mariner Self-disturbance Torques and Limit Cycles.* To be presented at the AIAA Guidance Control, and Flight Mechanics Conference, Princeton, N.J., Aug. 18-20, 1969.

11. Kizner, W. A., *A Method of Describing Miss Distances for Lunar and Interplanetary Trajectories,* External Publication No. 674. Jet Propulsion Laboratory, Pasadena, Calif., August 1, 1959.